UAM
UNIVERSIDAD AUTONOMA
DE MADRID
Departamento de Bioquímica
Facultad de Medicina

Dissecting the role of heartbeat-driven pericardiac fluid forces on epicardium morphogenesis through *in vivo* imaging in the zebrafish.

Tesis Doctoral
Marina Peralta López
Madrid 2014

Departamento de Bioquímica
Facultad de Medicina
Universidad Autónoma de Madrid

Tesis Doctoral

Dissecting the role of heartbeat-driven pericardiac fluid forces on epicardium morphogenesis through *in vivo* imaging in the zebrafish.

Marina Peralta López
Licenciada en Biología

Madrid 2014

Director: Dr. Nadia Mercader Huber
Fundación CNIC Carlos III

INDEX

GLOSSARY

***ace*: *acerebellar* (*fgf8*$^{-/-}$ mutants)**

***Acvr1l*: activin A receptor type I**

AHF: anterior heart field

apEPs: arterial pole epicardial precursors

At: atrium

AVC: atrio-ventricular canal

avcPE: proepicardial cluster located close to the atrio-ventricular canal

BDM: 2,3 butanedione monoxime

BMP: bone morphogenetic protein

Bmp2: bone morphogenetic protein 2

Bmp4: bone morphogenetic protein 4

dpf: days post fertilization

ECM: extracellular matrix

EMT: epithelial to mesenchymal transition

EPDCs: epicardial derived cells

FGF: fibroblast growth factor

fgf8a: fibroblast growth factor 8 a

FHF: first heart field

GFP: green fluorescent protein

hpf: hours post fertilization

hst: *heartstrings* (*tbx5*$^{-/-}$ mutants)

IFT: inflow track

Isl1: *Islet1*

***Itg*α4**: Integrin alpha 4

LPM: lateral plate mesoderm

myh6: myosin heavy polypeptide 6

OFT: outflow track

PE: proepicardium

RA: retinoic acid

Raldh: retinaldehyde dehydrogenases

SHF: second heart field

SV: *sinus venosus*

Tbx18: T-box transcription factor 18

Tbx5: T-box transcription factor 5

Tcf21: transcription factor 21

tnnt2: troponin T2

V: ventricle

VCAM1: vascular cell adhesion molecule 1

vpPE: proepicardial cluster located close to the venous pole of the heart

***Wt1*:** Wilms' tumor suppressor gene

SUMMARY

Mesothelial cells lining the pericardium generate the proepicardium (PE): the precursor cell population of the epicardium, the outer layer covering the myocardium. The epicardial layer is essential for myocardial maturation, formation of the heart valves and coronary vasculature. Two mechanisms have been proposed based on fixed samples:

1. The formation of a bridge between the PE and the ventricle.
2. The release of cysts into the pericardial cavity.

However, there is no evidence from *in vivo* studies showing how epicardial precursor cells reach and attach to the heart. Hydrodynamic forces play a central role in organ morphogenesis. The role of blood flow in shaping the developing heart is well established, but the role of fluid forces generated in the pericardial cavity surrounding the heart is unknown. Using optical tools for real-time analysis in the zebrafish, including high-speed imaging and optical tweezing, we show that the heartbeat generates pericardiac fluid advections that drive epicardium formation. These flow forces trigger PE formation and epicardial progenitor cell release and motion. The pericardial flow also influences the site of PE cell adhesion to the myocardium. We found primary cilia protruding into the pericardial cavity from PE and pericardial cells that could be mediating the mechanotransduction of fluid forces. Additionally, we identified a novel mesothelial source of epicardial precursors and show that precursor release and adhesion occur both through pericardial fluid advections and through direct contact with the myocardium. Thus, two hydrodynamic forces couple cardiac development with function: first, blood flow inside the heart, and second, the pericardial fluid advections outside the heart identified here. This pericardial fluid flow is essential for epicardium formation and represents the first example of hydrodynamic flow forces controlling organogenesis through an action on mesothelial cells.

RESUMEN

Las células mesoteliales que revisten el pericardio generan el proepicardio (PE): la población celular precursora del epicardio, la capa más externa que cubre el miocardio. El epicardio es esencial para la maduración del miocardio, la formación de las válvulas cardiacas y la vasculatura coronaria. Se han propuesto dos mecanismos basados en muestras fijadas:

1. La formación de un puente entre el PE y el ventrículo.
2. La liberación de cistos en la cavidad pericárdica.

Sin embargo, no hay evidencias *in vivo* mostrando como las células precursoras del epicardio alcanzan y se adhieren al corazón. Las fuerzas hidrodinámicas juegan un papel central en la morfogénesis de los órganos. El papel del flujo sanguíneo en moldear el corazón durante su desarrollo está bien establecido, pero el papel de las fuerzas de fluido generadas en la cavidad pericárdica rodeando al corazón se desconoce. Usando herramientas ópticas para el análisis en tiempo real en el pez cebra, incluyendo imagen de alta velocidad y pinzas ópticas, nosotros mostramos que el latido cardiaco genera advecciones de fluido que conducen a la formación del epicardio. Esas fuerzas de fluido desencadenan la formación del PE y la liberación y movilización de los precursores epicárdicos. El fluido pericárdico también influencia el lugar de adhesión al miocardio de las células PE. Encontramos cilios primarios protruyendo hacia la cavidad pericárdica desde células PE y pericárdicas que podrían estar mediando la mecanotransducción de las fuerzas de fluido. Adicionalmente, identificamos una nueva fuente mesothelial de precursores epicárdicos y mostramos que la liberación y la adhesión de los precursores ocurren mediante advección en el fluido pericárdico y por contacto directo con el miocardio. Por tanto, hay dos fuerzas hidrodinámicas implicadas en el desarrollo cardiaco: la primera, el flujo sanguíneo dentro del corazón y la segunda, el fluido pericárdico fuera del corazón identificado en este trabajo. Este fluido pericárdico es esencial para la formación del epicardio y representa el primer ejemplo de fuerzas de fluido hidrodinámicas controlando organogénesis mediante la acción sobre células mesoteliales.

INTRODUCTION

The heart is the first organ to form and to acquire its function in the embryo. This allows the oxygenation of organs, circulation of nutrients and removal of waste, as soon as the number of cells reaches a point where diffusion is no longer efficient.

In the human population around 1% of newborn children have some form of congenital heart defect and cardiac malformations explain around 30% of fetus loss during gestation (Bruneau, 2008). Furthermore, children with congenital heart diseases frequently develop neurological disorders. Heart morphogenesis requires a complex and proper regulation at the cellular and molecular level, whereby physical forces are also playing a crucial role. Understanding how this process occurs is vital for understanding the genesis of congenital heart disease, which has a huge impact on human health.

Moreover, understanding heart development might open avenues for regenerative medicine. Heart failure as a consequence of myocardial infarction is the first cause of death worldwide (WHO). Trying to find ways to promote cardiac regeneration, among others through the reactivation of developmental pathways, is therefore an important goal being pursued by the scientific community (Xin et al., 2013).

The heart lies in the anterior part of the body cavity. It is surrounded by the pericardium and is nourished by the coronary vessels. In mammals and birds, the heart is composed of four chambers: right atrium, right ventricle, left atrium and left ventricle (**Figure I 1**). The right atrium receives the deoxygenated blood from the body via the superior and inferior vena cava. The blood is pumped through the tricuspid valve to the right ventricle, which sends the blood to the lungs through the pulmonary artery, crossing the pulmonary valve. After being oxygenated, the blood goes back to the left atrium via pulmonary vein and passes through the mitral valve to the left ventricle, which pumps it towards the rest of the body by the aorta, through the aortic valve.

Three tissue layers compose the mature vertebrate heart: the endocardium, the myocardium and the epicardium. The endocardium is the innermost endothelial cell layer of the heart, facing the lumen. The myocardium is an involuntary striated muscle tissue specific to the heart, responsible of the heartbeat. In the adult heart, we can distinguish between the external compact layer and the internal trabecular layer. The epicardium is the mesothelial outermost layer covering the heart. The coronary vasculature delivers oxygen and nutrients to the heart and removes the waste allowing its function.

1. Heart development in model organisms.

The use of animal models for understanding cardiovascular diseases has contributed to improve our knowledge and capacity of diagnosis and treatment (Zaragoza et al., 2011). However, as they are not a perfect reproduction for human diseases and environments, the selection of the model organism has to be done taking into account the biological question that needs to be addressed. The mouse embryo is a mammalian model and thus more directly related to humans. One of its advantages is the large amount of genetic tools that allow gene targeting, gene replacement and other genome editing possibilities. Mice do present nonetheless some disadvantages for heart development studies, such as the embryonic development in utero and the necessity of

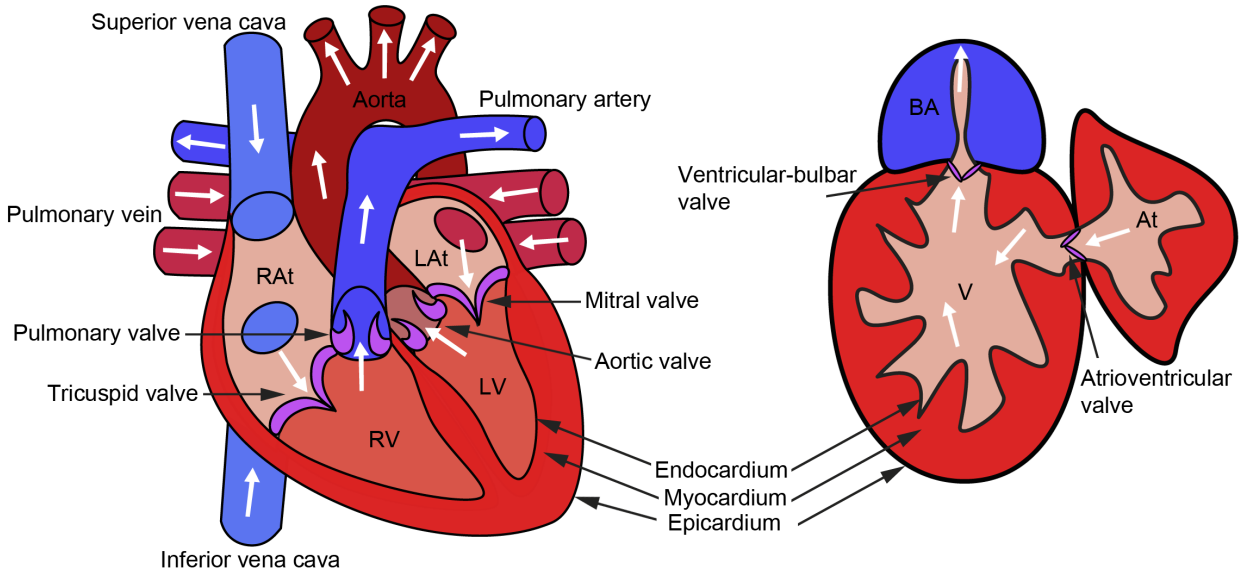

Figure I 1. The vertebrate heart. (A) Frontal view of a four chambered heart, as found in mammals and birds. The right atrium (RAt) receives the deoxygenated blood from the inferior and superior vena cava, the blood then passes through the tricuspic valve to the right ventricle (RV), from which the pulmonary artery emerges. The left atrium (LAt) receives the oxygenated blood from the pulmonary vein and pumps it into the left ventricle (LV) through the mitral valve, which distributes the blood via the aorta to the whole body. White arrows indicate the blood flow direction. Adapted from http://classroom.materials.ac.uk/caseHeart.php. (B) The teleost fish heart is composed of two chambers, one atrium (At) and one ventricle. The At collects the deoxygenated blood and sends it to the ventricle (V) through the atrioventricular valve. The V pumps the blood through the ventricular-bulbar valve to the bulbus arteriosus (BA). Both types of hearts have their walls formed by three layers: the endocardium, the myocardium and the epicardium.

the heartbeat and blood circulation for their survival. The chick embryo also presents several advantages for developmental studies like its rapid development and accessibility for visualization and experimental manipulation, but is less amenable to genetic manipulations. Lately, the zebrafish has become a powerful model organism for studying developmental processes. Its external development, transparency and fast generation time allow *in vivo* imaging and the possibility to use drug treatments or other direct manipulations. Besides, its ability to survive up to 7 days postfertilization (dpf) without a heartbeat (Sehnert et al., 2002) allows the study of the role of biomechanical forces during cardiovascular development.

1.1. Heart development in mouse and chick embryos.

In mammals and birds, cardiac progenitor cells arise from the mesodermal layer, which forms by ingression of cells into the primitive streak at gastrulation. (Vincent and Buckingham, 2010, Abu-Issa and Kirby, 2007) (**Figure I 2**). The first differentiated myocardial cells appear in the cardiac crescent, derived from the splanchnic mesoderm underlying the head folds. This population is called first heart field (FHF). A second pool of cardiac precursors lies medially to the FHF on either side of the midline; these progenitor cells constitute the second heart field (SHF). While the onset of endocardium formation in the mouse is mostly unknown, in chick embryos, endocardial cells form tubes medial to the myocardial mantle of progenitors on both sides of midline. These endocardial bilateral tubes fuse, like the FHF, at the midline to form the primitive cardiac tube. This tube gives rise mainly to the left ventricle and provides a scaffold for subsequent growth. As

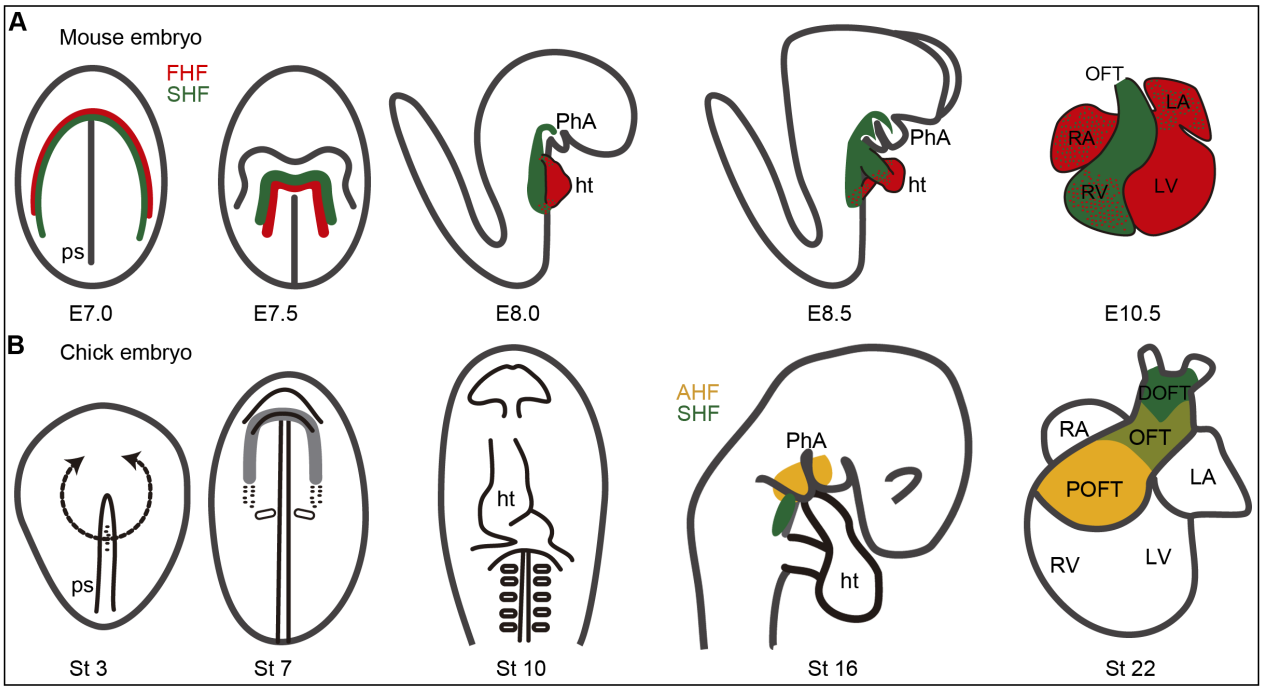

Figure I 2. Heart development in the mouse and chick embryo. (A) In the mouse, heart progenitors have reached the head folds by embryonic day (E) 7, and are separated into the first heart field (FHF) (in red) and the second heart field (SHF) (in green) at E7.5. The FHF contributes to the primitive heart tube, formed at E8.0. The SHF is subsequently added to the heart tube and gives rise to the outflow tract (OFT) and the RV. (B) In the chick embryo, heart progenitor cells invaginate into the anterior half of the primitive streak at Hamburger and Hamilton stage 3 (St 3) (Hamburger and Hamilton, 1951). By St 7, they have migrated under the head folds and start expressing *Nkx2.5* (grey zone). The tube is straight at St 10 and has looped at St 16. SHF (green) and anterior heart field (AHF) (yellow) have been defined at St 16 and will contribute to portions of the OFT at St 22. DOFT, distal outflow tract; ht, heart tube; LA, left atrium; LV, left ventricle; PhA, pharyngeal arches; POFT, proximal outflow tract; ps, primitive streak; RA, right atrium; RV, right ventricle. Adapted from Heart development and regeneration, volume 1.

the heart tube forms, the SHF comes to lie behind the cardiac tube, as well as extending more anteriorly and posteriorly.

Two principal components to the SHF have been described: (1) the anterior heart field (AHF), which contributes to the elongation of the arterial pole and (2) cells which contribute to the elongation of the venous pole of the heart (Buckingham et al., 2005). Lineage tracing experiments in mice indicated that the right ventricle, outflow track (OFT), *sinus venosus* (SV) and atria derive from the SHF. *Tbx5*, a T-box family member, is a molecular marker of the FHF (Bruneau et al., 2001). Mutant mice show severe defects in the inflow tract (IFT) and left ventricular hypoplasia. However, the OFT and right ventricle (V) of the mutants continue to grow, indicative of an effect of *Tbx5* loss of function specific to FHF proliferation. Several SHF marker such as Islet 1 (Isl1), a LIM homeodomain transcription factor, have been reported (Cai et al., 2003). *Isl1* null mutations lead to phenotypes affecting the SHF derived heart domains. In *Isl1* mutants SHF progenitor cells are progressively reduced in number, moreover, fibroblast growth factors (FGF) and bone morphogenetic proteins (BMP) are downregulated. *Isl1* mutants present a reduction in the domain of *Fgf8* expression. Their phenotype was more severe than that seen with *Fgf8* hypomorphs, which lack OFT (Abu-Issa et al., 2002). *Fgf8* is a member of the extracellular FGF family, required for a variety of patterning events during vertebrate development. In chick and zebrafish embryos, several studies have implicated Fgf8 in cardiovascular development (Alsan and Schultheiss, 2002, Reifers et al., 2000).

In later stages, the heart tube undergoes a process involving rightward looping and growth, leading to the formation of the four-chambered heart.

1.2. Heart development in zebrafish embryos.

The zebrafish heart is two-chambered. Atrium (At) and ventricle (V) are not septated. Nonetheless, it exhibits many similarities to the amniote heart.

At early blastula stages (256 to 512 cells), myocardial and endocardial progenitor cells are found at the ventro-lateral embryonic margin on both sides of the embryo, whereby endocardial progenitor cells hold more ventral positions (Lee et al., 1994). Myocardial chamber lineages are not yet separated; progenitor cells can contribute to both At and V (Stainier et al., 1993). At blastula stage, ventricular myocardial progenitors are positioned closer to the margin and to the dorsal midline than atrial ones (**Figure I 3**) (Keegan et al., 2004). However, endocardial progenitors are not spatially organized at this stage. After gastrulation, myocardial chamber progenitors occupy discrete regions of the anterior lateral plate mesoderm (LPM). During somitogenesis, these bilateral populations migrate medially until at 23 hours post-fertilization (hpf), they fuse at the midline to form a cardiac cone lined in its interior by the endocardial layer (Stainier et al., 1993).

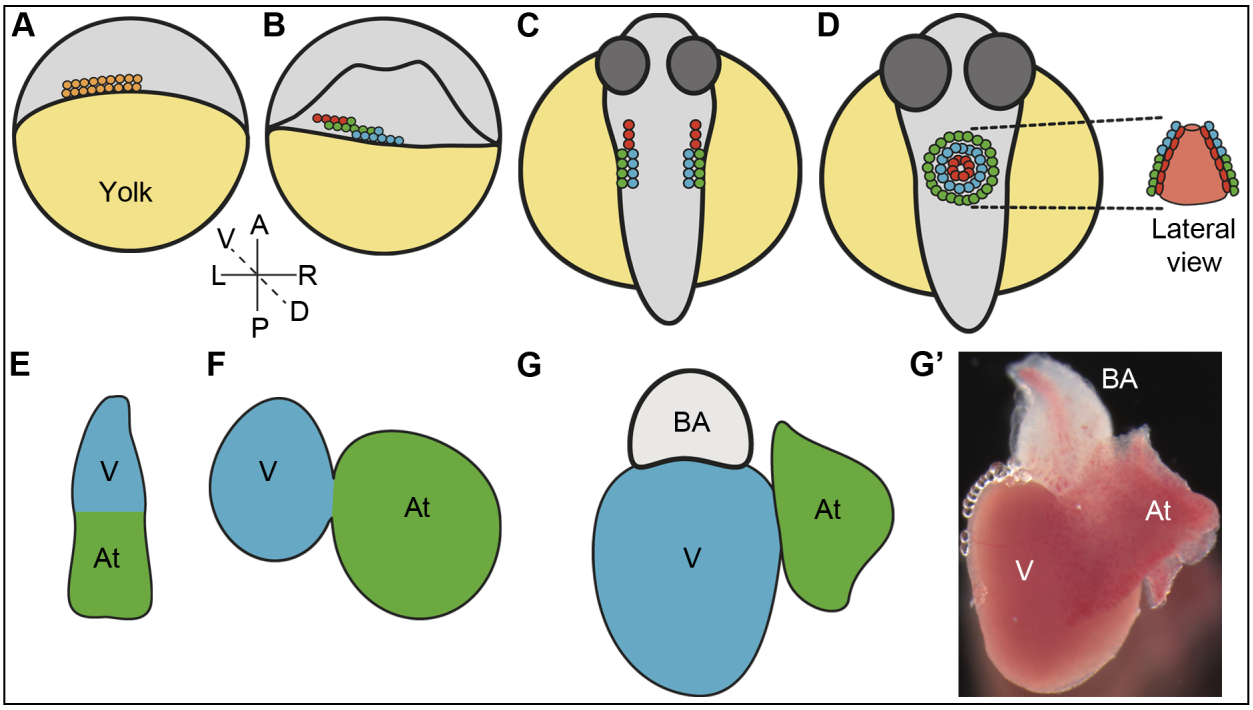

Figure I 3. **Heart development in zebrafish.** (A) At blastula stage, 3 hpf, the heart progenitor cells are located throughout the ventral and lateral regions of the embryo. (B) At gastrulation, 5hpf, the ventricular myocardial progenitors (blue) are positioned closer to the margin and to the dorsal midline than the atrial ones (green). The endocardial progenitors (red) appear close to the ventricular ones. (C) During somitogenesis, at 12 hpf, the ventricular myocardial progenitors are found more medial than the atrial progenitors. The endocardial progenitors lie anterior in the anterior lateral plate mesoderm (ALPM). (D) Myocardial and endocardial progenitors migrate to the midline and fuse by 19 hpf to create the cardiac cone. (E) The myocardium surrounds the endocardium and forms the linear heart tube by 24 hpf. (F) The heart loops to form a right-sided ventricle and left-sided atrium by 48 hpf. (G) Adult zebrafish heart. At, atrium; BA, *bulbus arteriosus*; V, ventricle. Based on Keegan et al., 2004; Stainier, 2001; Staudt and Stainier, 2012.

The embryonic heart starts to beat at 22 hpf. By 24 hpf, the cardiac cone has evolved into a linear heart tube, grows and loops rightwards. Next, the V and At form by ballooning out. At 48 hpf, the V and At become separated by the constriction of the atrio-ventricular canal (AVC). At this time, the heart grows through the addition of cardiac progenitors from the arterial and venous poles. Like in mammals and birds, the SHF population contributes to the arterial pole myocardium after the initial heart tube formation (Hami et al., 2011, Liu and Stainier, 2012). This process also requires *fgf8* signaling (de Pater et al., 2009). Around 72 hpf, the cardiac trabeculation process will be started by cardiomyocytes protruding out of the ventricular myocardium (Liu et al., 2010). When the heart starts to beat, forward and reverse blood flow are generated, and the initial reverse flow triggers the valve formation process (Vermot et al., 2009). During cardiac development, the heartbeat generated hemodynamic forces play an essential role promoting chamber differentiation, valve formation and myocardial trabeculation (Berdougo et al., 2003, Vermot et al., 2009, Peshkovsky et al., 2011, Staudt et al., 2014).

2. The proepicardium (PE).

The epicardium covering the myocardium arises from the PE, a cluster of mesodermal cells, which forms close to the venous pole of the cardiac tube (Manner, 1992). The PE had been described in several vertebrates from fish to human (Manner, 1992, Serluca, 2008, Jahr et al., 2008, Icardo et al., 2009, Viragh and Challice, 1981, Nesbitt et al., 2006, Kuhn and Liebherr, 1988, Komiyama et al., 1987, Hirakow, 1992). Different molecular markers are used to define epicardial and PE identity, such as the genes encoding the Wilms' tumor suppressor 1 (*Wt1*), the T-box transcription factor 18 (*Tbx18*) and the transcription factor *Tcf21* (Carmona et al., 2001, Haenig and Kispert, 2004, Tanaka and Tickle, 2004, Robb et al., 1998).

2.1. Origin and mechanisms inducing the PE.

Genetic fate mapping of Nkx2.5 and Isl1- positive cells in the mouse suggests that PE cells derive from the precardiac mesoderm (Zhou et al., 2008b). In the zebrafish, disruption of LPM migration through knockdown of *sphingosine-1-phosphate receptor 2* or *SRY (*sex determining region Y*)-box 32* leads to cardia bifida with each bilateral heart associated with its own PE, suggesting that the earliest progenitors of the epicardium lie in the LPM (Serluca, 2008). In the chick, there are also evidences about the PE arising from a region in the LPM. PE precursors remain adjacent to the cardiogenic mesoderm, without intercalating with it (Bressan et al., 2013).

The PE is composed of an outer layer of mesothelial cells and an inner core of mesenchymal cells, which produces extracellular matrix. Endothelial progenitors are also present in the PE, but their origin remains unclear. They have been proposed to be recruited either from the sinus endothelium, the liver primordium or both (Katz et al., 2012, Cossette and Misra, 2011, Perez-Pomares et al., 2004).

The mechanism of PE outgrowth is poorly understood. However, neighboring tissues haven been shown to influence PE positioning and inducing PE formation. *In vitro* and *in vivo* assays, using chick embryos, suggested that the liver bud induces PE marker genes expression (*Wt1*,

Tcf21 and *Tbx18*) in naïve mesothelial cells, during a specific time window (Ishii et al., 2007). Nonetheless, the mesothelial cells did not acquire a PE morphology. In the zebrafish, the liver does not seems to be required for PE induction. *hnf1ba*^{hi2169} mutants at 57 hpf lack a liver bud, but *tbx18* and *tcf21* expressions in the heart region are normal (Liu and Stainier, 2010). This species-specific difference could be due to the bigger distance between PE and liver bud in zebrafish embryos than in avians.

The secreted signaling molecules of the BMP family, as well as the FGF family, have been shown to play a role in PE formation. Activin A receptor type I (*acvr1l*) mutant zebrafish larvae, lacking a functional type I BMP receptor, loose *tbx18* and *tcf21* expression in the heart region, suggesting the absence of a PE (Liu and Stainier, 2010). The BMP ligand acting through *acvr1l* might be *bmp4,* as it is expressed in OFT, AVC and SV myocardium at 48 hpf. Indeed, *bmp4* mutant zebrafish show reduced expression of *tbx18* and *tcf21* only in the heart region at 57 hpf. *In vitr*o and *in vivo* assays in chick embryos have demonstrated that a very sensitive balance of BMP signaling is required for PE development. Altering the balance through supplying BMP (adding exogenous BMP2) or blocking this pathway (adding exogenous Noggin) leads to the loss of *tbx18* expression (Schlueter et al., 2006). In PE cultures both experimental situations lead to cardiomyocyte formation, but only in the cells close to the mesenchymal core, not in epithelial cells in the periphery of the PE explant. A signaling crosstalk between BMP and FGF drives precardiac mesoderm cells to enter the PE or contribute to the myocardium. BMP signaling via Smad (P-Smad 1/5/8) drives chick PE explants towards cardiomyocyte differentiation and exposure to FGF signaling via mitogen-activated protein kinase (Mek) 1/2 into epicardial lineage (van Wijk et al., 2009).

Regarding transcription factors, the most severe phenotypes were observed in mutants of the transcription factors *Tbx5* and *Gata4*. The transcription factor *Gata4*, a downstream effector of BMP signaling in the LPM (Rojas et al., 2005), is also important for PE development. GATA4-null mouse embryos lack a PE and present myocardial defects that seem to be a consequence of epicardium loss (Watt et al., 2004). In the zebrafish, *tbx5a* has been proposed to confer a subset of anterior LPM cells the capacity to respond to Bmp signals derived from the myocardium and initiate PE development (Liu and Stainier, 2010). In the chick, *Tbx5* is expressed in the PE. *Ex vivo* PE cultures showed that PE cells downregulate *Tbx5* expression during cell migration (Hatcher et al., 2004). Overexpression and knockdown of chick *Tbx5* prevent PE cells migration, impairing epicardial development. In human embryos, *TBX5* is expressed in the myocardium, in the epicardium and coronary vessels. Nonetheless, epicardial derived cells (EPDCs) do not express it as they migrate through the subepicardial space. Mutations in *TBX5* lead to haploinsufficiency that cause autosomal dominant Holt-Oram syndrome (OMIM #142900), a rare autosomal dominant human disease (Basson, 1997, Basson et al., 1999), which is characterized by upper limb malformations and cardiac septation defects. Hand and heart malformations in Holt-Oram syndrome vary considerably, even among affected family members with identical mutation. Also, patients with pericardial agenesis have been reported, which point out the importance of TBX5 in pericardium development (Dias et al., 2007).

In many vertebrates, *tbx18, wt1, tcf21* expression can be found bilaterally at the beginning of the PE formation, but only the right-sided PE will develop and give rise to the epicardium. The most important signaling cascade involved in left-right asymmetrical development is the NODAL/PITX2

pathway (Gritsman et al., 2000). Downstream of it, in the chick embryo, FGF8 induces SNAI1 on the right side, which is repressing PITX2 (Boettger et al., 1999, Patel et al., 1999). This triggers the expression of *Tbx18* and *Wt1* in the PE (Schlueter et al., 2006). At later stages, FGF signaling is needed for PE survival and its further outgrowth on the right side of the heart tube (Torlopp et al., 2010). The lack of FGF on the left side leads to upregulation of the proapoptotic caspase 3, which induces cell death (Schlueter and Brand, 2009). In *Xenopus*, and the *axolotl*, like in the chick, the PE develops on the right side of the IFT (Jahr et al., 2008, Fransen and Lemanski, 1990). In contrast, the mouse embryo PE does not display a prominent left-right asymmetry (Schulte et al., 2007). The original two PE anlagen fuse to form one medial cluster. In zebrafish embryos, the bilateral origin of the PE was tested by inducing *cardia bifida*, which revealed *wt1a*-positive cells close to both bilateral heart tubes, contrary to what occurs for the same experiment in chick embryos, where a PE developed only on the right side of the heart (Serluca, 2008, Manner et al., 2001) (**Figure I 4**).

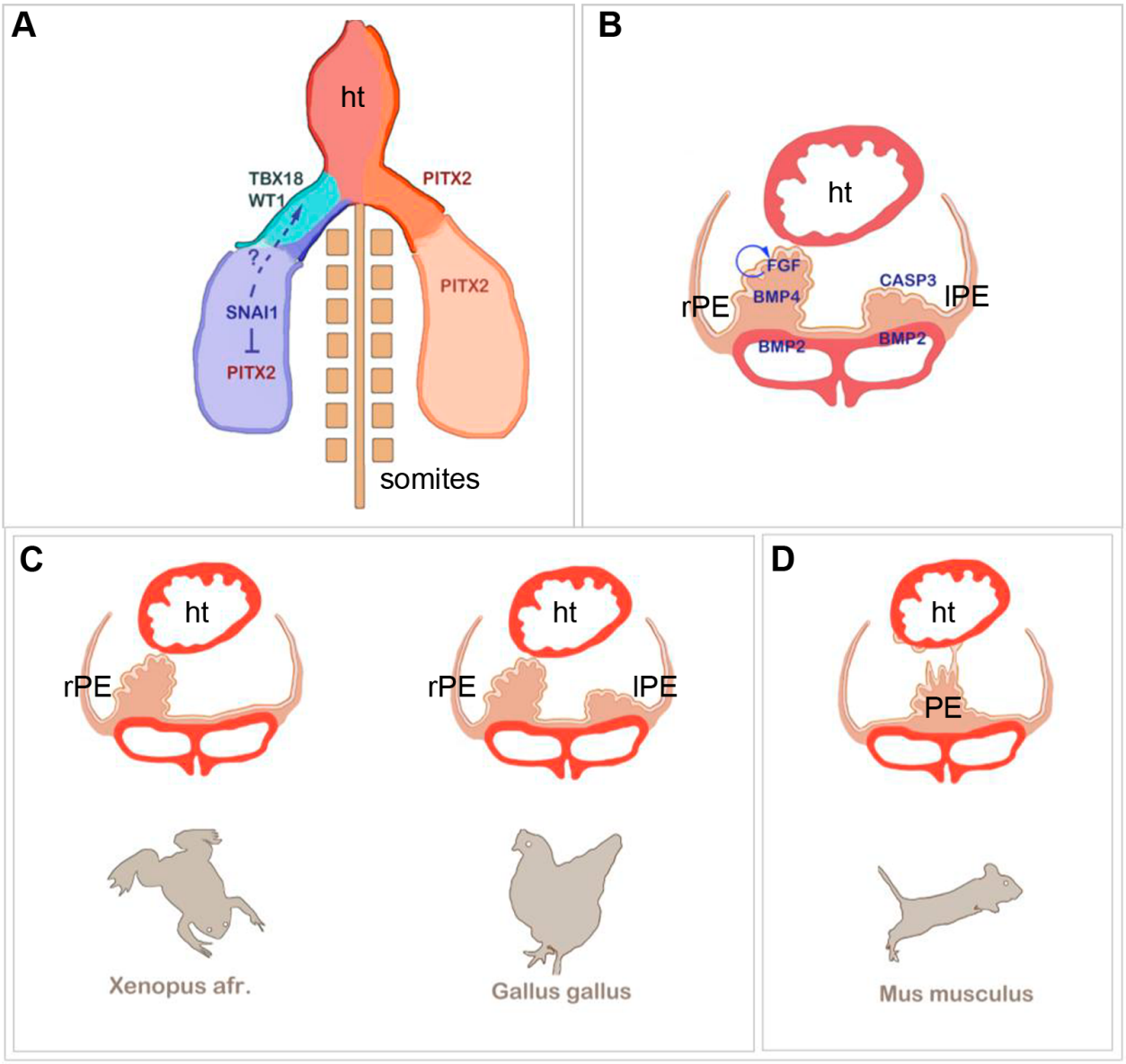

Figure I 4. Left-Right Asymmetry and PE development. (A) During somitogenesis and heart tube formation in the chick, *PITX2* is expressed in the left lateral plate mesoderm and the left inflow tract (IFT).

On the right side of the embryo, *SNAI1* represses *PITX2* expression. *TBX18* and *WT1* are the first PE markers expressed on the right side. (B) At later stages, BMP and FGF signaling regulate the asymmetric PE outgrowth. *BMP4* is required at low concentration to maintain PE marker gene expression, while *BMP2* high levels are needed in the *sinus venosus* to repress PE formation. A positive FGF signaling feedback loop supports the survival and growth of PE cells on the right side. The lack of FGF on the left side leads to massive retardation of the PE primordium and upregulation of *CASP3*, which induces apoptosis. (C-D) Examples of asymmetric and symmetric PE development among vertebrates. (C) Xenopus and the chick exhibit a right-sided PE cluster that establishes a tissue bridge to the heart. (D) In mouse embryos, asymmetric PE formation has not been observed. The bilaterally formed PE clusters fuse at the midline of the sinus venosus, and PE cell transfer is either accomplished by the release of PE cysts into the pericardial cavity or by being plucked off by the contracting ventricle. ht, heart; rPE, right-sided proepicardium; lPE, left-sided proepicardium. Adapted from Schlueter and Brand, 2013.

2.2. Evolutionary origin of the PE.

The evolutionary origin of the PE remains unclear. Invertebrates lack a PE. It has been proposed that in vertebrates the PE could derive from an ancient pronephric external glormerulus that has lost its excretory role (Cano et al., 2013). This hypothesis is supported by the way epicardium formation occurs in the lamprey *Petromyzon marinus,* one of the most primitive vertebrates, an agnathan. The epicardial layer arises by cell migration from the primordia of the right pronephric external glomerulus upon contacting the ventricular surface. Posteriorly, this primordium continues its differentiation to give rise to a functional external glomerulus. A possible developmental link between the heart and the kidney can be supported by the existence of a heart-kidney complex in hemichordates.

The fact that zebrafish and *Xenopus* embryos develop an independent PE and pronephric glomeruli would not support the hypothesis of the pronephric external glomerulus as a PE origin. However, this could be explained by the uncoupling of the cardiac and the pronephric domains in gnathostomes, which are coupled in agnathans, leaving the most cranial glomerular primordium devoid of its excretory potential.

2.3. Transfer of PE cells to the myocardium during epicardium formation.

In the chick, after onset of *Tbx18* and *Wt1* expression, the right PE increases size by until attaching to the dorsal side of the beating ventricle (**Figure I 5**) (Manner, 1992, Manner, 1999). The attachment of the mesothelial villi to the AVC leads to the release of extracellular matrix from the core of the PE, allowing the formation of a bridge, which is composed of heparan sulfate and fibronectin (Nahirney et al., 2003). PE cells then spread over the myocardial surface until completely enveloping the cardiac tube. Interestingly, the epicardial cells covering the cardiac OFT do not derive from the PE, but from the cephalic pericardium (Perez-Pomares et al., 2003).

A similar process has been proposed for *Xenopus:* the PE appears on the right side of the lFT. Next, the tip of the PE attaches the ventricular myocardium and a bridge is formed allowing the transfer of PE cells to the ventricle (Jahr et al., 2008).

However, in mice, no evident PE-myocardial bridge has been observed. Rather, the epicardium forms islands across the myocardial surface (Komiyama et al., 1987) (**Figure I 6**). This finding

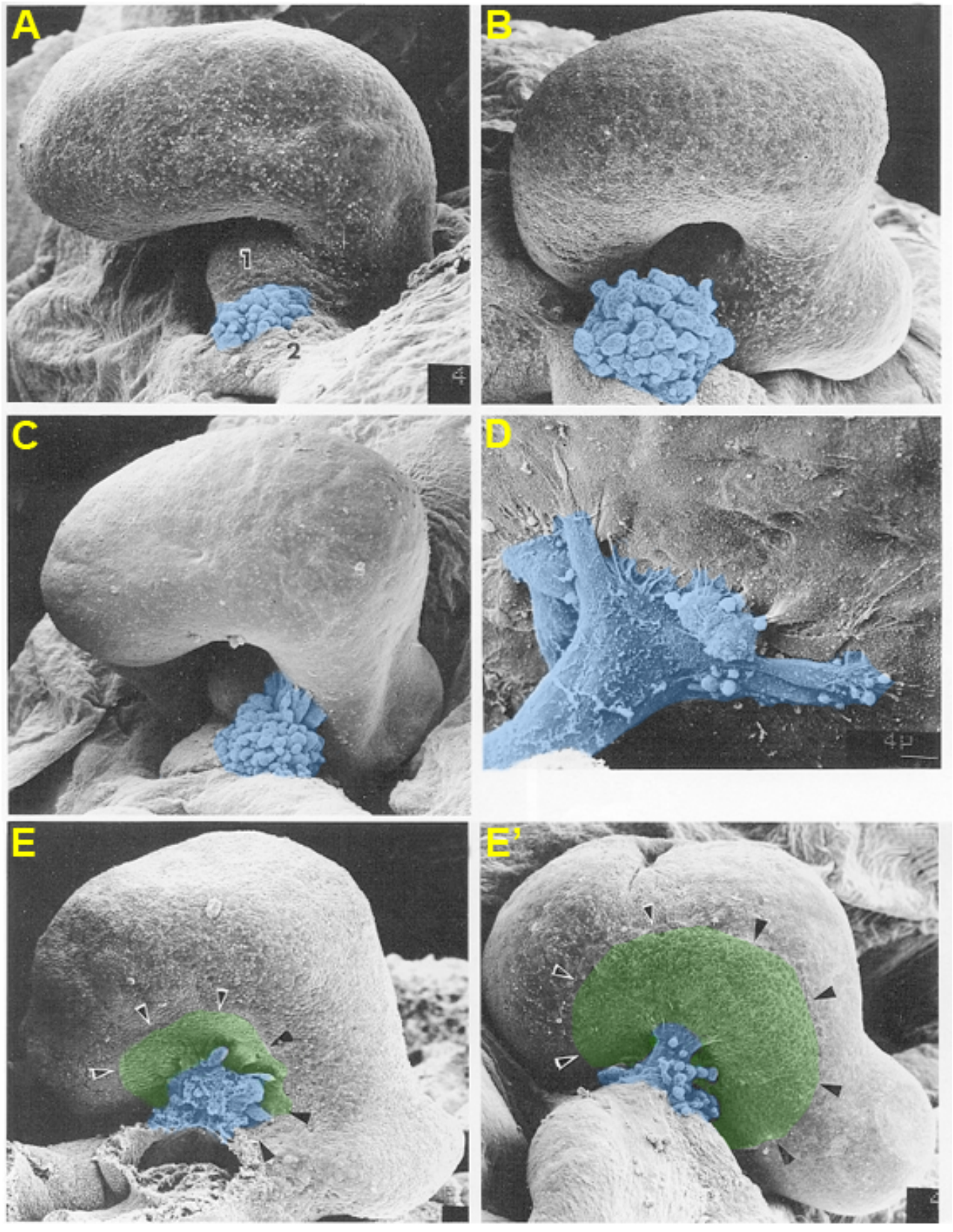

Figure I 5. Epicardial formation in the chick embryo. (A) At stage 14, the epithelium covering the ventral wall of the SV forms villous protrusions directed into the pericardial cavity (blue). (B) These protrusions increase in number and grow in length, acquiring the cauliflower-like phenotype typical of the PE. (C) Posteriorly, the PE begins to establish contact with the dorsal wall of the heart. Filopodia extending from the tips of some villi adhere to the myocardial surface. (D) Higher magnification showing a pericardial villus adherent to the cardiac surface. The tip of this villus is branching at the cardiac surface. (E, E') A bridge between the PE and the myocardium is formed when most villi are in firm contact with the heart. From the point of attachment, the epicardial layer (green) starts to spread over the cardiac surface (arrowheads mark the borderline). Adapted from Männer, 1992.

suggests the release of PE cysts into the pericardial cavity and subsequent adhesion to the myocardial surface. It has also been noted that multicellular villi expand toward the beating heart and contact with the myocardium (Hirose et al., 2006, Rodgers et al., 2008). Given the fact that PE formation occurs at a stage at which the heart is already beating, myocardium-PE contact or fluid flows generated during cardiac contraction cycles have been suggested as a mechanism of PE cyst release (Rodgers et al., 2008, Fransen and Lemanski, 1990).

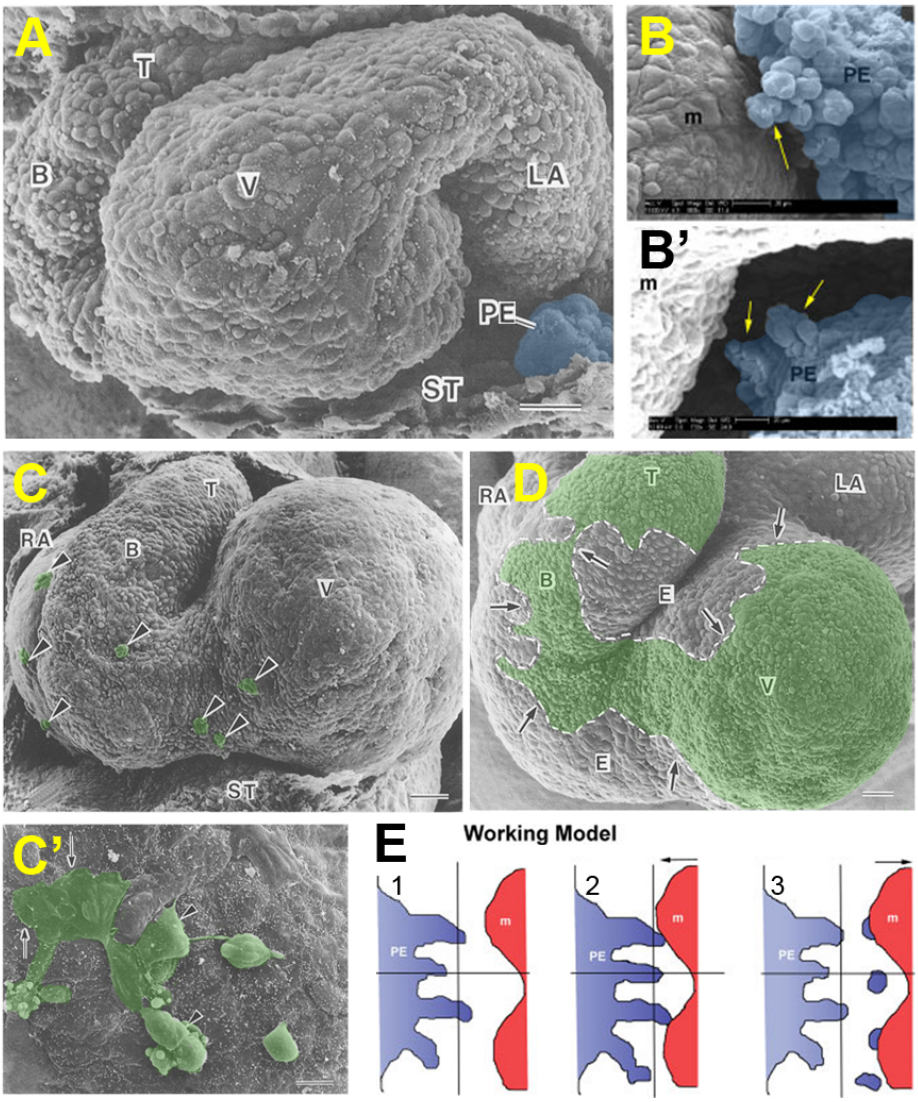

Figure I 6. Epicardial formation in the mouse embryo. (A) Cranioventral view of the heart of an embryonic day (E) 8 embryo. The PE is formed at the *septum transversum*. (B, B') Outgrowth of villous extensions toward the myocardium. Arrows mark large multicellular villi. (C) At E 9.5, many cell aggregates (arrowheads) are seen at various areas on the heart wall. (C') Higher magnification of the atrial wall. Cell aggregates (arrowheads) are flattened and form irregular patches of epithelial-like cells, revealing ruffled borders (arrows). (D) Later, whole the atrial wall and some areas of the ventricle and *bulbus cordis* are covered with epicardium. (E) Proposed model of PE translocation during mouse heart development. 1. PE cells initially grow toward the heart as multicellular villous extensions. The heartbeat will alter the distance between the myocardium and the outgrowth of PE. 2. The villi will reach a necessary length to make direct contact with the relaxed heart, and adhere to it in a velcro-like manner 3. Cardiac contraction leads to increase of the distance between the PE and myocardium and the adhered tips of the villi break off the PE. Villi at the atrioventricular sulcus and outer edges of the heart are less likely to directly contact the heart due to its distance to the myocardium. Once a critical villi length is reached in this area, they become unstable and the tips are sheared off due to the dynamic fluid forces within the pericardial cavity, creating free-floating cysts. Arrows indicate direction of heart movement. B, bulbus cordis; LA, left atrium; m, myocardium; PE, proepicardium; RA, right atrium; ST, septum transversum; T, truncus arteriosus; V, ventricle. Scale bars: (A) 30 µm; (B-C) 50 µm; (C') 10 µm; (D) 50 µm. Adapted from Komiyama et al., 1987 and Rodgers et al., 2008.

3. The epicardium.

At the time of heart looping, the outer layer of the heart, the epicardium starts to form (Bakkers, 2011). The epicardial layer is a single-layered flat mesothelium, covering the myocardium. Between the myocardium and the epicardium, the connective tissue-rich subepicardial space is being formed. The epicardium plays an important role during cardiac development by nourishing the myocardium with trophic factors, promoting and maintaining its mitotic activity.

3.1. Genes involved in epicardium formation.

Several genes have been described as important for epicardial development. *Wt1* encodes a zinc-finger protein, expressed in the epicardium, the subepicardial mesenchyme and in migratory EPDCs (Carmona et al., 2001). When EPDCs start to differentiate, *Wt1* expression is downregulated (Perez-Pomares et al., 2002). The protein plays an important role for heart and kidney development (Kreidberg et al., 1993). The epicardium does not form correctly, large gaps appear at the cranial end of the heart and there is an absence of the epicardial layer over the ventral surface of the aorta (Moore et al., 1999). Mutant animals die displaying ventricular hypoplasia and bleeding into the pericardial cavity due to myocardial wall rupture. Integrin alpha 4 (*Itg*α4) is a *Wt1* target gene involved in epicardium formation (Kirschner et al., 2006), it is important for the adhesion of epicardial precursors to the myocardium, through its interaction with vascular cell adhesion molecule 1 (VCAM1) (Yang et al., 1995, Kwee et al., 1995, Sengbusch et al., 2002).

Tbx18 belongs to the T-box transcription family. It is specifically and strongly expressed in the PE and in the epicardium (Haenig and Kispert, 2004, Tanaka and Tickle, 2004). The mutant mice exhibit structural and functional defects in the epicardium, coronary vasculature (Wu et al., 2013) and venous pole formation is affected (Christoffels et al., 2006).

Tcf21, a gene encoding a helix-loop-helix transcription factor, is specifically expressed in the PE, the epicardium and in the pericardium (Robb et al., 1998). Mouse and chick embryos, lacking *Tcf21* present epicardial blistering (Braitsch et al., 2012). In *Xenopus*, depletion of *Tcf21* results in a disruption in PE cell specification and failure to form the epicardium (Tandon et al., 2013).

3.2. Role of the epicardium as a paracrine factor source.

Chicken embryo experiments, in which epicardial formation was surgically blocked, have proven that the epicardium is essential for proper myocardial development (Manner, 1993, Gittenberger-de Groot et al., 2000, Manner et al., 2005). In absence of an epicardium, the compact myocardial layer is thinner, problems in chambers septation and valvulogenesis appear, and there are defects in the coronary vasculature. In addition, abnormal tissue bridges between the ventricles and the pericardial wall can be observed. Interestingly, the phenotype of PE ablation is similar to the one observed in *Wt1* mutant mice (Moore et al., 1999).

These experiments, together with many others, suggest that the epicardial layer is a paracrine factor source for the myocardium. Retinoic acid (RA) is a potent morphogen synthesized by retinaldehyde dehydrogenase (Raldh) enzymes, Raldh2 being the predominant one in mesodermal tissues (Niederreither et al., 2001). Raldh2 has been reported as a direct transcriptional target of Wt1 in epicardial cells (Guadix et al., 2011). RA signaling within the epicardium has been suggested to play an important role for cardiomyocyte proliferation by the production of epicardially-derived mitogens, such as Fgf9 (Lavine et al., 2005). FGF signaling is received by FGF receptors 1 and 2 acting together to promote cardiomyocytes proliferation. Mice deficient in FGF9 display decreased myocardial proliferation and ventricular hypoplasia.

In several species, after cardiac injury, the epicardial layer responds by secreting proangiogenic factors and contributing to fibrotic repair (Zhou et al., 2011, Gonzalez-Rosa et al., 2012, Kikuchi and Poss, 2012, Limana et al., 2011).

3.3. Epicardial derived cells (EPDCs).

A subpopulation of epicardial cells undergoes epithelial-to-mesenchymal transition (EMT) and migrates into the subepicardial space and underlying myocardium. Important regulators of this EMT are vascular endothelial growth factor (VEGF) and FGFs (Wessels and Perez-Pomares, 2004, Carmona et al., 2010). The transcription factors Snail1 and Snail2 in mammals and Slug in avians are important EMT regulators and they are expressed in the embryonic epicardium (von Gise and Pu, 2012). Their role is to repress epithelial markers and promote mesenchymal markers. Interestingly, in mice, *Snail1* is under the transcriptional control of Wt1 (Martinez-Estrada et al., 2010). However, it has been described that epicardial-specific *Snail1* mutants do not display cardiac abnormalities (Casanova et al., 2013).

In chicken embryos, retroviral single cell labeling was used for epicardial lineage tracing. The results evidenced that EPDCs give rise to coronary vasculature (endothelial and smooth muscle cells) and intracardiac fibroblasts (Mikawa and Fischman, 1992, Mikawa and Gourdie, 1996). These data were confirmed using quail-chick chimeras. Besides, EPDCs have been shown to populate the atrioventricular cushions during development and give rise to the *annulus fibrosus* (Dettman et al., 1998, Manner, 1999, Wessels and Perez-Pomares, 2004).

In mice, Cre-loxP based lineage tracing using Wt1-Cre, WT1-CreERT2 and Tbx18-Cre have shown that smooth muscle, pericytes of coronary vessels, intracardiac fibroblast and mitral and tricuspid valves derive of Wt1 and Tbx18 positive cells. More controversial is the contribution of EPDCs to the myocardium due to the persistence of low levels of Tbx18 expression in the myocardium and technical problems of the Wt1-Cre lines (Zhou et al., 2008a, Cai et al., 2008, Wiese et al., 2009, Rudat and Kispert, 2012). Tcf21-Cre demonstrated that the majority of Tcf21-positive epicardial cells are committed to the cardiac fibroblast lineage (Acharya et al., 2012). *Scleraxis* (Scx) and *Semaphorin3D* (Sema3D) expressing PE cells give rise to coronary vascular endothelium, besides Scx- and Sema3D- positive cells contribute to the early *sinus venosus* and endocardium respectively (Katz et al., 2012). Recently, an adult cardiac-resident mesenchymal stem cells (MSC) population with a PE origin has also been described (Chong et al., 2011).

In zebrafish, *tcf21*-CreERT2 lines revealed that epicardial fates are limited to perivascular cells, but not contributing to myocardium nor vascular endothelial cell types (Kikuchi et al., 2011).

Taken all these data together, the epicardial layer is a molecularly heterogeneous structure giving rise several cell types. Also, species-specific differences regarding the differentiation potential of EPDCs might be present.

Due to the importance of the epicardial layer for heart development, in this thesis, we aimed to analyze the mechanism through which it is formed. We explored in real time PE formation in the zebrafish to understand whether bridge or PE cyst release are processes occurring *in vivo* in an organism. In addition, our goal was to assess how initiation of cardiac function and progression of morphogenesis are coupled and thus we studied the impact of the heartbeat on epicardium formation.

OBJECTIVES

The objectives of this thesis were:

1. To analyze epicardium development using zebrafish embryos as a model organism.
2. To assess the role of heartbeat triggered fluid flow forces during epicardium morphogenesis.
3. To explore the possible role of primary cilia as mechanosensors of heartbeat-induced fluid forces during proepicardium formation by analysis of their distribution within the pericardial cavity.

MATERIAL AND METHODS

Animal handling

Experiments were conducted with zebrafish embryos from the AB strain (ZIRC, Eugene, OR, USA), as well as the Tg(-*6.8kbwt1a:GFP*) (Bollig et al., 2009), Tg(*wt1b:GFP*) (Perner et al., 2007), Et*(-26.5Hsa.WT1-1gata2*:*EGFP*)^{cn1} transgenic line (Peralta et al., 2013), *tbx5a* null mutant *heartstrings* -the mutation causes premature termination at amino acid 316- (Garrity et al., 2002), *fgf8* mutant *acerebellar* (Reifers et al., 1998) -a 5' splice site is mutated, leading to skipping of exon 2 and causing a frame shift in the open reading frame resulting in a premature stop in translation- and the Tg(β-actin:*arl13b:GFP*) (Borovina et al., 2010) lines.

Animal procedures conformed to EU Directive 2010/63EU and Recommendation 2007/526/EC, enforced in Spanish law under Real Decreto 1201/2005.

Epi:GFP line generation

The enhancer trap line contains an insertion of the ZED vector (Bessa et al., 2009), carrying GFP under the control of a minimal *gata2* promoter plus a 500 bp fragment of the -26kb. Hsa Wt1 region, 4 kb upstream of the *wilms tumor 1 a* (*wt1a*) transcription initiation site. To characterize the insertion, we performed nested PCR using degenerate primers. To determine the 3' end of the insertion, the first amplification was performed with a pool of four degenerate primers (AD3 5-WGTGNAGNANCANAGA, AD5 5-WCAGNTGWTNGTNCTG, AD6 5-STTGNTASTNCTNTGC and AD11 5-NCASGAWAGNCSWCAA) and combining this with Tail3-1 5-CTCAAGTACAATTTTAATGGAGTAC. To determine the 5' end of the insertion, the degenerate primers were combined with the primer Tail5-1 5-GGGAAAATAGAATGAAGTGATCTCC. This first round was followed by a second PCR using the nested primers Tail3-2 5-ACTCAAGTAAGATTCTAGCCAGA and Tail5-2 5-GACTGTAAATAAAATTGTAAGGAG, again combined with the 4 degenerate primers. Finally, a third PCR step was performed with Tail3-3 5-CCTAAGTACTTGTACTTTCACTTG or Tail5-3 CCCCAAAAATAATACTTAAGTACAG (**Figure MM 1**).

In situ hybridization (ISH) in whole mount embryos

Antisense mRNA probes used were against *gfp* (provided by J.L. Gómez-Skarmeta, CABD, Sevilla, Spain), *wt1a* (provided by C. Englert, FLI, Jena, Germany), *tbx18* and *tbx5* (provided by G. Begemann, University Bayreuth, Germany).

Embryos were fixed overnight in 4% para-formaldehyde (PFA) (Merck) diluted in phosphate buffered saline (PBS) at 4ºC (rocking if embryos are older than 24 hpf). After two rinses in PBS (10 min), embryos were dehydrated through methanol:PBS series: 25%, 50%, 75% (10 min in each step, 20 min washed were performed for larvae older than 3 dpf) and 100% (2x30 min). The embryos can be stored at -20ºC at this step until use.

Embryos were rehydrated in methanol:PBS 75% (10 min), 50% (10 min), 25% (10 min) and washed in 0.1% PBSTw (2x5 min). Samples were digested with proteinase K (10 µg/ml) (for

24 hpf embryos: 10 min; 48 hpf: 15 min; 72 hpf: 20 min) and rinsed in 0.1% PBSTw (2x5 min). Then, they were fixed with 4% PFA (20 min), washed in 0.1% PBSTw (2x5 min) and transferred to prehybridization buffer (50% formamide, 4x SSC pH 4.5, 1% SDS, 100 µg/ml tRNA, 50 µg/ml heparin, 1% Blocking reagent (Roche) in MAB pH 7.4) (1 hour) at 65ºC. The Riboprobe was diluted in prehybridization buffer (at 1-2 ug/ml) and embryos were incubated overnight at 65ºC. Subsequent to hybridization, samples were washed at 65ºC in 50% formamide /2x SSCT (2x SSC, 0.1% Tween 20) (2x30 min), 2x SSCT (15 min) and 0.2x SSCT (2x30min). Then, the embryos were rinsed in MABT (2X5 min) at room temperature (RT), blocked with 2% blocking reagent

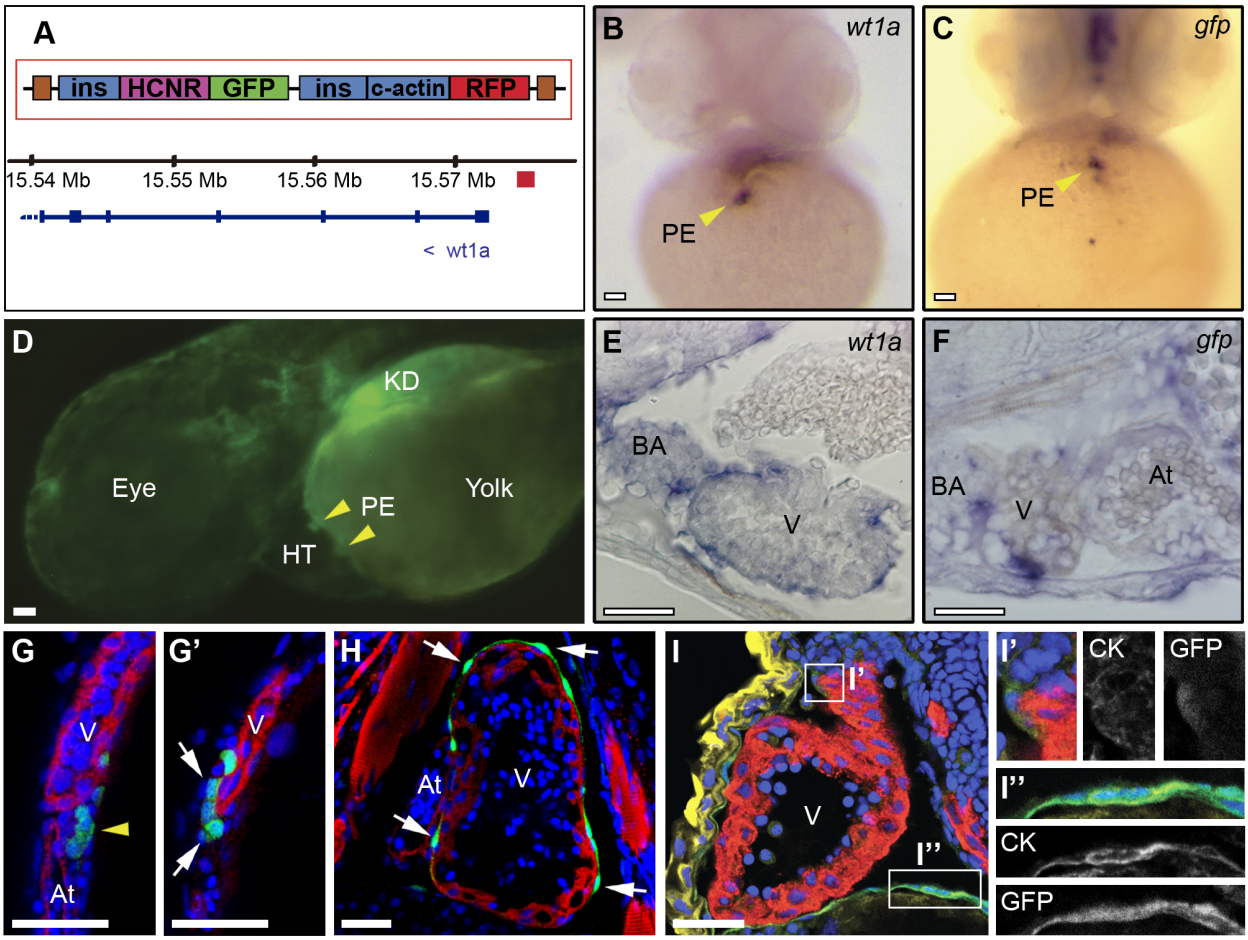

Figure MM 1. Generation of the Et(-26.5Hsa.WT1-gata2:EGFP)cn1 enhancer trap line. (A) A 500 bp region upstream of human Wilm's tumour gene (*WT1*) was cloned into the ZED vector (Bessa et al., 2009), containing a cassette driving RFP expression under the control of cardiac actin and GFP from a minimal Gata2 promoter. One founder line was obtained in which the plasmid was inserted 4 kb upstream of the Wilms tumor 1 a (*wt1a*) transcription initiation site (Red box). (B-C) *wt1a* and *gfp* whole-mount mRNA *in situ* hybridization (ISH) in larvae at 2 dpf. Frontal views reveal staining of the proepicardium (PE). (D) Fluorescent image of a laterally positioned *Et(-26.5Hsa.WT1-gata2:EGFP)cn1* larva revealing GFP expression in two PE clusters at the atrioventricular canal and venous pole and the kidney anlage (KD). (E-F) ISH on sections showing *gfp*- and *wt1a*-positive cells on the myocardial surface. (G-H) Sections of whole mount immunostained hearts shown in Figure R 7B and 7C showing GFP-positive PE and epicardial cells on the myocardial surface at 3 dpf (G-G') and 6 dpf (H). (I-I'') Immunohistochemistry on heart sections at 65 hpf. Epicardial and pericardial cells expressing GFP (green) co-express cytokeratin (CK, yellow). Anti-myosin heavy chain (MHC) is shown in red, cell nuclei are marked with DAPI (blue). In all panels, yellow arrowheads mark the PE and white arrows epicardial cells. Scale bars (B-D) 10 µm, (E-I) 40 µm. At, atrium; BA, *bulbus arteriosus*; c-actin; cardiac actin; Epi, epicardium; GFP, green fluorescent protein; HCNR, highly conserved non-coding region; HT, heart tube; ins, insulator; KD, kidney; Myo, myocardium; RFP, red fluorescent protein; PE, proepicardium; V, ventricle.

(Roche) in MABT (1 hour) and incubated with sheep anti-digoxigenin Fab fragments antibody conjugated to alkaline phosphatase (Roche), diluted 1:2000 in blocking solution, overnight at 4ºC. The embryos were washed in MABT (2x30 min and 2x1 hour) and washed in NTMT (100 mM Tris HCl pH 9.5, 50 mM $MgCl_2$, 100mM NaCl, 0.1% Tween 20) (3x10 min). The reaction was developed adding BM Purple (Roche) (in the dark), monitored and then stopped when a good staining intensity appeared by rising in PBS (3x5 min). Samples were fixed with 4% PFA, washed in 0.1% PBSTw (3x5 min) and stored in 80% glycerol in 0.1% PBSTw.

ISH on paraffin sections

Paraffin embedding: Embryos were fixed overnight in 4% PFA (Merck) diluted in PBS at 4ºC (while rocking for embryos older than 24 hpf). After two rinses in PBS (10 min), embryos were dehydrated through ethanol:water series: 30%, 50%, 70%, 90% and 100% twice, (20 min in each step), at RT. Then they were washed twice in xylol (Merck) (30 min) and two times in paraffin wax at 65ºC (30 min). Embryos were orientated in the warm paraffin and the blocks left solidify overnight.

7 µm sections were collected on Superfrost plus slides, dried overnight at 37ºC and stored at 4ºC until use. After dewaxing in xylol (2x10 min) and rehydration in ethanol:water 100% (2x10 min), 90% (5 min), 70% (5 min), 50% (5 min) and 30% (5 min), slides were washed in PBS (5 min). All washes were performed in glass troughs. Sections were postfixed with 4% PFA for 10 min by pouring the fixative over the slides placed horizontally in a humid chamber (grey plastic box with PBS on the bottom). Later, sections were washed twice in PBS (2x5 min) and digested with proteinase K (10 µg/ml) (10 min). Sections were washed again in PBS (2x5 min). Then, they were postfixed with 4% PFA (5 min) reused from the previous step. Both, postfixation and digestion steps were carried out in a moist chamber with PBS. After a wash in PBS, samples were permeabilized with 0.07N HCl (15 min), washed again in PBS (2x5 min) and blocked against unspecific binding with 0.25% acetic acid in 0.1M trietanolamine pH 8 (10 min). Permeabilization and blocking steps were carried out while gently rocking the slides in a glass trough. Later, the sections were washed in PBS (5 min), in RNase-free water (5 min) and stayed in prehybridization buffer (50% formamide, 5x SSC pH 5.5, 1x Denhardt's, 0.1% Tween 20, 0.1% Chaps, 50 µg/ml tRNA) (2 hours) at 65ºC in a moist chamber with posthybridization buffer I (50% formamide, 5x SSC pH 5.5, 1% SDS). Probe was diluted in prehybridization buffer (at 1-2 ug/ml) and applied to the slides (150 µl total volume per slide), which were covered with a glass cover slide and incubated overnight at 65ºC. Subsequent to hybridization, samples were washed in posthybridization buffer I (2x30 min) and then in posthybridization buffer II (2x30 min) (50% formamide, 2x SSC pH 5.5, 0.2% SDS), both steps at 65ºC. The samples were rinsed in MABT (100 mM Maleic acid (Sigma), 150 mM NaCl, 0.1% Tween 20) (3x5 min) at RT, samples were blocked with blocking solution (10% goat serum, 1% Blocking reagent in MABT) (2 hours) in a moist chamber with MABT and incubated with sheep anti-digoxigenin Fab fragments antibody conjugated to alkaline phosphatase (Roche, diluted 1:2000 in blocking solution) overnight at 4ºC, using the same moist chamber. The slides were then washed in MABT (2x10 min and 3x1 hour) and washed in NTMT (100 mM Tris HCl pH 9.5, 50 mM $MgCl_2$, 100mM NaCl, 0.1% Tween 20) (3x10 min). The reaction was developed by adding BM Purple (in the dark) in a moist chamber with NTMT, monitored and

then stopped when a good staining intensity appeared by rising in PBS (2x5 min). Slides were fixed with 4% PFA, washed in PBS (3x5 min) and mounted with Aquatex (Merck).

Double ISH / Immunohistochemistry on paraffin sections

After ISH, sections were fixed with 4% PFA, washed in PBS (3x5 min) and mounted in 80% glycerol in PBS for imaging. After imaging, sections were washed in 0.1% PBTw (0.1% Tween20 in PBS) (3x5 min) and permeabilized with 0.5% PBSTx (0.5% Triton-X100 in PBS) (15 min). Then, slides were washed in 0.1% PBSTw (3x5 min). Anti-myosin heavy chain (MF20, DSHB) was added at 1:20 dilution in 0.1% PBSTw and sections incubated overnight. Antibody was detected with the Vectastain Elite ABC staining kit (Vector) and sections mounted in Aquatex.

Immunohistochemistry on whole mount embryos

Larvae were fixed overnight in 4% PFA in PBS, washed in 0.1% PBSTw (0.1% Tween20 in PBS) and permeabilized with 0.5% PBSTx (0.5% Triton X-100 in PBS) (20 min). Several washing steps (3x10 min) were followed by 2 h blocking with blocking solution (3% albumin from bovine serum, 5% goat serum, 20 mM $MgCl_2$, 0.3% Tween 20 in PBS) and overnight incubation (while rocking) at 4°C with anti-myosin heavy chain (MF20, DSHB) at a 1:20 dilution in blocking solution. After several washing steps in 0.1% PBSTw (3x30 min), secondary antibody anti-mouse-Cy3 (Jackson Laboratories) was diluted 1:500 in 0.1% PBSTw and incubated overnight at 4ºC (while rocking). After several washes in 0.1% PBSTw, nuclei were counterstained with DAPI (Invitrogen) at 1:1000 in 0.1% PBSTw (15 min) and washes 3x10 min in 0.1% PBSTw. Larvae were directly acquired using confocal microscope or mounted in Vectashield (Vector) if the acquisition is delayed more than 3 days.

Embryos were imaged with a Zeiss 780 confocal microscope fitted with a W Plan-Apochromat 20x N.A.1,0 DIC M27 75mm objective. Z-stacks were taken every 3 µm. 3D images were reconstructed with IMARIS software (Bitplane Scientific Software). The pericardial ventral wall was digitally removed to provide a clearer view of the heart.

Proliferation and apoptosis assays

For proliferation analysis, we used anti-pH3 antibody (Millipore) at 1:100 dilution in combination with the MF20 antibody at a 1:20 dilution. Secondary antibodies were anti-rabbit-Alexa 647 and anti-mouse-Cy3 (Jackson Laboratories) diluted 1:500. We followed the protocol previously described above. Embryos were imaged with a Zeiss 780 confocal microscope fitted with a 20X, N.A. 1.0 objective with a dipping lens. Z-stacks were taken every 4 µm. TUNEL staining was performed with the *in situ* cell death detection kit (Roche). After fixation overnight in 4% PFA in PBS, embryos were washed in 0.1% PBSTw (0.1% Tween20 in PBS) (2x10 min) and permeabilized with 0.5% PBSTx (0.5% Triton X-100 in PBS) (20 min). Endogenous biotin was blocked using biotin blocking kit (Vector). Several washing steps in 0.1% PBSTw (5 x 5 min) were followed by 1 h incubation

with freshly prepared equilibration buffer (1mM TdT 1x, 1mM $CoCl_2$ in PBS) at RT. Later the buffer was removed and the TdT reaction mix was added for 2 h at 37 ºC. Then, embryos were washed in 0.1% PBSTw (3x5 min) and incubated with blocking solution (3% albumin from bovine serum, 5% goat serum, 20 mM $MgCl_2$, 0.3% Tween 20 in PBS) for 2h at RT. We incubated with anti-myosin heavy chain (MF20, DSHB) at a 1:20 dilution in blocking solution overnight at 4°C (while rocking). After several washing steps in 0.1% PBSTw (3x30 min), secondary antibodies were (anti-mouse-Cy3 (Jackson) and streptavidin-Cy5 diluted 1:500 in 0.1% PBSTw) and were incubated overnight at 4ºC (while rocking). On the next day, embryos were washed (5x30 min) in 0.1% PBSTw. Nuclei were counterstained with DAPI (Invitrogen) at 1:1000 in 0.1% PBSTw (15 min). After several washes (at least 3x10 min) larvae were acquired using confocal microscope or mounted in Vectashield (Vector) if the acquisition is delayed more than 3 days. Images were obtained with a Zeiss 780 confocal microscope fitted with a W Plan-Apochromat 20x N.A.1,0 DIC M27 75mm objective. Z-stacks were taken every 4 µm.

For quantification, the pericardial cavity was divided in 3 areas (**Figure MM 2**) and cells were counted manually on z-sections. Significance of the observed results was determined by one-way ANOVA followed by Tukey's multiple comparison. Statistical assays were performed by GraphPad Prism 5.

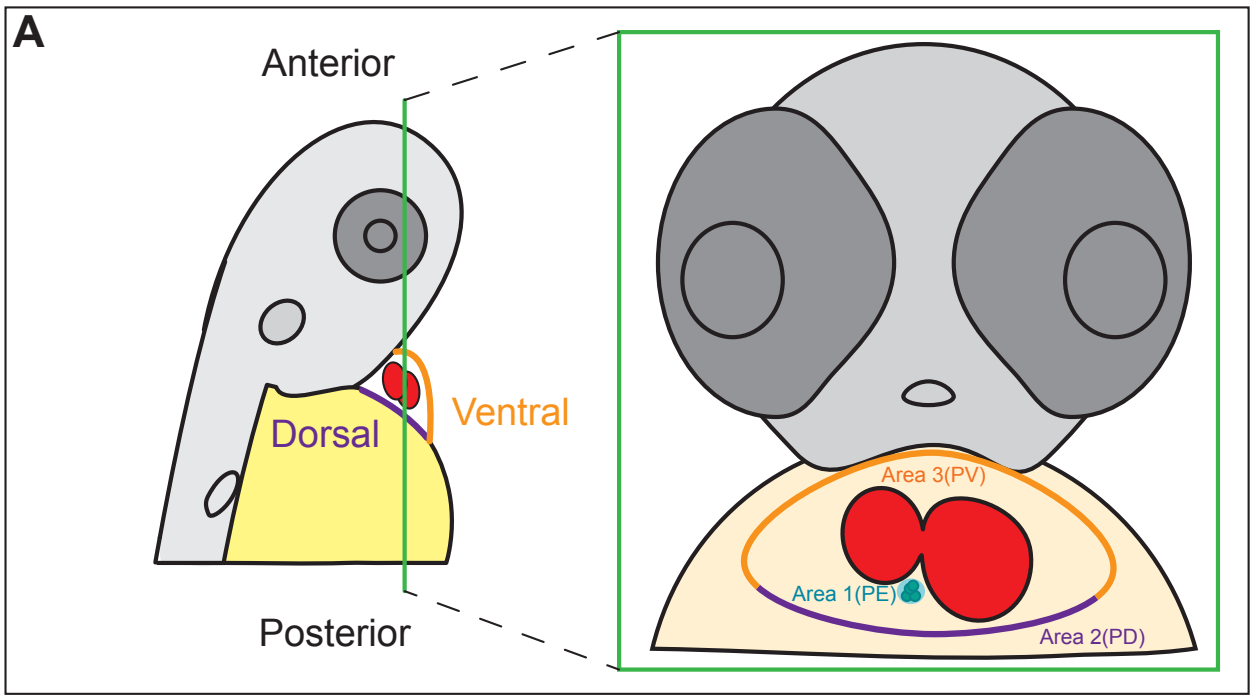

Figure MM 2. Pericardial cavity segmentation for proliferation and apoptosis quantification. (A) Schematic representation of a z-stack section on confocal microscope (inside of green box). For easier quantification, the pericardial cavity was divided in 3 areas: Area 1 (PE), proepicardial cluster; Area 2 (PD), pericardial dorsal wall and Area 3 (PV), pericardial ventral wall.

Immunohistochemistry on cryostate sections

Larvae were fixed at RT for 2 hours with PFA 4%, then they were washed twice in PBS at 4ºC and transferred into a PBS:sucrose 15% solution at 4ºC till the samples went to the botton of the tube. Next, they were incubated in PBS:sucrose 15%:gelatin 7.5% for 30-60 minutes at 37ºC and embedded at RT. The blocks were left to cool at 4ºC and then frozen in isopentane at -72ºC for 1 minute and stored at -80ºC until cryostat sectioning.

8 µm cryosection slides were left at RT for 20 minutes before degelatinizing them in PBS at 37ºC (15 min). They were washed in TBSTw (0.1% Tween 20 in TBS) (2x5 min), permeabilized with TBSTx (0.5% Triton X-100 in TBS) (10 min) at RT and incubated in blocking solution (3% albumin from bovine serum, 5% goat serum, 20 mM $MgCl_2$, 0.3% Tween 20 in PBS). Slides were incubated overnight at 4ºC with the primary antibodies: anti-cytokeratin (Dako) (1:100 in blocking solution) and anti-myosin heavy chain (MF20 clone, Developmental Studies Hybridoma Bank) (1:20 in blocking solution). The samples were washed in TBSTw (2x5 min) and incubated with biotin goat anti-rabbit (Jackson) (1:500 in TBSTw) (1 hour) at RT to amplify the cytokeratin signal. After washing with TBSTw (2x5 min), the cryosections were incubated with the other secondary antibodies: streptavidin-Cy5 (Jackson) (1:500 in TBSTw) and Cy3 goat anti-mouse (Jackson) (1:500 in TBSTw) (1 hour) at RT. Samples were washed in TBSTw (2x5 min), nuclei were counterstained with DAPI (Invitrogen) (1:1000 in TBSTw) (15 min), washed again in TBSTw (2x5 min) and mounted with Vectashield (Vector).

In vivo imaging

Larvae were transferred to fish water containing 0.2 mg/ml tricaine and 0.0033% PTU, orientated with forceps and immobilized in 0.7% agarose (NuSieve GT Agarose, Lonza) in a 35 mm petridish with a glass cover (MatTek Corporation) (**Figure MM 3**). Zebrafish hearts between 2 dpf and 3 dpf (eventually until 4 dpf also) were scanned bidirectionally at 30 frames per second (fps) with an SP5 confocal microscope (Leica) in resonant mode using a HCX PL APO lambda blue 20x N.A. 0,7 multi-immersion objective. 15 second long videos were acquired every 10 µm, with a line average of 6 and a pinhole of 1.9 AU. Around 30 Z-stack videos were acquired per heart. GFP and DIC channels were acquired simultaneously. The recorded images were at 8 bits and had a resolution of 512 x 256 pixels. For quantification of PE cells, GFP-positive and GFP-negative cells were counted on merged brightfield and fluorescence images. Manual cell tracking was performed using ImageJ. A mean of 4 to 5 cells or cell clusters was used for quantifications. Tracks were then imported into Imaris and fitted to the original images for the track displays.

Brightfield imaging experiments were performed on a Leica DMIRBE microscope using a Photron SA3 high speed CMOS camera (Photron, San Diego, CA). Time-lapse sequences were acquired at a 250-500Hz frame-rate, in transmission configuration using white light illumination and a Leica 20x, N.A 0.9 water immersion objective.

For the pericardial volumetric cavity analysis, hearts of embryos incubated with bodipy TR

(Invitrogen) were imaged at 60 frames per second (fps). 4D imaging was performed using consecutive xy(c)tz time-lapse acquisitions with a Zeiss 780 live fast confocal microscope fitted with a 40x, N.A. 1.1 objective. Z-stacks were taken every 2 µm. Time series of two-dimensional sections were temporally analyzed using customized Matlab software (Liebling et al., 2005). Realigned 4D data sets were displayed and analyzed using Imaris (Bitplane AG) or Image J. Statistical differences were analyzed by Kruskal-Wallis followed by Dunn's test.

For cilia analysis, live *Arl13b:GFP* zebrafish pericardial cavity at 48 and 55 hpf were scanned bidirectionally at 30 frames per second (fps) with an SP5 confocal microscope (Leica) in resonant mode using a Leica 20x, N.A 0.9 water immersion objective.

We performed 1 second videos on z-sections at an inverval of 1 µm. The datasets were temporally aligned using the previously published Matlab software (Liebling et al., 2005, Liebling et al., 2006) and the aligned files were viewed and analyzed in Fiji (Schindelin et al., 2012).

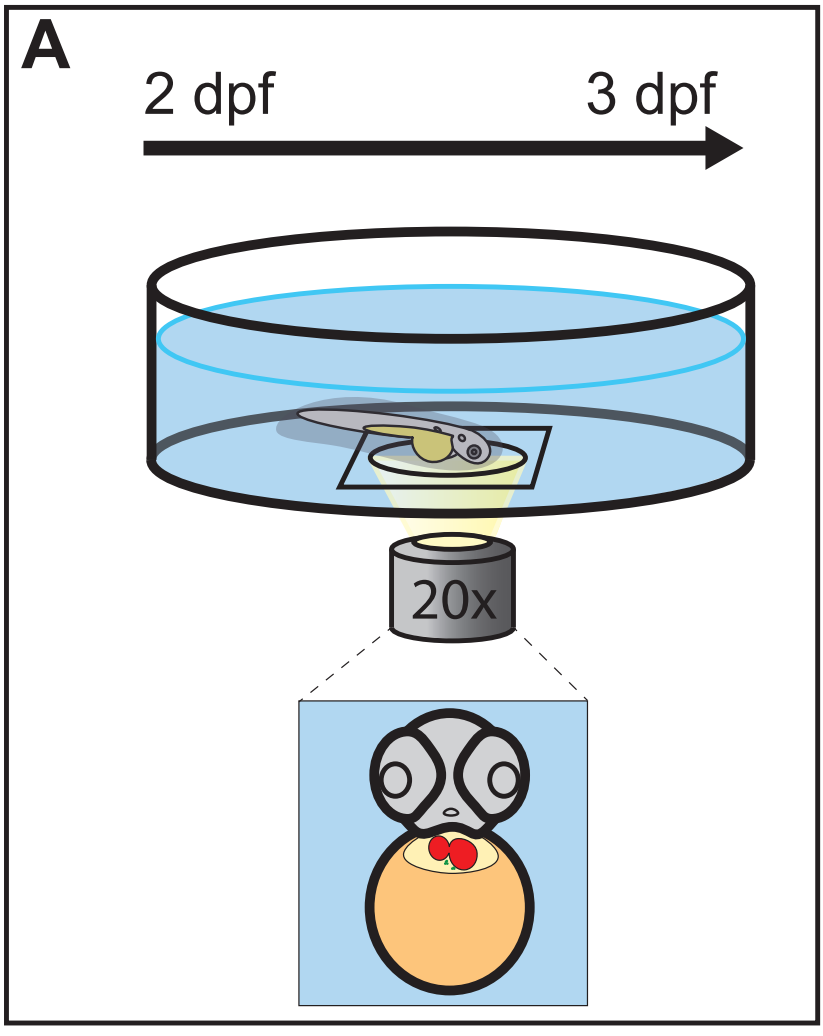

Figure MM 3. Zebrafish embryos agarose embedding and orientation for *in vivo* imaging. (A) Inside of a glass bottom microwell dish, embryos were embedded in an 0.7% agarose drop (grey) and orientated ventrally to the glass. The agarose was covered by fish water with tricaine and PTU diluted (blue). HCX PL APO lambda blue 20x N.A. 0,7 multi-imm objective of a SP5 Leica confocal was used for the acquisitions, in resonant mode, through time at 28ºC.

Microinjection and drug administration

1 nl of the *tnnt2* MO (Genetools Inc) (CATGTTTGCTCTGATCTGACACGCA) was injected at a concentration of 0.4 mM, 1-5 nl of the *myh6* MO (ACTCTGCCATTAAAGCATCACCCAT) at 0.1 mM and 2-3 nl of the *cmlc1* MO (TGCCATGATGCTGATGGGAAAAGGC) at 0.4 mM were injected into 1 to 8 cell stage embryos using a FemtoJet microinjector (Eppendorf).

Red fluorescent 1 µm carboxylated microspheres (Invitrogen) were diluted 1:10 in PBS, sonicated for 10 minutes (Hove and Craig, 2012), and injected into the pericardial cavity using a Leica AS TP microinjection set up.

2,3-Butanedione monoxime (Sigma) was diluted to 20 mM in fish tank water with 0.0033% PTU, and caffeine (Sigma) at 100 µg/ml, in which larvae were placed for the required times.

Optical tweezing

Optical tweezer experiments were performed using a home-built microscope as described (Drobczynski et al., 2009; Berg-Sorensen and Flyvbjerg, 2004). The optical setup uses a Spectra Physics YAG laser (1064nm) focused through a high numerical aperture oil immersion objective (Zeiss achromat X100 1.25 N.A.). The light scattered by the trapped cell is collected through a second objective (Olympus X40 0.6 N.A). Subsequent signal treatment was performed using LabView 7.2 (National Instruments) in Windows XP. The laser power used to trap the PE cells varied from 0.9 to 2W (laser head output) depending on the location of the cell. The beam energy was dissipated by the flow, trapping cells without inducing any other visible effect on the fish.

Using a calibration grid, we directly converted the displacements to µm. The movie was first opened with ImageJ to enhance the contrast (0.4% for the whole stack). We then built an orthogonal view of the trapped cell or heart displacements. These views were saved as text files for post-processing with IgorPro Wavemetrics.

Forces were calculated from the displacements of the trapped cell. The displacements, dX, were directly proportional to the applied force through $F = k_{trap}.dX$, where k_{trap} is the optical trap stiffness obtained from the Power Spectrum of the time displacements. Trap stiffness is described elsewhere (Berg-Sorensen and Flyvbjerg, 2004) and is proportional to the cut-off frequency:

$$K_{\text{trap}} = 2.\pi\xi \ .,$$

where ζ is the friction, calculated as a first approximation for a spherical particle

$$\zeta = 6.\pi.\eta.R \ ,$$

η is the fluid viscosity (here approximated to $\eta=10^{-3}$ Pa.s), and R is the cell radius (R≈2.5µm).

The maximum velocity of the fluid is attributed to the maximum force amplitude found by

$$v_{\max} = \frac{F_{\max}}{6.\pi\eta R} .$$

Each measurement was repeated twice. Between four and six cells were measured for each position. Statistical differences were analyzed by One-way ANOVA and Kruskal-Wallis (forces) or Tukey (speed) tests.

ImageJ and Wavemetrics IgorPro were used for kymographs and to analyze PE cell motions within the trap. The traces were saved as text files and were quantified with IgorPro.

Scanning and transmission EM

For TEM, wildtype zebrafish at 48, 72, and 96 hpf were fixed for 3–5 hr in 2.5% glutaraldehyde/0.1M sodium caccodylate at 4°C, washed for an equal time in 0.1M sodium caccodylate/5%sucrose, and post-fixed for 2 h in the dark with 1% osmiumtetroxide/0.1M sodium caccodylate. After washing in 0.1M sodium caccodylate/5% sucrose, the fish were dehydrated rapidly in increasing concentrations of acetone to 100%. Fish were then washed twice (5 min each) with acetone. Fish were removed from acetone to a 2:1 mixture of acetone: Durcopan ACM resin (Fluka) overnight at RT, then to a 1:1 mixture of the same components for 10 h, and finally pure Durcopan overnight. Blocks were polymerized at 70°C overnight in fresh Durcopan. Sections were obtained with a Reichert OM-U3 ultramicrotome. Semi-thin sections stained with an alkaline solution of 1% toluidine blue were used for light microscopy. Ultra-thin sections, obtained from selected areas on the semi-thin sections, were double stained with uranyl acetate and lead citrate, examined and photographed in a JEOL 10.10 electron microscope.

For SEM, zebrafish embryos were fixed in 2% glutaraldehyde in 0.1 M PBS at 4°C overnight, washed with 5% sucrose in 0.1 M PBS for 15 min, and fixed in 1% osmium tetroxide in 0.1 M PBS for 60 min. Fixed embryos were washed with 5% sucrose in 0.1 M PBS for 15 min and dehydrated in a graded series of acetone. The embryos were critical-point dried using liquid CO2, mounted on a sample holder, covered with gold, and viewed using a JSM-6400 scanning electron microscope (JEOL).

RESULTS

1. Characterization of the PE in zebrafish embryos.

The presence of the proepicardium (PE) has been previously described in zebrafish embryos (Serluca, 2008), but the details of the process leading to epicardium formation remain unknown.

1.1. Epicardial development visualized by electron microscopy.

In order to analyze epicardium formation in zebrafish embryos, we performed scanning and transmission electron microscopy imaging on 2, 3 and 4 days postfertilization (dpf) embryos.

Scanning electron microscopy images showed a cluster of about 6 PE cells located on the dorsal pericardial wall, close to the atrioventricular canal (AVC), between late 2 dpf and early 3 dpf embryos (observed in n=2 out of 4 embryos) (**Figure R 1A-B'**). At 4 dpf, the epicardial layer covers the myocardium of the ventricle (V) (n= 5 larvae) (**Figure R 1C,C'**).

Transmission electron microscopy images showed some rounded PE cells surrounded by flat pericardial cells. Rounded cells were covered by extracellular matrix (ECM) on their apical surface facing the cavity. This observation suggests that mesothelial cells break their adhesion unions and change their shape from flat to round to form the PE. Additionally, these cells seem to increase the ECM secretion (**Figure R 1D-D''**). At 3 dpf, there are epicardial cells attached to the myocardial cells of the V (**Figure R 1E**).

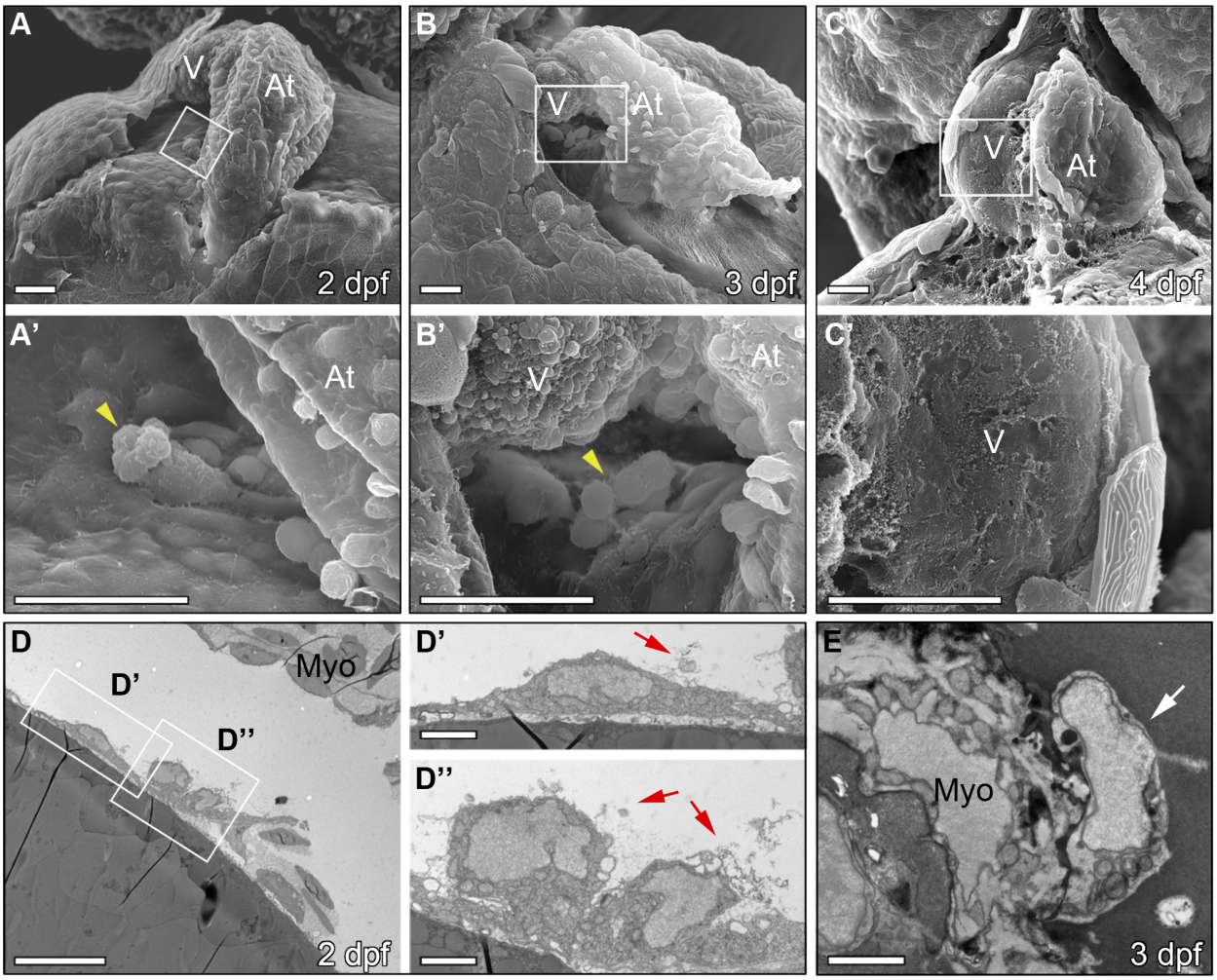

Figure R 1. Epicardial development in the zebrafish visualized by electron microscopy. (A-C') Scanning electron microscopy images showing ventral views of hearts at 2, 3 and 4 dpf. Anterior is to the top. A'-C' show zoomed views of boxed areas in A-C. A' and B' show clusters of about 6 proepicardial cells (yellow arrowheads) on the dorsal pericardial wall positioned at the level of the AVC, which are not in direct contact with the myocardium. At 4 dpf, the myocardial wall is covered by a layer of flattened epicardial cells (C,C'). (D-E) Transmission electron microscopy images of sagittal sections through hearts of larvae at 2 (D-D'') and 3 dpf (E). D' and D'' show zoomed views of boxed areas in D. Pericardial mesothelial cells reveal a flattened morphology with little extracellular matrix (D'); in contrast, the cells of the nascent PE cluster are rounded and show more extracellular matrix deposition on their apical surface (D'', red arrows). White arrow in E marks an epicardial cell attached to the myocardium. At, atrium; dpf, days postfertilization; Myo, myocardium; V, ventricle. Scale bars (A-C') 20 μm and (D'-E) 2 μm.

1.2. Epicardial development visualized by immunohistochemistry and *in vivo* imaging.

Given the extracardiac origin of epicardial precursors, an important question arises: how do PE cells find their way to the myocardial surface? To answer that question, first we analyzed reporter lines marking the PE and epicardium by immunohistochemistry, which provided us with a global vision of the process and allowed us to determine the best reporter line to work with. Next, we elucidated the way PE cells adhered to the myocardium to form the epicardial layer through *in vivo* imaging.

1.2.1. Characterization of *wt1* transgenic reporter lines during epicardium formation.

We tested several reporter lines in order to choose the best tool to study epicardium formation including the following lines: *Tg(wt1b:GFP) (Perner et al., 2007)*, *Tg(-6.8kbwt1a:GFP) (Bollig et al., 2009)* and *Et(-26.5Hsa.WT1-1gata2:EGFP)*^{cn1} (hereafter called *Epi:GFP*) (Peralta et al., 2013).

We first performed whole mount immunohistochemistry on larvae at different stages of development (**Figure R 2**). In 60 hpf *Tg(wt1b:GFP)* larvae, GFP is expressed in few PE cells (**Figure R 2A**). From 72 hpf onwards, it can be detected in few epicardial cells (**Figure R 2B,C**). In addition, GFP is broadly expressed in the *sinus venosus* (SV) at all stages analyzed (**Figure R 2A-C**). In the *Tg(-6.8kbwt1a:GFP*) line, at 60 hpf, few PE cells expressed GFP (**Figure R 2D**). From 72 hpf onwards, GFP expression was observed in some epicardial cells (**Figure R 2E,F**). In the *Epi:GFP* line, at 60 hpf, GFP expression highlights PE cells (**Figure R 2G**) and, at 72 hpf, epicardial cells attached to the myocardium (**Figure R 2H**) (**Table R 1**). While the majority of epicardial cells were GFP-positive (over 70% of cells counted in 8 larvae), also some GFP-negative cells were found covering the outer surface of the myocardium (Peralta et al., 2013). *Epi:GFP* also labels the rest of the pericardial mesothelium (**Movie S 1**), as in the *Tg(-6.8kbwt1a:GFP)* line (data not shown).

In vivo imaging of the *Epi:GFP* line revealed that GFP expression was dynamic: we could observe examples of GFP-negative PE cells, which activate GFP expression after adhesion to the myocardium (**Movie S 2**). Furthermore, analysis of GFP expression revealed that from 48 hpf

Lines	Proepicardial expression	Epicardial expression	Pericardial expression	Sinus Venosus expression
Tg(*wt1b:GFP*)	++	++	+++	+++
Tg(*-6.8kbwt1a:GFP*)	+	++	++	+
Epi:GFP	+++	+++	+++	++

Table R 1. Comparison of GFP expression in the epicardial reporter lines. Ratio of cells expressing GFP in each region for the reporter lines (+, few cells; ++, several cells; +++, most of the cells).

onwards, in *Tg(wt1b:GFP)* embryos, GFP expression is also detected in few atrial cardiomyocytes at the venous pole of the heart tube (**Figure R 2A,B**). Similarly, few atrial cardiomyocytes at the base of the heart tube, express GFP in the *Epi:GFP* line (**Figure R 2G**).

In sum, our studies reveal that from the tested lines, the *Epi:GFP* is the most suited line to study PE and epicardium morphogenesis, as it marks most of the cells and persist from the very onset of PE formation until completion of epicardial layer formation.

1.2.2. *In vivo* characterization of PE and epicardium formation using the *Epi:GFP* reporter line.

To analyze how PE cells reach the myocardial surface, we performed *in vivo* time lapse on *Epi:GFP* larvae between 40 hpf and 80 hpf.

At 42 hpf, GFP was expressed homogeneously by the mesothelial cells lining the pericardial cavity (**Movie S 1**). From 48 hpf onwards, GFP expression remains high in the emerging PE at the dorsal pericardial wall and declines in pericardial cells. Between 48 and 55 hpf, a group of PE cells from the dorsal pericardial wall first rounded up and protruded into the pericardial cavity to form a cluster (**Movie S 3**). We observed the presence of two PE clusters over the dorsal pericardial wall. The bigger one located at the level of the AVC; was named avcPE. The second one emerged on the right side, adjacent to the venous pole; which we named vpPE (**Figure R 3A** and **Movie S 4**). Additionally, after 60 hpf, individual pericardial cells rounded up and attached to the myocardial surface from a region of the pericardial mesothelium close to the arterial pole. We called these cells arterial pole epicardial precursors (apEPs) (**Movie S 5**). Cells from the avcPE and vpPE clusters were released, individually or in small groups, into the pericardial cavity (**Movie S 6**). Once released, cells were advected around the ventricle for varying periods (from a few seconds to 1 h), during which, from a ventral view, they moved in an anticlockwise direction. Eventually, the advected PE cells adhered to the myocardial surface (**Movie S 7**). Unlike cells from the avcPE and vpPE clusters, apEP cells attached to the myocardium without being first released into the pericardial cavity (**Figure R 3A'** and **Movie S 5**). apEP cells, prior to attachment, revealed a slight motion, which was coordinated with that of the myocardium (**Figure R 3B-B''**). After transfer, apPE cell motion was comparable to that of a previously attached PE cell. Similar to apEP cells, vpPE cells were advected with a periodical motion coupled to the heartbeat (**Figure R 3C-C''**), with increased amplitude after detachment from the pericardial wall. Once released, cells moved in an anticlockwise direction around the ventricle. Kymograph analyses confirmed the coupling of this motion to contraction of the myocardium (**Figure R 3D-D'''**).

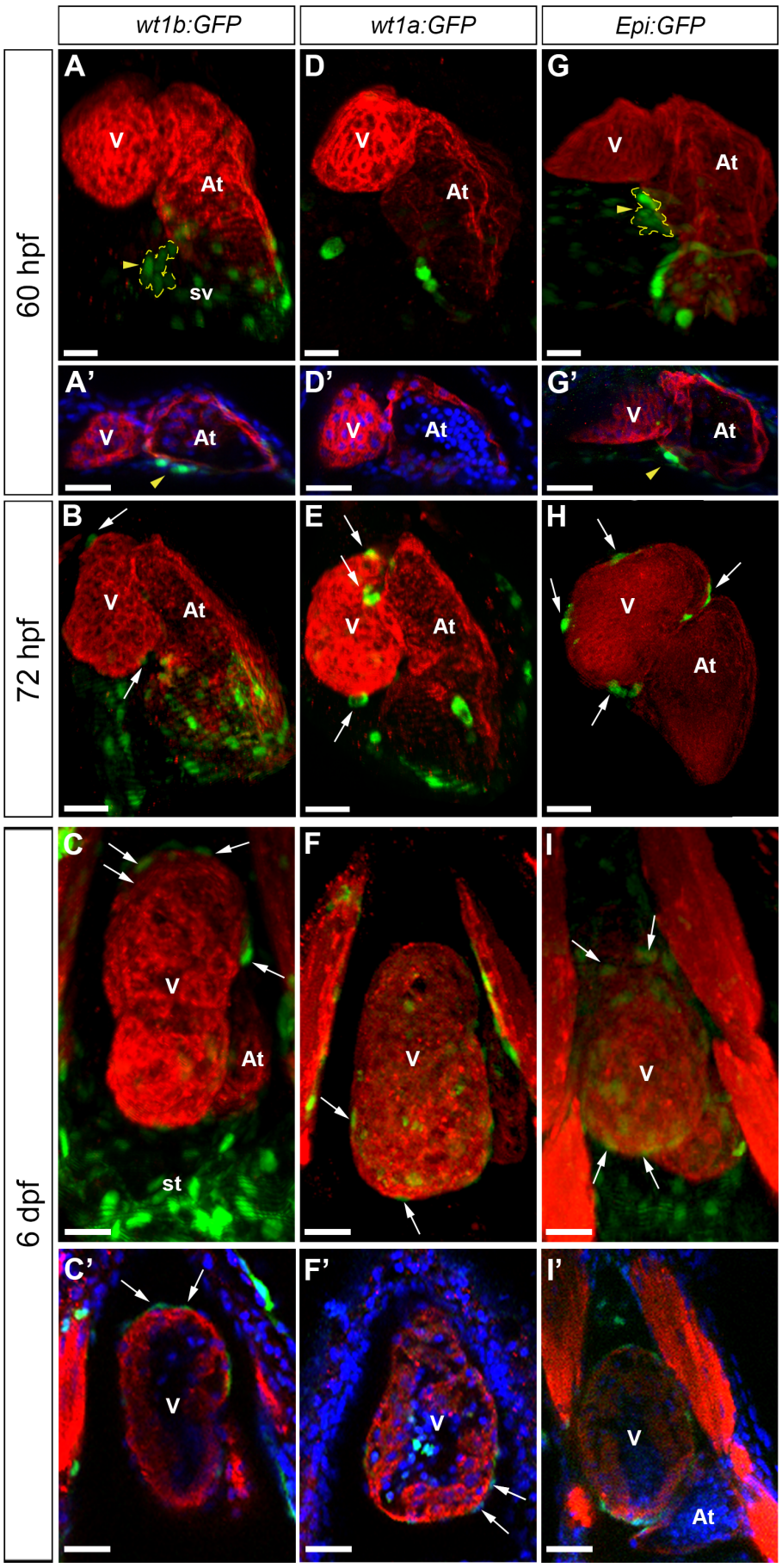

Figure R 2. Wilm's tumor 1 reporter lines to study epicardium development in the zebrafish. Whole mount immunofluorescence of hearts from the lines *Tg(wt1b:GFP)* (Perner et al., 2007), *Tg(-6.8kbwt1a:GFP)* (Bolling et al., 2009) and *Et(-26.5Hsa.WT1-1gata2:EGFP)cn1* (Epi:GFP) (Peralta et al., 2013) at developmental stages indicated on the right side of the panels using myosin heavy chain antibody (red). GFP expression is shown in green. In some panels, nuclear DAPI staining is shown in blue. (A-I) 3D projections. Ventral views are shown; anterior is to the top. (A'-I') Confocal sections of the whole-mount hearts shown in A-I. Arrowheads and yellow dotted lines mark the PE; arrows mark epicardial cells. (A-C) *Tg(wt1b:GFP)* labels few PE cells and epicardial cells and strongly marks the sinus venosus and septum transversum. (D-F) GFP expression in *Tg(-6.8kbwt1a:GFP)* labels epicardial cells, but the PE is not clearly visible. (G-I) Epi:GFP labels the sinus venosus and septum transversum as well as the PE clusters and epicardial cells. At, atrium; st, septum transversum; sv, sinus venosus; V, ventricle. Scale bars, 30 μm.

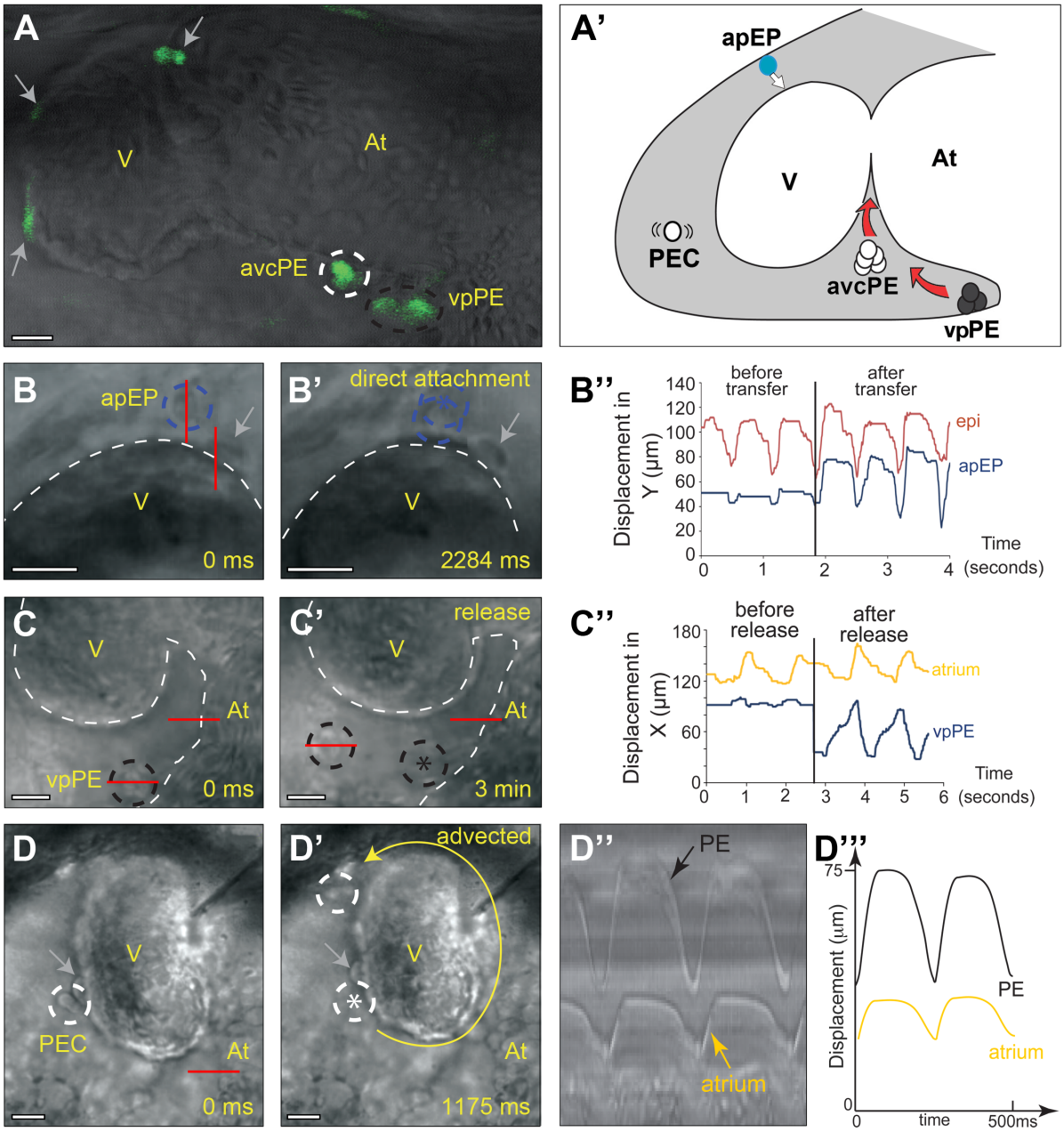

Figure R 3. Proepicardial cells are released from three distinct sources. (A) Confocal imaging of a 48 hpf Epi:GFP heart showing GFP-positive PE clusters at the atrioventricular canal (avcPE) and venous pole (vpPE) (Movie S 4). (A') Location of the PE cells shown in panels A-D: advected PE cells (PEC), avcPE, vpPE cells and epicardial progenitors arising from the arterial pole pericardial mesothelium (apEP). The white arrow indicates direct transfer from the pericardial mesothelium to the myocardium; red arrows indicate release into the pericardial cavity (gray shading). (B) apEP cells transfer directly to the myocardium. At the onset of acquisition (0 ms), the apEP cell (blue dotted circle) is attached to the pericardial wall. (B') Later (2284ms), the apEP cell has transferred to the myocardial surface (Movie S 5). (B'') Tracking of an apEP cell. Note the limited movement in response to contact with the ventricle before transfer (blue trace). Red lines mark the regions in which displacement was measured for kymographs. Motion after transfer is comparable to that of an epicardial cell attached at an earlier time point (red trace). (C,C') A vpPE cluster (black dotted circle) moving in response to heart contraction, which leads to its release (Movie S 6). (C'') Tracking of the vpPE cluster reveals a limited motion before release and increased oscillatory motion afterwards, coupled to atrial wall contraction. (D and D') A pair of advected PE cells (PEC white dotted circles) in the cavity circumnavigate the ventricle in the direction denoted by the yellow arrow (Movie S 7). (D''-D''') Kymograph analysis and highlighted representation showing coupling of this motion to atrial contraction. In all kymograph analyses, displacement values enable the synchronization of PE cell motion after attachment to the myocardium or release from the cluster to be seen. In all panels, gray arrows mark epicardial cells on the myocardial surface prior to acquisition and asterisks indicate PE cell positions before release. At, atrium; V, ventricle. Scale bars 20 µm.

Overall, *in vivo* imaging thus revealed that epicardial precursor cells derive from three different pericardial sources: the avcPE, the vpPE and apEP (**Figure R 4**). The avcPE is the biggest PE cluster, followed by the vpPE cluster and a small contribution coming from individual apPE cells

A

		Wildtype	
		mean size	nº larvae
Source of epicardial cells	vpPE	4 ± 1 cells	10
	avcPE	7 ± 3 cells	14
	apPE	1 cell	5
		nº events	nº larvae
PE cluster release into the pericardial cavity	vpPE	6	6
	avcPE	72	16
	apPE	0	5
Direct transfer of PE cluster to myocardium	vpPE	0	6
	avcPE	0	16
	apPE	8	5
Colonization of the ventricle	1st cell cluster to distal (D)	15	16

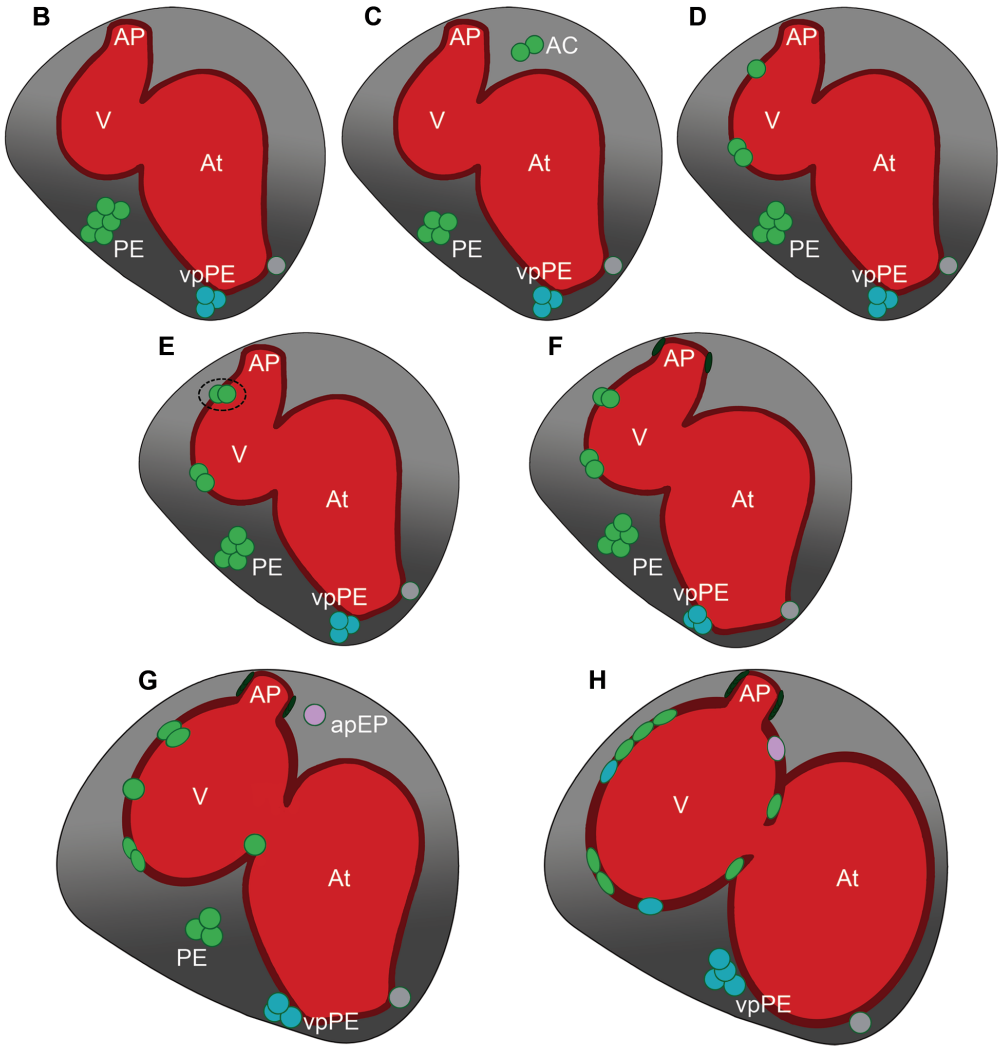

Figure R 4. Chronological annotation of events during epicardium morphogenesis. (A) Summary of events observed during epicardium formation in 16 embryos from 48 hpf to 78 hpf. (B-H) Events leading to epicardium formation. (B) Between 48 and 55 hpf the avcPE cluster of 4-10 cells arises from the dorsal pericardial wall at the level of the atrioventricular canal. More caudally, the vpPE appears as a smaller group of cells at the right side of the venous pole (blue). On the left side, a single Epi:GFP-positive cells appears, which does not develop a PE (grey). (C) vpPE and avcPE cells or cell clusters are released into the pericardial cavity. (D) PE cells attach to the ventricular myocardium, first at distal locations and then at more proximal regions. (E) PE cells on the myocardial surface divide. (F) The forming *bulbus arteriosus* is covered by a thin layer of epicardial cells, which does not derive from the PE. (G) Epicardial progenitors from the arterial pole mesothelium source (apEP, pink) are transferred to the myocardium. (H) After 72 hpf, epicardial cells continue to divide and flatten until they completely cover the ventricle. AP, arterial pole; At, atrium; PE, proepicardium; V, ventricle.

(**Figure R 4A**). At the left side of the cardiac venous pole, a single rounded GFP-positive cell is present, but we have not seen it to contribute to the epicardial formation. The release of epicardial precursors cells form the avcPE, vpPE and apEP occurs over an extended period beginning late 2 dpf and finishing late 3 dpf. Cells were mostly released as individual cells or in pairs (n=22/27 events of avcPE release observed in 6 embryos). Most epicardial cells derived from the avcPE. Epicardial cells preferentially adhere first to the distal half of the ventricle and later colonize the proximal half. Once epicardial cells attach, proliferation leads to complete coverage of the myocardium at 6 dpf (**Figure R 4B-H**).

1.3. Validation of the two epicardial origins in zebrafish: PE -derived and arterial pole derived epicardium.

Quail-to-chick PE chimeras had shown there are different epicardial populations:

- The PE gives rise to the epicardial layer covering the ventricle and the atrium.
- The pericardium of the arterial pole generates the epicardium of the OFT (Perez-Pomares et al., 2003).

To further explore the differences between both epicardial populations we studied mutants with problems in epicardial development and OFT formation.

In the chick, ablation of the PE leads to outgrowths from the arterial pole pericardium, which partially compensate for the missing PE and form an incomplete epicardial layer (Gittenberger-de Groot et al., 2000). We wanted to test if such a compensatory mechanism could operate in the zebrafish embryo. To answer this question we analyzed epicardium formation in the *tbx5a* null mutant *heartstrings (hst)*, and the *fgf8a* mutant *acerebellar (ace)*.

1.3.1. tbx5a function is necessary for PE formation, but dispensable for the formation of the OFT epicardium.

Loss of *tbx5a* function had been previously been shown to disrupt PE formation in the zebrafish (Liu and Stainier, 2010). Our group also confirmed these results (Peralta et al, unpublished). We

characterized the expression pattern of both zebrafish paralogues of *tbx5*, namely *tbx5a* and *tbx5b* (Albalat et al., 2010) by whole mount ISH at 24, 48 and 72 hpf. *tbx5a* expression was found in the heart tube at 24 hpf. At 48 and 72 hpf expression was found in the ventricle and the part of the atrium close to the atrio-ventricular canal, as well as in the pericardium (**Figure R 5A-C**). *tbx5b* was expressed in the myocardium of the heart tube at 24 hpf and only in the ventricle and in the pericardium at 48 and 72 hpf at lower levels than *tbx5a* (**Figure R 5D-E**). Neither *tbx5a* nor *tbx5b* were expressed in the PE or epicardium, as confirmed also by ISH on sections (data not shown). Analysis of PE formation by scanning electron microscopy at late 2 dpf revealed that while a PE cluster was clearly visible close to the AVC region in siblings (n=2 larvae), it was absent in *hst* embryos (n=4 larvae) (**Figure R 5F,G**). *In situ* hybridization with *tbx18* and *wt1a* probes in control siblings (n=6 larvae) and mutants (n=5 larvae) at 3 dpf revealed that the ventricle was devoid of an epicardial layer in *hst* (**Figure R 5H-K**). However, the developing OFT was covered by *tbx18*- and *wt1a*-positive cells. Thus, OFT epicardium formation is not perturbed by *tbx5a* loss of function. This finding is in agreement with the description in the chick, that the distal arterial pole epicardium is derived from the cephalic pericardium and not from the PE (Perez-Pomares et al., 2003). Our results furthermore suggest that *tbx5a* is indispensable for ventricular epicardium formation and that this epicardial layer cannot be formed by compensatory alternative mesothelial sources, such as the cephalic epicardium, in this mutant.

1.3.2. fgf8a function plays a role in the proper timing of the PE development and its location.

In the chick, *Fgf8* signalling determines the formation of a PE at the right side of the heart (Schlueter and Brand, 2009). In zebrafish embryos, *acerebellar* (*ace*) mutants had been shown to have a diminished contribution of second heart field progenitors to the arterial pole (de Pater et al., 2009). We observed PE formation was severely delayed in *ace* embryos. *In situ* hybridization on sections using the *tbx18* probe in *ace* at 3 dpf revealed nearly no epicardial cells covering the ventricular myocardium (2 ± 1 epicardial cells in 5 out of 7 mutant embryos), while all their siblings had epicardial cells attached to their ventricle (21 ± 9 epicardial cells in 4 out of 4 wildtype embryos) (**Figure R 6A-B'**). Unexpectedly, *ace* embryos showed an OFT at 3 dpf and epicardial cells coating it, although its formation is delayed. Contrary to wildtypes, at 4 dpf, a PE cluster was still present in mutants (n=6 larvae) (**Figure R 6C-D'**). While usually two distinct clusters can be seen, one located at the right side of the venous pole (vpPE) and the other close to the AVC (avcPE), only one cluster was visible in *ace* embryos, located closer to the atrium instead of being closer to the AVC. Moreover the cluster appeared abnormally expanded towards the dorsal pericardial wall. At 4 dpf, control larvae showed epicardial cells covering the ventricle (35 ± 4 epicardial cells in 3 out of 3 larvae), even though the majority of *ace* larvae revealed a reduced number of epicardial cells (9 ± 5 epicardial cells in 5 out of 6 larvae). Later, at 6 dpf, the epicardium of controls and *ace* larvae looked more similar (**Figure R 6E,F**). This partial recovery of the epicardium might be accomplished by the proliferation of the few PE cells, which had attached to the ventricle.

We also explored whether epicardium formation of the arterial pole was affected in *ace* mutants. *tbx18* expression could be detected covering the arterial pole of the heart (**Figure R 6A-F**),

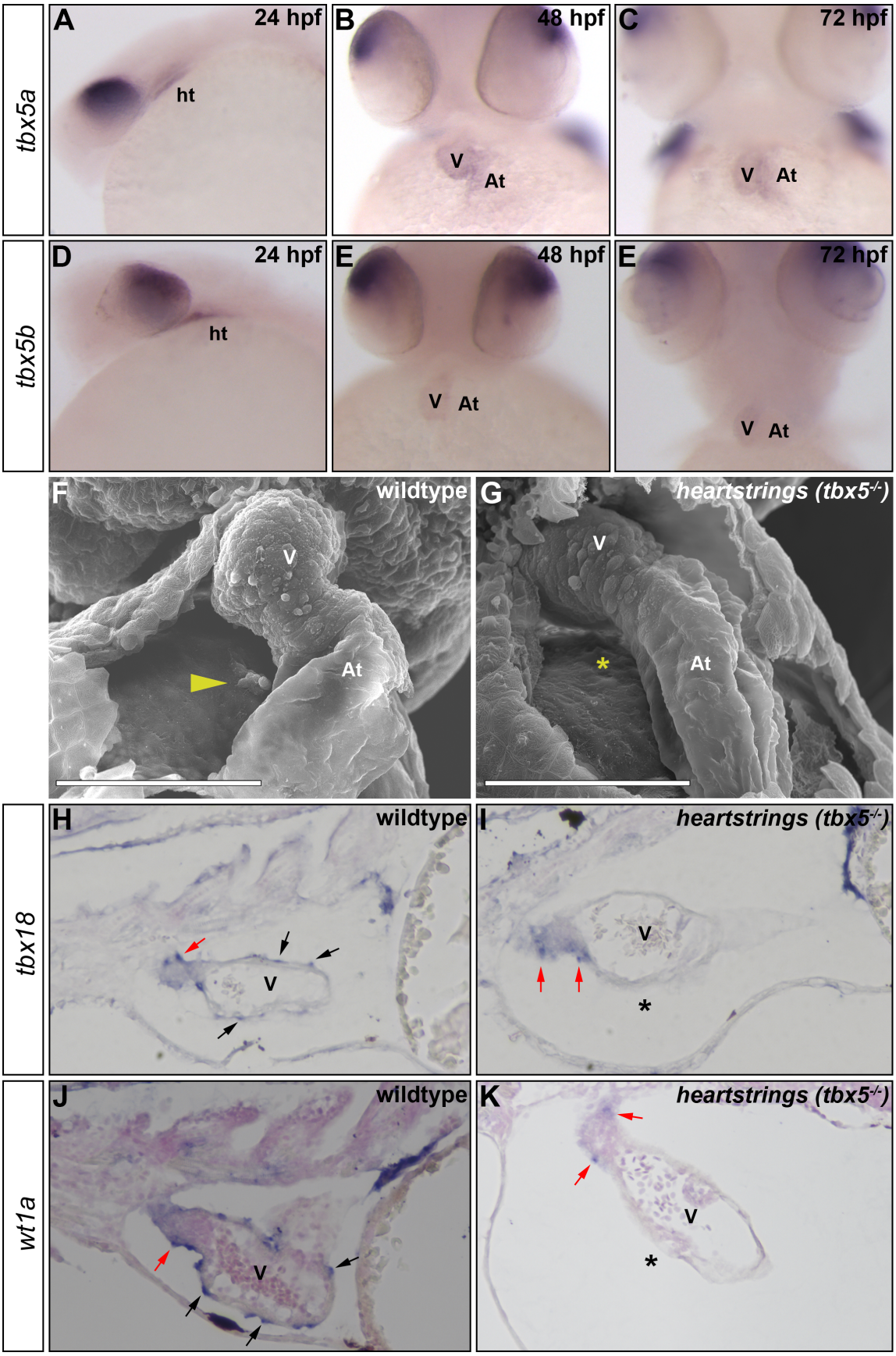

Figure R 5. Expression pattern and role of *tbx5* during morphogenesis of proepicardium-derived and arterial pole derived epicardium formation. (A-E) mRNA ISH analysis of *tbx5a* and *tbx5b* in whole mount zebrafish embryos from 24 hpf to 72 hpf. Anterior is on the top. (A-C) *tbx5a* expression marks the heart tube at 24 hpf, the ventricle and part of the atrium close to the atrio-ventricular canal at 48 and 72 hpf.

(D-E) Expression of *tbx5b* is visible at lower levels than *tbx5a.* It is expressed in the myocardium of the heart tube at 24 hpf and later, between 48 and 72 hpf, in the ventricle. (F-G) Scanning electron microscopy images from wildtype and *heartstrings (hst)* mutant hearts. Shown are ventral views. Arrowhead in F highlights the avcPE. Note the absence of a similar cluster in the *hst* mutant shown in G (asterisk). (H-K) mRNA ISH on sections of wildtype and *hst* mutant larvae at 72 hpf with *tbx18* and *wt1a* riboprobes. Red arrows mark epicardial cells on the outflow tract; black arrows epicardial cells on the ventricle. Asterisks show absence of ventricular epicardium in *hst* larvae. V, ventricle; At, atrium; ht, heart tube. Bars in F and G, 90 µm.

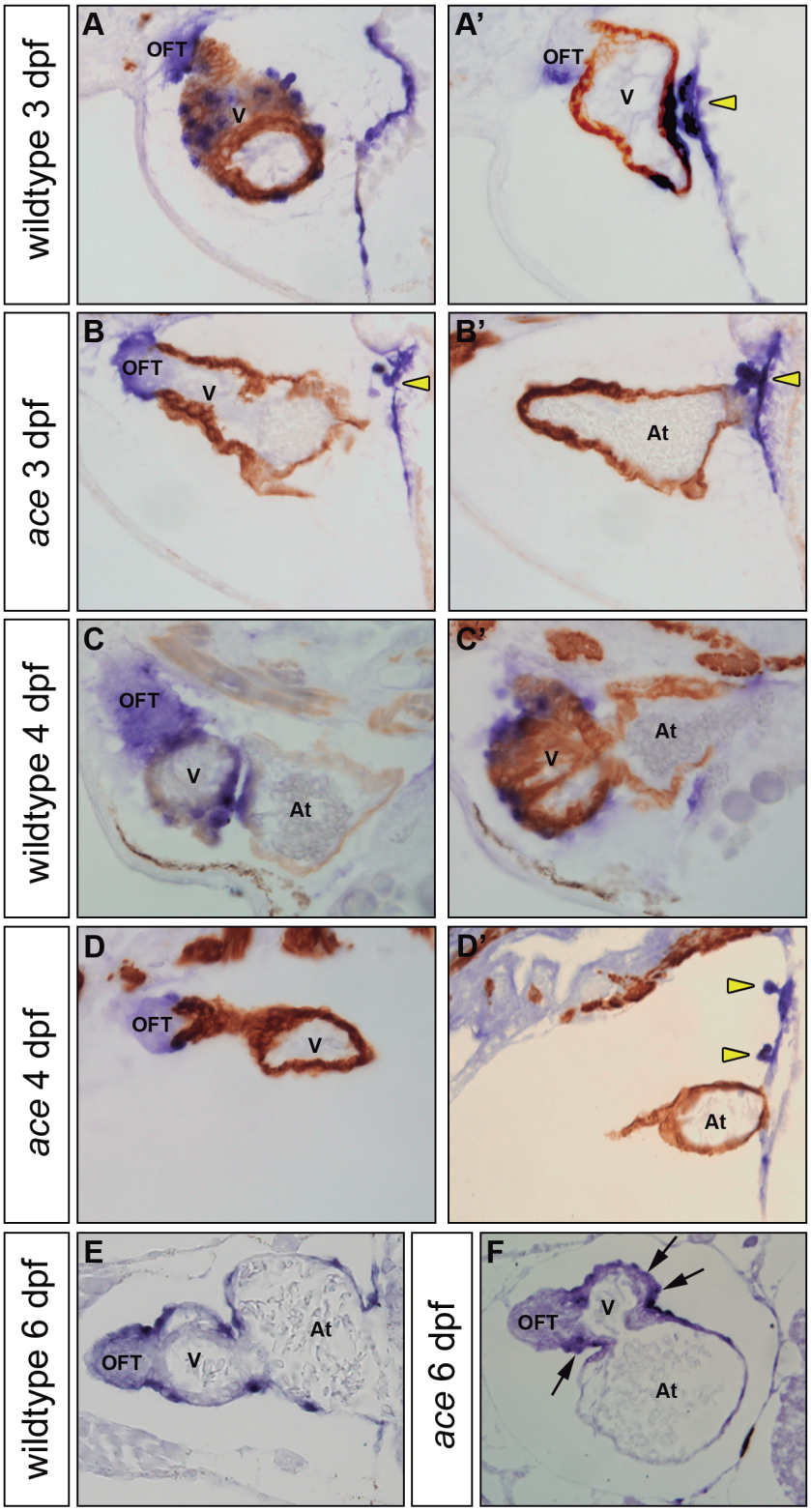

Figure R 6. Proepicardium formation in *acerebellar (ace)* mutants (*fgf8a*$^{-/-}$). (A-F) *tbx18* mRNA in situ hybridization on sections of *ace* and wildtype embryos at indicated stages, followed by myosin heavy chain immunostaining to visualize the myocardium. Yellow arrowheads reveal PE cells bulging out into the pericardial cavity and arrows mark epicardial cells. Note the absence of epicardial cells in the *ace* mutants at 3-4 dpf and the odd PE location. At, atrium, dpf, days postfertilization; OFT, outflow tract; V, ventricle.

suggesting that arterial pole epicardial development was normal in *ace* mutants. In conclusion, our results suggest that *fgf8a* is needed for correct PE positioning and timing of PE cluster formation, leading to less PE cells attaching to the ventricle and causing a delay in ventricular epicardium formation. However, *fgf8a* seems to be dispensable for arterial pole epicardium formation.

2. Role of fluid forces in proepicardium and epicardium formation.

2.1. PE and epicardium formation is controlled by the heartbeat.

In vivo data showing the way PE cells were released from the clusters and reached the myocardial surface, suggested a role for heartbeat in the process. To determine whether heart contraction mediates epicardium development, we monitored the effect cardiac contractility inhibition, both genetically with a *tnnt2* antisense RNA morpholino (Sehnert et al., 2002) and chemically, using 2,3- Butanedione monoxime (BDM) (**Figure R 7**). In *Epi:GFP* embryos, we usually observed the presence of avcPE and vpPE clusters at 2 dpf (**Figure R 7A**). At early 3 dpf, scattered GFP-positive cells were detected on the myocardial surface (**Figure R 7B**) and at 6 dpf, epicardial cells covered the ventricular myocardium (**Figure R 7C**). In *tnnt2* morphants, which lacked a heartbeat, no PE clusters were visible (**Figure R 7E**). Only a few GFP-positive cells were observed on the pericardial wall, and these had a flat morphology and did not cluster together (**Movie S 8**). In contrast to controls (**Figure R 7B**), *tnnt2* morphants had no ventricle-adhered PE cells at 72 hpf (n= 17/17 larvae) (**Figure R 7E'**). Moreover, the heartbeat was blocked at specific time points by treatment of larvae with 20 mM BDM, in order to avoid possible side effects of blocking heartbeat since the beginning. BDM treatment from 48 to 60 hpf prevented PE adhesion to the myocardium (n= 28/28 larvae) (**Figure R 7F,F'**), contrasting with the presence of epicardial cells in untreated embryos (**Figure R 7G,G'**). *In vivo* imaging of *Epi:GFP* larvae revealed that during PE formation pericardial mesothelial cells first round up and protrude into the cavity (**Figure R 8A,A'** and **Movie S 3**), a process reverted by BDM treatment (**Figure R 8B,B'**). At 60 hpf, myocardium-adhered epicardial cells start to proliferate (n= 4 imaged larvae) (**Figure R 8C,C'**). BDM affected neither the adhesion of epicardial cells nor their proliferation on the myocardial surface (n= 7 imaged larvae) (**Figure R 8D,D'**). Analysis of phosphohistone 3 and TUNEL staining revealed that heartbeat inhibition with BDM reduced pericardial cell proliferation without significantly increasing apoptosis of pericardial cells (**Figure R 8E,E'**). The absence of a heartbeat thus impairs PE formation, possibly through reduced pericardial cell proliferation (**Figure S 1**), but the subsequent expansion of the epicardial layer on the myocardial surface seems to be less dependent on heart contraction.

Heart malfunction leads to pericardial effusion, which could affect the pericardial wall tension at later stages. However, the pericardial cavity volumes of BDM-treated and control larvae did not differ at time points at which PE formation was affected (**Figure R 8F,F'**). Moreover, in some *tnnt2* morphants in which the phenotype was not completely penetrant (n= 6 larvae), severe pericardial effusion was accompanied by a weak heartbeat, and in these embryos, some epicardial cells were attached to the myocardium (**Figure R 8G,G'**), suggesting that pericardial effusion is unlikely to be the main mechanical stimulus impeding PE formation. While usually a region distal to the

AVC was colonized first (n= 16/16 larvae) (**Figure R 8H**), in *tnnt2* morphants exhibiting a weak heartbeat epicardial cells were mostly found close to the AVC (n= 5/6 larvae) (**Figure R 8H'**). The effect of cardiac dysfunction on epicardium formation was also tested by caffeine treatment and silencing of the gene encoding the atrial-specific myosin heavy polypeptide 6 (*myh6*) (Stainier et al., 1996, Berdougo et al., 2003). Caffeine treatment at 55 hpf led to nonhomogeneous contraction

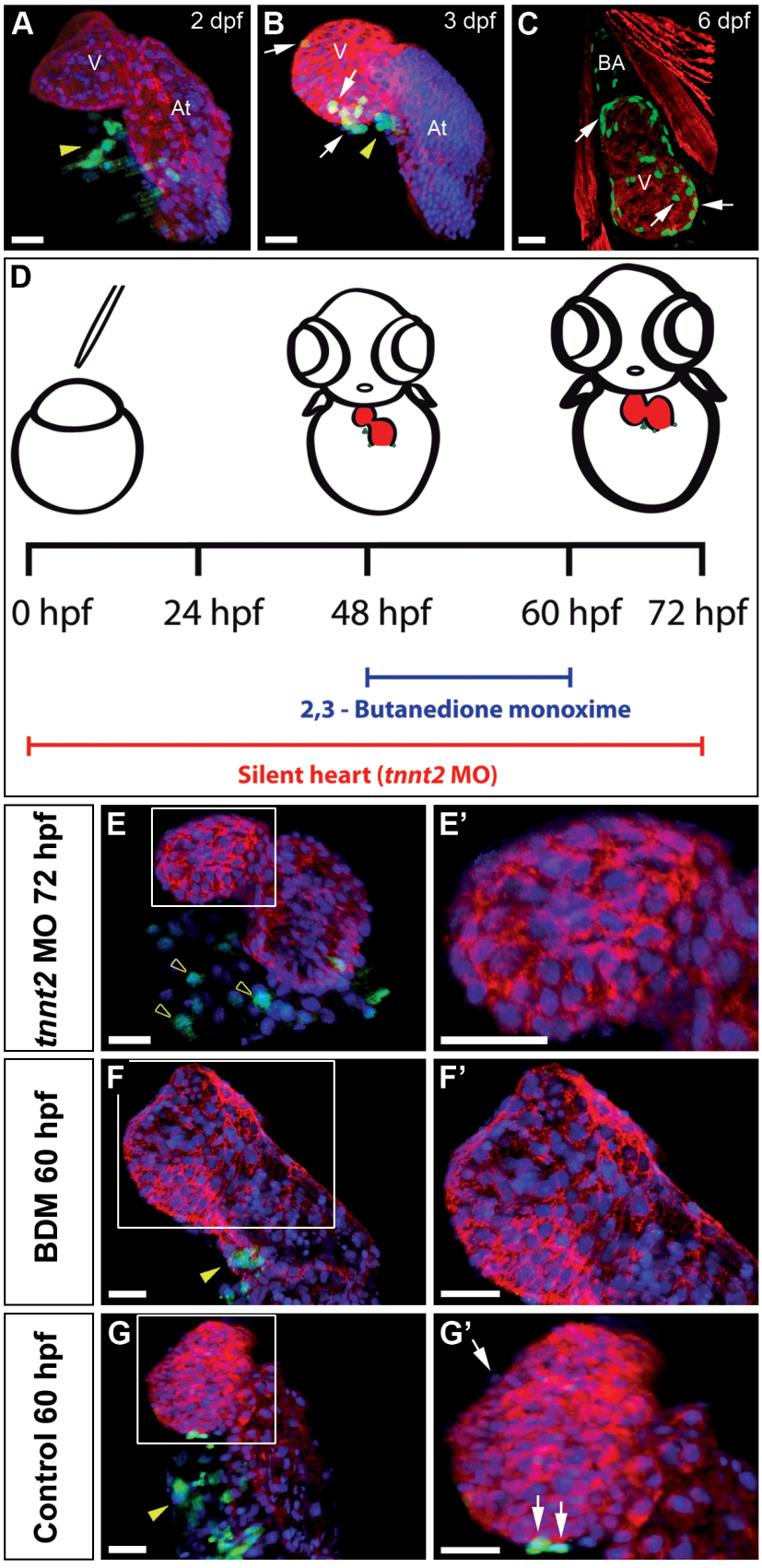

Figure R 7. Epicardium formation is inhibited in the absence of a heartbeat. (A-C and E-G') Immunohistochemical analysis of proepicardial (PE) and epicardial development. Panels show 3D projections of whole hearts from Epi:GFP zebrafish larvae at different developmental stages stained with anti-myosin heavy chain to detect myocardium (red) and DAPI to counterstain nuclei (blue). DAPI is not shown in (C) to improve visualization of the myocardium. GFP expression is shown in green. Yellow arrowheads mark PE cell clusters; white arrows mark epicardial cells. (D) Scheme of experiments for inhibiting heart function by tnnt2MO-injection into 1-cell stage embryos or BDM treatment between 48 and 60 hpf. Myocardium is shown in red and GFP-positive cells in green. (E) Heart of a *tnnt2* morphant at 72 hpf. Empty arrowheads mark scattered GFP-positive mesothelial cells at the venous pole, which do not form a PE cluster (Movie S 8). (F) Heart of a BDM-treated larvae. (G) Control at 60 hpf. E'-G' are zoomed views of boxed areas in E-G. At, atrium; BDM, 2,3-butanedione monoxime; dpf, days postfertilization; hpf, hours postfertilization; *tnnt2* MO, *troponin t2* Morpholino; V, ventricle. Scale bars, 30 µm.

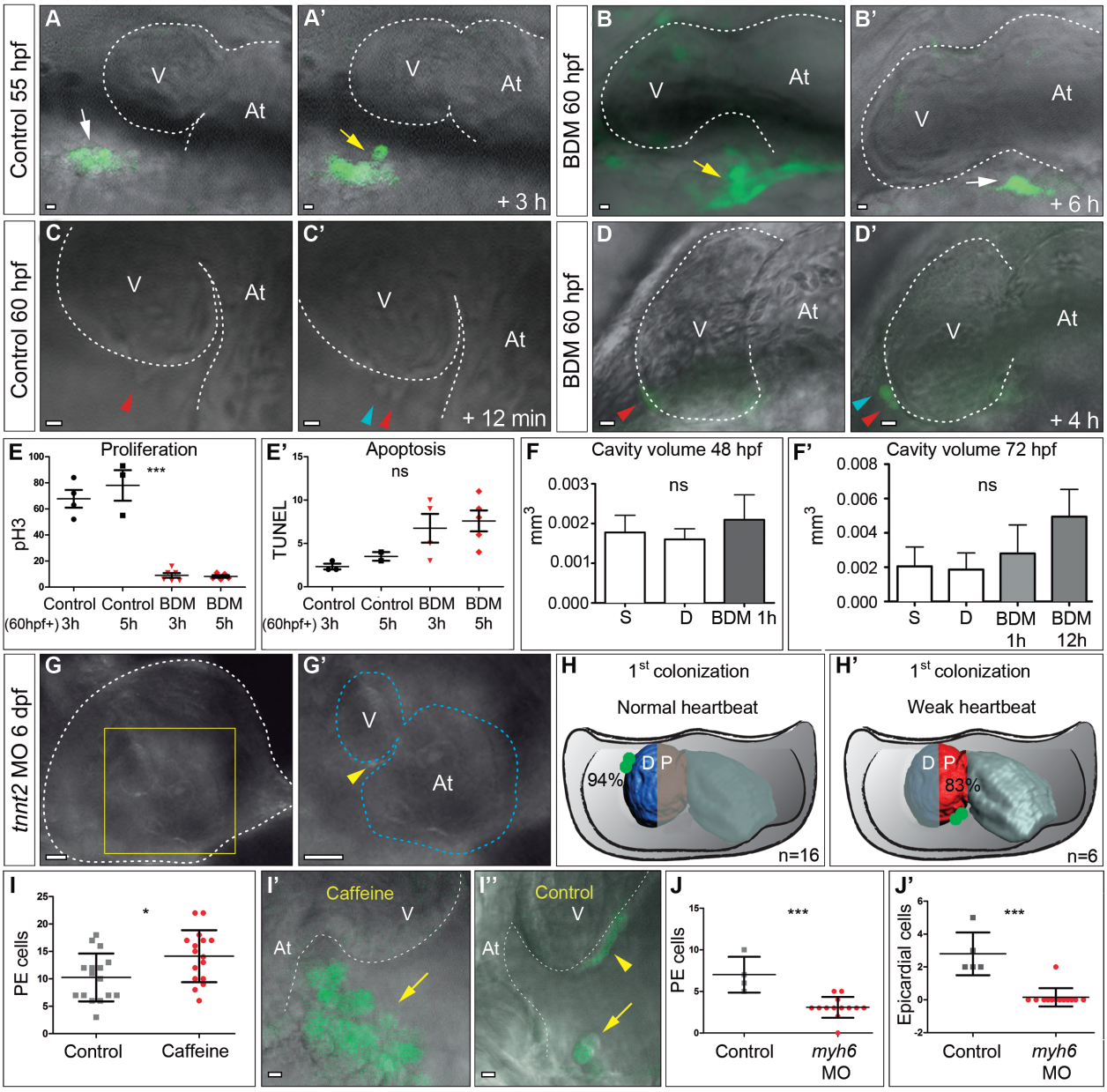

Figure R 8. The heartbeat is necessary for proepicardial cluster formation and correct transfer to the myocardium. Panels show experiments performed with Epi:GFP larvae. (A-D') Confocal imaging of hearts at different stages. Dorsal is to the top. (A-A') In wildtype larvae at 55 hpf (control), mesothelial cells of the pericardial wall (white arrows) form a PE cluster (yellow arrow) (Movie S 3). (B,B') BDM treatment inhibits PE formation and PE cells flatten (white arrow) instead of rounding up. (C-D') Epicardial cells proliferate normally in the absence of a heartbeat. Red arrowheads mark cells about to proliferate; blue arrowheads mark newly formed cells. (E, E') Quantification of proliferation (pH3 staining) (Figure S 1) and apoptosis (TUNEL staining) of pericardial mesothelial cells in the presence or absence of a heartbeat; 3 and 5 hour BDM-treatments from 60 hpf onwards were compared with controls fixed at the same stage. Y-axis shows number of pericardial cells. ***, $p<0.001$. (F,F') Pericardial cavity volume at 48 and 72 hpf in systole (S) and diastole (D) in untreated larvae (n= 2 and 3) and after BDM treatment initiated 1 or 12 h before, as indicated (n= 4 and 6). (G-H') Larvae with an altered heartbeat show a different pattern of myocardial ventricle colonization. (G-G') A few epicardial cells (yellow arrowhead) are observed in tnnt2 morphants with <100% penetrance, which have a weak heartbeat and strong edema. (H,H') Order of myocardial colonization by PE cells. In control larvae epicardial cells first colonize the distal ventricle surface (D), while in weak-heartbeat *tnnt2* morphants epicardial cells mostly colonized the proximal ventricle (P). Numbers indicate the percentages of animals with the reported colonization pattern and the total numbers of animals analyzed (I-I'') Enlarged PE cluster in caffeine-treated animals (Movie S9). (I) PE cell quantification of caffeine-treated (n=16) versus untreated larvae (n=16) revealed significant differences (*, $p=0.023$; two-tailed Student's t-test). (I' and I'') Merged brightfield and fluorescent images of PE clusters (yellow arrows) from a control and a caffeine-treated larva. Arrowhead indicates epicardial

cells. (J-J') Impaired PE and epicardium formation in *myh6* morphants revealed by cell quantification at 70 hpf (n=21 control and 45 *myh6* morphants; ***, p<0.0001, two-tailed Student's t-test). In all graphs, bars indicate means and standard deviations. At, atrium; D, distal; *myh6*MO, myosin heavy polypeptide 6 morpholino; ns, not significant; P, proximal; pH3, phospho-Histone 3; V, ventricle. Scale bars (A-D' and I-I') 10 µm, (G-G') 20 µm.

due to ventricle wall collapse (**Movie S 9**) and an increased PE cluster size after 10 h of treatment (**Figure R 8I-I"**). At 70 hpf, the number of PE and epicardial cells was significantly lower in *myh6* morphants (**Figure R 8J,J'**). Whereas a PE was clearly visible in 70% of wildtype larvae at 60 hpf, only 20% of morphants displayed a PE cluster (data not shown). Thus, heartbeat impairment perturbs PE cluster formation and PE cell transfer to the myocardium.

2.2. The heartbeat generates pericardiac fluid advections.

The coupling of PE cell advection with heart contractions (**Figure R3**) suggests a role for myocardium contractility in PE cell motion. Confirming this, administration of BDM after a PE cluster has formed prevented cell release over a 5 h imaging period (n= 5 larvae), during which PE cells or cell clusters in untreated larvae were released (20 events of release observed in 4 larvae). Furthermore, stopping the heartbeat after PE cell release stopped PE cell motion, and advection was restarted upon reactivation of the heartbeat by BDM washout (**Movie S 10**).

We next examined pericardial cavity topology and measured the space between the heart chambers and the pericardial wall *in vivo* (**Figure R 9A,A'**). The space between the ventricle and the pericardial wall was almost fully occluded during ventricular diastole, but it opened to 20.6 ± 9.4 µm at systole, allowing passage of PE cells. In contrast, the separation of the atrium and pericardial wall was much smaller (5.5 ± 0.9 µm) and varied less during the heart cycle. Thus, the topology of the pericardial cavity might favour accumulation of PE cells around the ventricle. Analysis of the position of 30 advected cells or cell clusters (n= 13 larvae) confirmed that cells localized most frequently around the distal region of the ventricle (region 1), less often in the cranial domain of the pericardial cavity (region 2) and in a few cases around the atrium (region 3) (**Figure R 9B**).

Interestingly, tracking of PE cell motion during the advection phase (**Figure R 9C-E**) revealed that PE cells or clusters move quickly along the AVC and the uppermost side of the ventricle (corresponding to a region of late cell adhesion) and slow down along the surface of the ventricle (corresponding to a region of early cell adhesion; **Figure R 9D** and **Movie S 11**). Speed was lowest at sites far from the myocardium (region a: 164 µm/s ± 13; n = 3 larvae) and along the distal surface of the ventricle (region b: 337 µm/s ± 79; n = 4 larvae) and increased through the AVC (region c: 546 µm/s ± 20; n = 3 larvae) and cranial domain of the cavity (region d: 828 µm/s ± 103; n = 3 larvae) (**Figure R 9E**). Optical tweezing confirmed the velocity profile and revealed the flow forces advecting PE cells (**Figure R 9F-H**). PE cells were trapped sequentially in five locations of the pericardial cavity (**Figure R 9F**). Flow velocities and forces were highest at the AVC, and in regions of the dorsal pericardium where the vpPE and avcPE form (positions 1 and 5) and were lower close to the distal ventricle and periphery of the cavity (positions 4 and 3) (**Figure R 9G** and **Table R 2**). The directionality of the forces was consistent with the observed motion of PE cells.

Forces were lowest in positions 3 and 4. Forces close to the AVC were higher (positions 1, 2 and 5) (**Figure R 9H** and **Table R 2**).

The flow profiles of intercarboxylated microscopheres injected into the pericardial cavity revealed pericardial flow motions similar to those observed for PE cells (**Figure R 9I-K'** and **Movie S 12**). Furthermore, blocking the heartbeat resulted in an immediate cessation of bead advection (**Movie S 12**).

These results lead to two major conclusions: the avcPE and vpPE are located in areas of high flow forces and the distal ventricle is an area of weak flow forces. Thus, PE cells are released in regions of high flow forces and PE cells adhesion occurs in regions of low flow forces (**Figure R 9L**).

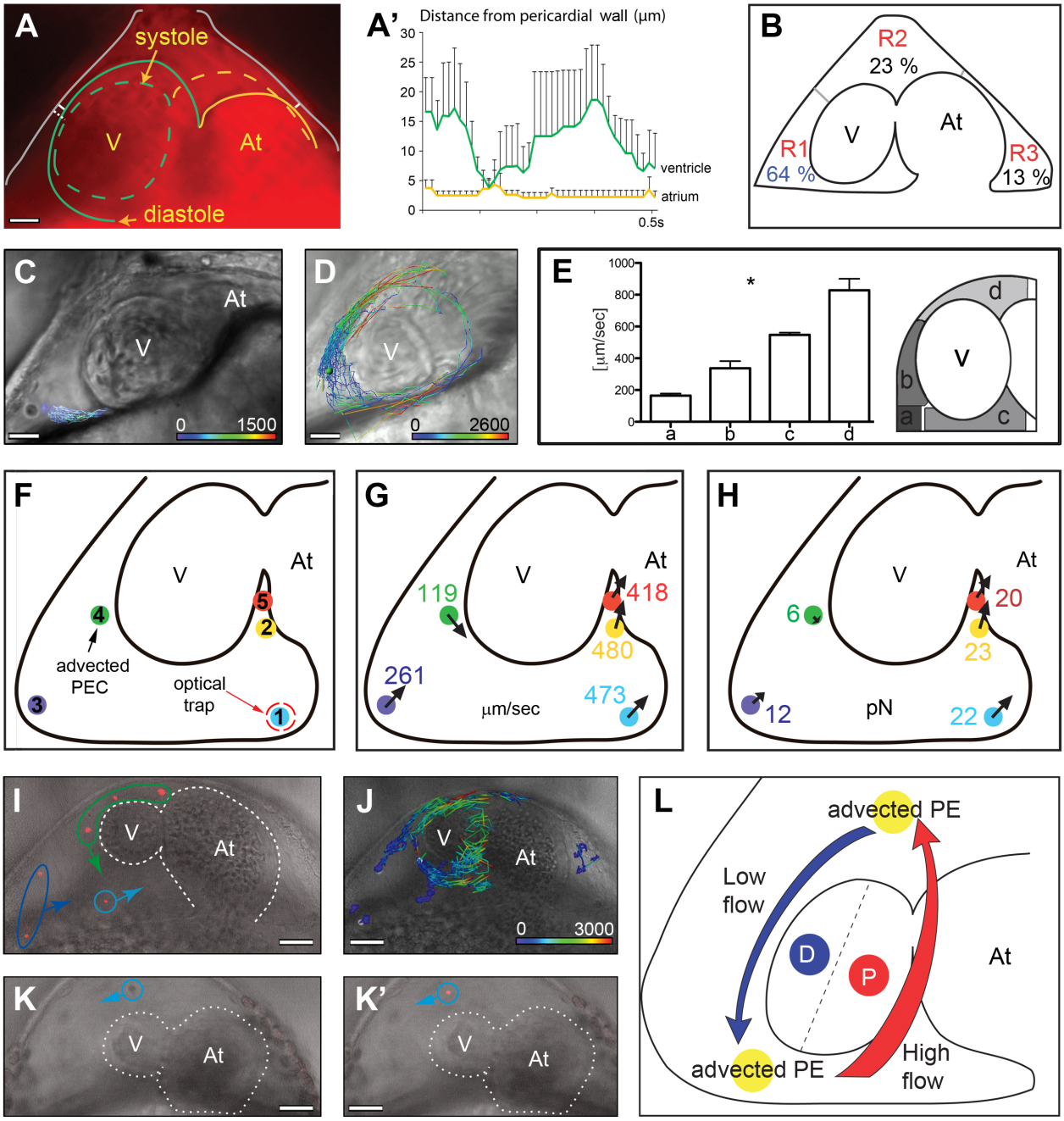

Figure R 9. Characterization of flow forces within the pericardial cavity. (A, A') Measurement of the distance between the myocardium and the pericardial wall during heart contraction. (A) Ventral view of

a 48 hpf heart immersed in Bodipy TR. The continuous and discontinuous lines outline the myocardium at diastole and systole, respectively: ventricle in green; atrium in yellow. (A') Average maximum distance over 4 heartbeats between the pericardial wall and ventricle (green) and pericardial wall and atrium (yellow). (B) Localization of PE cells within three regions (R1, R2 and R3) of the pericardial cavity. Numbers are the percentages of cells within each region from a total of 30 cells or cell clusters. (C) Tracking of a PE cell (dot) at the periphery of the pericardial cavity and (D) tracking of a PE cell flowing around the ventricle (Movie S 11). Speed (μm/sec) of advected PE cells is represented by a color code; minimum and maximum speeds are indicated. (E) Speed of advected cells within the pericardial cavity (means ± SD), varied significantly in different areas, indicated by letters a-d (One-way ANOVA followed by Tukey's mixed effect test. *; $p<0.05$ for all pairwise comparisons). (F) Positions probed with optical tweezers: 1, cell positioned close to the vpPE site; 2, cell close to the avcPE site; 3, cell at a distance from the ventricle; 4, cell close to the ventricle; 5, cell positioned at the AVC. (G,H) Vector and force maps obtained by optical tweezing. (I-K') In vivo confocal imaging and tracking of fluorescent beads injected into the pericardial cavity; beads recapitulate the pattern of advected PE cells (Movie S 12). Advected PE cell (K) and bead (K') following the same flow. (L) Model summarizing the circulatory pattern of PE cells moving with the pericardial flow in conjunction with the observed order of myocardial adhesion. At; atrium; D, distal; P, proximal; PEC, proepicardial cells; pN, picoNewton; V, ventricle. Scale bars 50 μm.

Position	1	2	3	4	5	Significant differences
Speed (μm/s)	480 ± 278	473 ± 25	216 ± 13	119 ± 12	418 ± 90	1–4, $p = 0.003$; 2–4, $p = 0.002$; 4–5, $p = 0.02$
Forces (pN)	22 ± 1	23 ± 13	12 ± 1	6 ± 1	20 ± 4	1–4, $p < 0.05$; 2–4, $p < 0.05$; 4–5, $p < 0.05$

Table R 2. Speed and Force Measurements of PE Cells and Cell Clusters in the Pericardial Cavity by Optical Tweezing. Shown are mean ± SD of speed and force measurements from PE cells trapped at the five positions within the pericardial cavity as shown in Figure R 9.

2.3. Ordered adhesion to the ventricular myocardium depends of pericardial fluid advections.

Given the observed ordered adhesion to the myocardial surface, we sought to determine whether PE cells could attach to any part of the myocardium, provided they are able to access it. Optical tweezing allowed advected PE cells to be trapped and placed close to the myocardium, both at distal (1) and proximal (2) positions (**Figure R 10**). Tweezed cells placed close to the ventricular surface in any positions attached to the myocardium (**Figure R 10A-A'''** and **Movie S 13**). To determine whether heart contraction was necessary for attachment, we stopped the heart after trapping the PE cell and moved it close to the myocardial surface (**Figure R 10B,B'**). The trapped PE cells adhered so strongly to the myocardium that it was not possible to subsequently remove cells with the optical tweezers (**Figure R 10C,C'** and **Movie S 14**). Together, these results suggest that ordered PE cell attachment is an active process resulting from the complex balance between PE cell adhesiveness to the myocardium and the differential flow forces generated in the pericardial cavity by the beating heart.

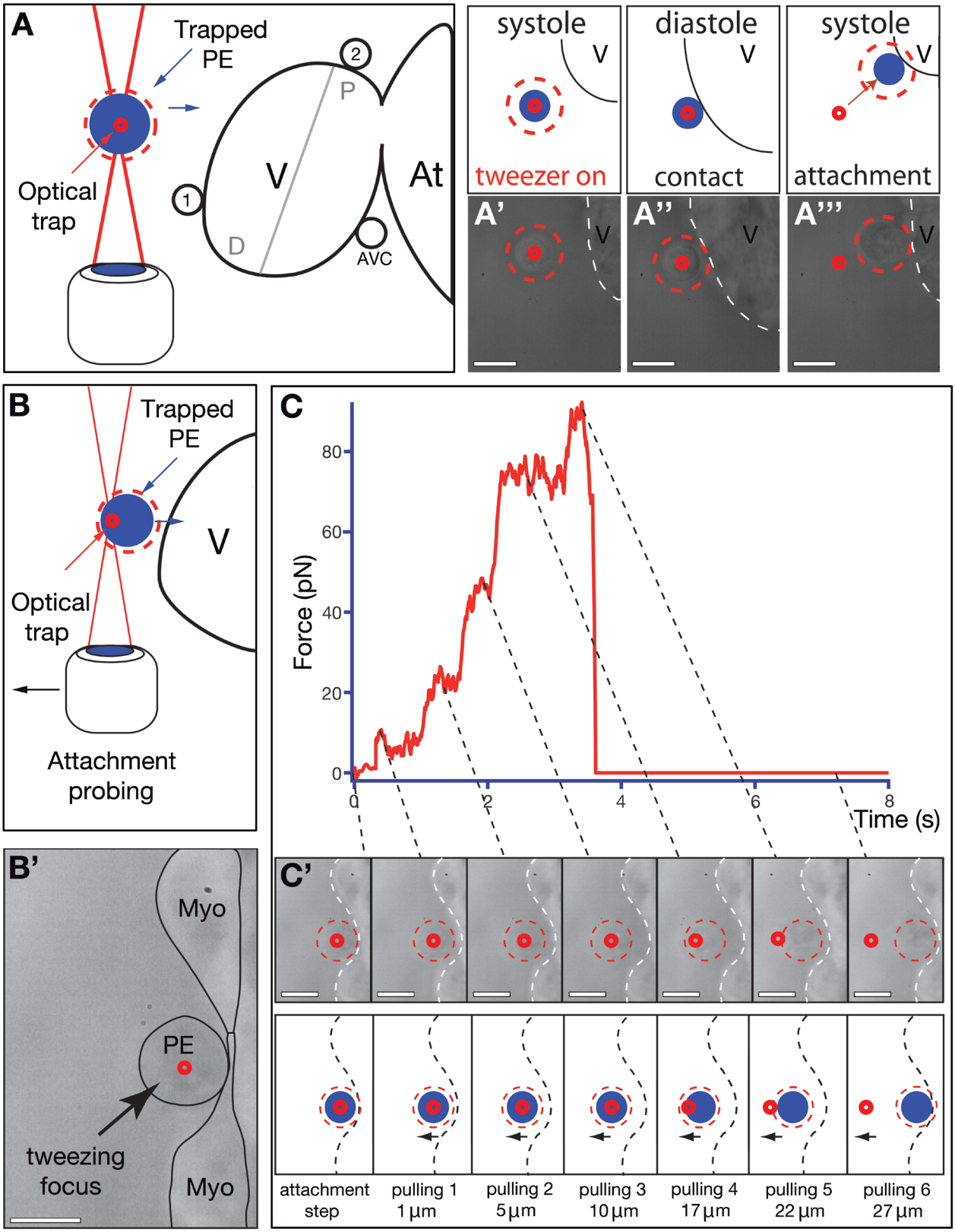

D

Condition	Location	Adhesion	n° of cells tested
Control	1	Yes	2
Control	AVC	Partial	2
Control	2	Yes	2
+BDM	1	Yes	3

Figure R 10. Characterization of proepicardial cell adhesion to the myocardium. (A) Optical tweezer set-up used to study the propensity of PE cells to adhere to different myocardial regions including the AVC, a region distal to it (region 1) and a region proximal to the AVC (region 2). The blue

circle illustrates the trapped cell and the small red circle the approximate location of the optical trap. The red dotted circle around the cell facilitates its visualization during the experiment. (A'-A"') Trapped PE cells adhere firmly to the ventricle if placed close to it. (Movie S 13). (B-C') Optical tweezer pulling test to determine the role of the heartbeat during PE cell attachment to the myocardium. After BDM treatment, a PE cell was trapped and forced to attach to the myocardium (time 0s, B'-C). After 30 seconds, the trapped cell was progressively pulled away from the myocardium. (C,C') Optical tweezer forces applied to a cell over time during the pulling test. With increased distance, the magnitude of the force within the tweezer increases (10pN, 20pN, 40pN, 70pN, 90pN), eventually resulting in the cell moving out of the tweezer because of its attachment to the myocardium (pulling 5). Further pulling resulted in the cell springing back to its original position on the surface of the heart (pulling 6) (Movie S 14). The dotted lines link the force changes observed in the trap (C) with the images of the trapped cell at the same time (C'). (D) Table summarizing the number, location and types of adhesion events tested with the optical tweezers. At, atrium; Myo, myocardium; V, ventricle. Scale bars 10 μm.

3. Primary cilia as possible mechanosensors during pericardial cavity and PE formation.

Primary cilia are well known chemical and/or mechanical sensors (Berbari et al., 2009) and have been reported in the embryonic pericardium of the chick and the mouse (Rash et al., 1969). Our next step was to explore whether cilia were present in the pericardial cavity. To address this question, we used the ciliary axonema reporter line Tg(β-actin:arl13b:GFP) (Borovina et al., 2010), which also marks some cells membranes. *In vivo* imaging revealed that there are cilia protruding into the pericardial cavity in pericardial and PE cells (**Movie S 15**). They showed different motion patterns depending of their location in the pericardial cavity.

3.1. Primary cilia display a heterogeneous distribution in the pericardial cavity.

In vivo imaging analysis of the pericardial cavity showed cilia distributed heterogeneously protruding into the pericardial cavity (**Figure R 11**). For cilia quantification, we divided the ventral and dorsal pericardial wall in three regions each one (**Figure R 11B**):

- Ventral pericardial wall:
    - OFT: Region closer to the OFT.
    - VP V: Ventral pericardial wall close to the V.
    - VP At: Ventral pericardial wall close to the At.
- Dorsal pericardial wall:
    - SV: Region close to the *sinus venosus.*
    - PE: Region where the avcPE appears.
    - Deeper: The deepest region of the pericardial cavity as seen from a frontal view.

These three regions were divided in right and left half, mainly comprising the ventricle or atrium, respectively.

At 48 hpf (n=9 analyzed larvae), a stage previous to PE formation, the cilia distribution protruding from some pericardial cell in the ventral pericardial wall was (**Figure R 11C**): 9 ± 3 cilia in the OFT region; 17 ± 3 cilia in the VP V and 15 ± 4 cilia in the VP At domain. The dorsal pericardium also showed a heterogeneous distribution: the right half of the SV region presented a higher number of cilia (6 ± 1) than left part (3 ± 3). Interestingly, the PE region presented a huge difference between the right side, where the avcPE will form (17 ± 3) and the left side (4 ± 3). Most of the dorsal pericardial cilia were concentrated in that area. The Deeper region presented the lowest number of cilia: 3 ± 2 on the right side and 1 ± 1 on the left part.

At 55 hpf, when the PE clusters are formed, the cilia distribution in the cavity was similar to the one observed at 48 hpf (analyzed in 6 larvae) (**Figure R 11D**). There was also not a significant change in the cilia number. The ventral pericardium presented 9 ± 3 cilia protruding from the OFT area, 22 ± 6 from the VP V and 20 ± 6 from the VP At. The dorsal pericardium showed 8 ± 1 cilia on the right and 3 ± 2 on the left SV. The PE also presented some cilia. However, they were immotile and bent, as being trapped by what seemed to be ECM (**Movie S 16**). Additionally, there were consistently 4 ± 2 cilia protruding from the left part of the PE region. The deeper area revealed 3 ± 1 cilia at the right side and 1 ± 2 at the left side.

3.2. Primary cilia show different motion patterns depending on their localization.

In depth analysis using *in vivo* imaging revealed that cilia possessed different motion patterns depending on the region in the pericardial cavity where they protruded from (**Figure R 12**). Cilia at the OFT region displayed a circular rotation (**Movie S 17**); however, cilia at the VP At were bending up and down due to the influence of the V and At motion (**Movie S 18**). Cilia in the dorsal pericardium also revealed characteristic motions. The cilium in the deeper area displayed a more restricted bending movement (**Movie S 19**). The peculiarity of the cilia motion was visible even within the same region, as shown on the right side of PE area (**Movie S 20**). The cilium closer to the heart bent completely when the V was close to it; while the cilium more distant from the cardiac tube was bending in a smaller angle. The particularities observed in cilia motion suggest they are due to the turbulent flow generated in the pericardial cavity by the heartbeat. Besides, their motion is influenced by the distance between cilium and the heart.

3.3. The heartbeat triggers primary cilia motion in pericardial mesothelial cells.

To test whether the cilia movement was coupled to the heartbeat or whether they were motile cilia, we analyzed their behavior upon stopping cardiac contraction by BDM treatment. When the heartbeat was stopped, the cilia did not shown any motion (n=6 larvae) (**Movie S 21**). After washing out of the BDM, the heart recovered the contractility gradually. Simultaneously, the cilia started to move coupled to the heartbeat, however the cilia motion is different to the normal motion for that are found in that area, due to the abnormal cardiac contraction (**Movie S 22**). Thus, cilia motion is triggered by heartbeat generated pericardial fluid forces.

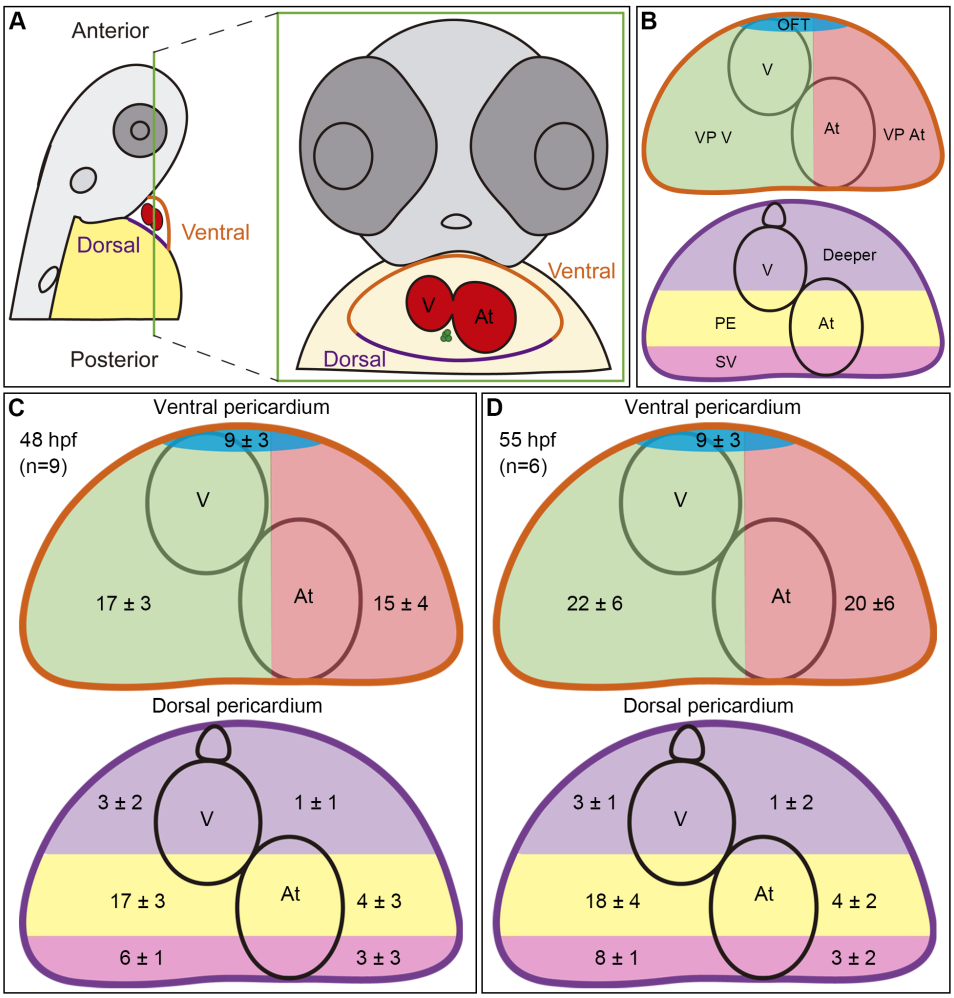

Figure R 11. Spatial distribution of primary cilia protruding into the pericardial cavity (A) Schematic representation of a z-stack section (inside of green box). For easier quantification, the ventral and dorsal pericardial walls were divided into 3 areas, respectively. (B) The ventral pericardium (VP) was divided into: OFT area (OFT); the area close to the ventricle (VP V) and the area close to the atrium (VP At). The dorsal pericardium was divided into: the area closer to the *sinus venosus* (SV); the area closer to the atrioventricular canal (PE) and the deepest area (Deeper). This three areas were divided into right (closer to the ventricle) and left (closer to the atrium) half. (C) Cilia distribution in 48 hpf embryos of the *Arl13b:GFP* line (n=9 larvae analyzed) on ventral and dorsal pericardial walls (means ± SD). (D) Cilia distribution in 55 hpf larvae (n=6 larvae analyzed), at the time of PE formation (means ± SD). Note the presence of more ciliated cells in the right PE area. At, atrium; V, ventricle.

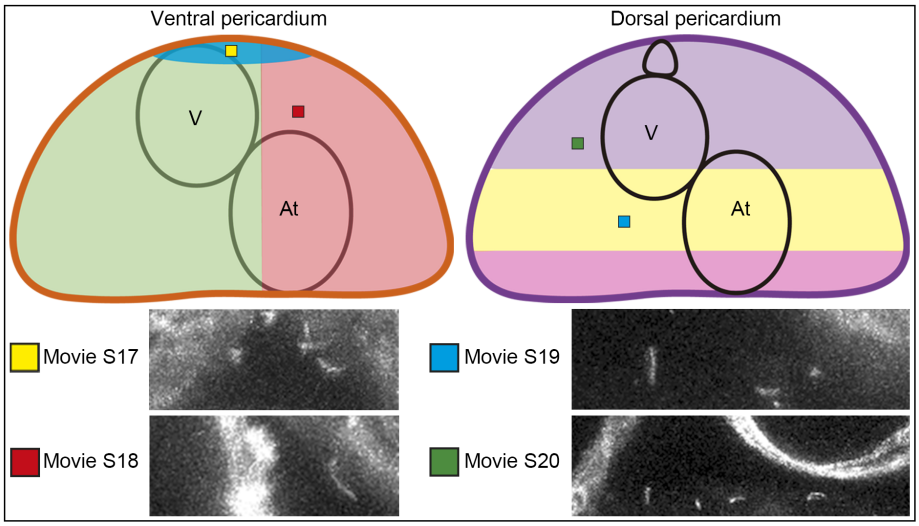

Figure R 12. Primary cilia movement is specific of their location within the pericardial cavity. Schematic representation of the regions in which cilia motion was recorded (Movies S17-20). Movie S17 shows cilia on the ventral pericardium, OFT area. Movie S18 shows cilia on the ventral pericardium close to the At. Movie S19 shows cilia in the dorsal pericardium deeper area and Movie S20 in the dorsal pericardium PE area. At, atrium; V, ventricle.

DISCUSSION

1. What *in vivo* imaging can teach us about PE formation: bridge versus PE cells release.

Different ways of PE cell attachment to the myocardium have been described among species. In chick embryos, PE cells have been suggested to be transferred through an ECM bridge between the PE and the myocardium (Nahirney et al., 2003). A bridge formation between the PE and the ventricular myocardium also has been proposed to occur in *Xenopus* (Jahr et al., 2008). Interestingly, in the sturgeon *Acipenser naccarii* besides bridge formation, PE cell aggregates were shown attached to the myocardial surface. This epicardial cells have been suggested to derive from free-floating PE cells (Icardo et al., 2009). Similarly, in the axolotl *Ambystoma mexicanum* PE cell aggregates appear attached to the myocardial surface, posteriorly these rounded cells flatten over and spread to form the epicardial layer (Fransen and Lemanski, 1990). To explain the way PE cells reach the myocardium, the authors propose that the PE cells are released into the pericardial cavity, where the cells are able to float in the pericardial fluid before attach to the myocardial surface. A similar mechanism has been proposed for the mouse (Komiyama et al., 1987) and the heartbeat has been proposed to play a role in PE release and adhesion (Rodgers et al., 2008). Our data provide for the first time *in vivo* evidence of how PE cells are released into the pericardial cavity. In the zebrafish, we observe that after PE cluster release, PE cells are advected in the pericardial cavity and subsequently attach to the myocardium. Supporting the importance of *in vivo* imaging, we observed what seemed to be a bridge between the PE and the ventricular myocardium by *in situ* hybridization (**Figure D 1**) (**Movie S 23**), but direct transfer to the heart from the PE was never observed *in vivo*. Our results are consistent with the hypothesis that in species, in which the coelomic cavities (pericardial, pleural and peritoneal) are not closed at the time of PE formation, such as the chicken, a bridge is formed to avoid loss of PE cells to the neighboring cavities (Fransen and Lemanski, 1990). In contrast, PE cell release might predominate in species with a pericardial cavity isolated from the rest of the coelom during epicardium formation, as occurs in mammals and fish. Moreover, we show that the mechanisms of PE cell release and direct epicardial precursor transfer to the myocardium can coexist. Both mechanisms might be also working together in other species, as proposed for the sturgeon (Icardo et al., 2009).

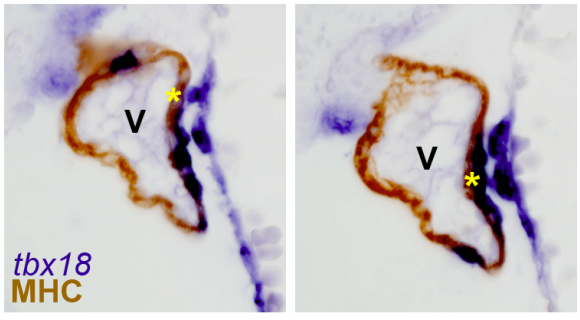

Figure D 1. Observation of Proepicardial-myocardial bridge formation in fixed samples is not confirmed by in vivo imaging. *tbx18* mRNA in situ hybridization on sections of wildtype embryos at 60 hpf, followed by myosin heavy chain (MHC) immunostaining to visualize the myocardium. Yellow asterisk mark PE cells contacting with the ventricle forming a bridge. V, ventricle.

In the *Epi:GFP* line we found that rounded GFP-positive cells could be observed on both sides of the venous pole, whereby the left side always displayed only one individual rounded cell, and the right side a group of 3 to 5 cells. Importantly, *in vivo* imaging revealed that PE cells were released exclusively from the right PE. This situation resembles the PE asymmetry observed in the chick and Xenopus, exhibiting a right-sided PE cluster, while the left sided PE primordium regresses (Schlueter and Brand, 2013a). In mouse embryos, asymmetric PE formation has not

been observed, and the bilaterally formed PE clusters fuse at the midline of the *sinus venosus*.

Interestingly, the epicardium covering the distal OFT, is being added along with the arterial pole formation. These epicardial cells do not derive from the PE and they are incorporated to the heart after the PE had started to release cells. Our data confirmed in the zebrafish what had been also described in the chick embryo (Perez-Pomares et al., 2003). It is interesting to note that while the OFT is covered with an epicardial layer from the earliest time points, the myocardium becomes covered at a slightly later time point. This shift in timing of epicardial formation could suggest that the primitive heart tube needs to lack an epicardium or that it does not need it at that moment. Once the heart reaches a certain size or developmental stage, the myocardium might require epicardial-derived trophic factors. It is also interesting to note that the epicardial layer is growing when the SHF population is added to the heart tube. This could mark the initial moment when the epicardium becomes necessary for further myocardial development.

The morphological changes and the cellular mechanisms involved in the formation of the PE clusters are not well understood. Through *in vivo* imaging we have observed that PE cells change their shape from flat to rounded, break their cell adhesions and lose their contact with the basal lamina. Also in accordance to our EM data, during this process, ECM seems to accumulate at the site of PE formation. Further experiments need to be performed to dissect the molecular mechanisms underlying the changes in cell shape and cell adhesion leading to PE formation. We have found expression of *twist1a* in the PE in zebrafish, a gene that has been linked to loss of cell adhesion and the acquisition of a migratory phenotype in several contexts (VanDusen and Firulli, 2012), (**Figure D 2**). In the chick embryos, Twist1 has been described as necessary for proper PE formation (Schlueter and Brand, 2013b). Thus, it will be interesting to study its role in controlling the change from an epithelial to mesenchymal phenotype of PE cells in the zebrafish.

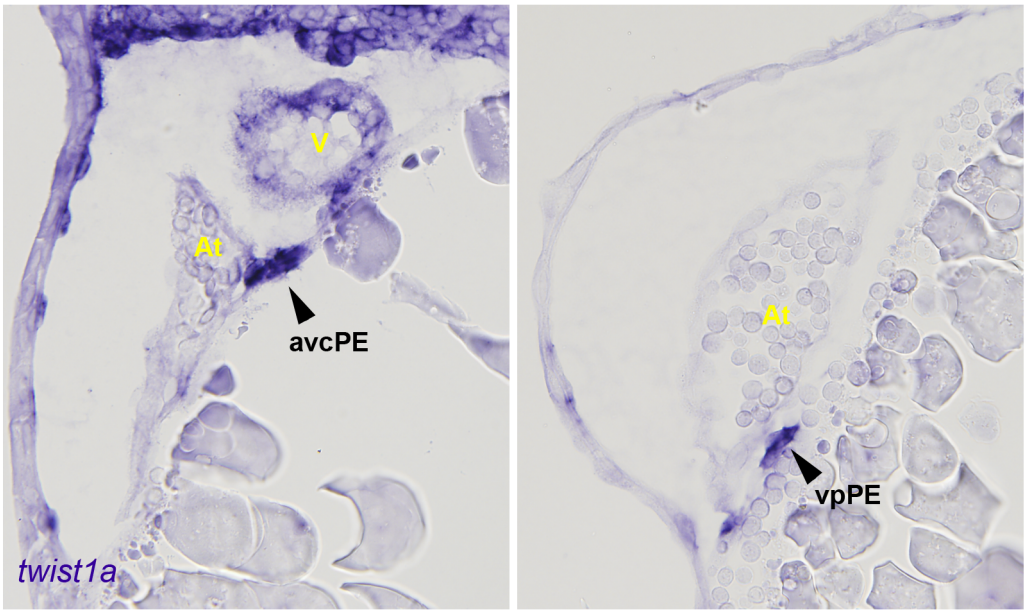

Figure D 2. *twist1a* expression in PE cells. *twist1a* mRNA in situ hybridization marks proepicardial cells at 60 hpf. At, atrium, V, ventricle.

Unexpectedly, we found that the PE does not proliferate; the main pericardial area undergoing proliferation is the ventral pericardial wall. How this highly proliferating area within the pericardial cavity relates to PE formation and maintenance remains unsolved. A possible explanation would be that the proliferative pericardial ventral wall “squeezes” the pericardial dorsal wall. This bilateral mechanical force could lead to cluster emergence. To test this hypothesis, labeling of pericardial cells and tracking them would be necessary. Epithelia must maintain constant cell numbers; a phenomenon known as “crowding” induces apical extrusion (Eisenhoffer and Rosenblatt, 2013). A similar process might occur during PE formation, where extruded mesothelial cells might constitute the PE.

2. PE and epicardial heterogeneity.

The PE is a heterogeneous cluster of mesothelial cells. Several PE cell populations can be observed depending on the marker gene used. No pan-PE cell marker gene is known so far.

In the mouse and the chick, the PE is composed of an outer layer of mesothelial cells and an inner core of mesenchymal cells. However, the zebrafish PE is composed of mesothelial cells of the inner pericardial wall only, and has an average size of 7±3 cells (avcPE), being much smaller than a mouse or chick PE. These differences could explain the lower number of cells lineages reported by EPDCs in the zebrafish.

Our data showed that zebrafish harbor two PE clusters. One located adjacent to the venous pole (vpPE) and a second at the AVC canal level (avcPE). Besides these two clusters, we have found a third source of PE cells: single cells rounding up from a region of the pericardial mesothelium close to the arterial pole, which are transferred to the ventricular myocardium. It is interesting to speculate on the presence of such an epicardial cell source located at the atrial pole to be present also in other species. This progenitor pool might contribute to EPDC heterogeneity. The identification of different sources of epicardial cells from the pericardial mesothelium described for the zebrafish agrees with results obtained in the chick. There, PE ablation is partially compensated by increased proliferation of the pericardial mesothelium, leading to ectopic PE-like protrusions (Manner, 1993, Gittenberger-de Groot et al., 2000, Perez-Pomares et al., 2002). It seems likely that overlapping strategies have evolved to ensure epicardium formation, including multiple PE cell sources. Whether the three different epicardial cell sources described in zebrafish give rise to progenitors with different differentiation potential requires further investigation.

In the chicken, the epicardium covering the cardiac OFT, does not derive from the PE but originates from the cephalic pericardium (Perez-Pomares et al., 2003). *In vivo* imaging in the zebrafish confirmed that PE-derived cells do not colonize the OFT, which rather is covered by the pericardial mesothelium as it is added to the growing heart. Also, in *hst* mutants which lack a PE, the OFT epicardium develops normally. While in the chick, the ablation of the PE leads to a partial compensation by the arterial pole derived epicardium, this was not observed in *hst* zebrafish embryo. While more investigation is needed to understand this different behavior, an explanation could be that the arterial pole epicardium possesses less proliferative potential. A second explanation could be that *tbx5a* is necessary for this process to occur. In *ace* mutants, PE formation is delayed, but epicardium formation was also not rescued by the OFT epicardium,

which developed normally. This could be due to the existence of a differential profile of adhesion molecules between the ventricular myocardium and the smooth muscle of the OFT. Interestingly, the few epicardial cells attached to the ventricle seem to present a high proliferative capacity; they are able to develop an epicardial layer although with some delay. In wildtype embryos, epicardial cells attached to the ventricular myocardium proliferate until covering it completely. We suggest the following mechanism*:* less PE cells are transferred to the myocardium in *ace*, but later, the adhered cells proliferate and can compensate for the reduced number of PE cells and form a nearly complete epicardial sheet.

3. Role of the heartbeat and flow forces during PE cluster formation.

Fluid flow forces have recently emerged as an important factor in the control of organogenesis and organ homeostasis (Cartwright et al., 2009, Freund et al., 2012). Extensive study of intracardiac fluid forces during cardiovascular development has demonstrated important roles in valvulogenesis and trabeculation (Vermot et al., 2009, Peshkovsky et al., 2011, Hove et al., 2003, Santhanakrishnan and Miller, 2011). Our data suggest that cardiogenesis is also regulated by extracardiac flow forces generated in the pericardial cavity. The heartbeat generates pericardial fluid forces necessary for PE cluster formation. Genetic disruption of the heartbeat using *tnnt2* antisense morpholinos lead to the absence of PE clusters. When the *tnnt2* MO was injected in the *Epi:GFP* line, scattered GFP-positive cells were detected on the pericardial wall, but their morphology was flat and they did not cluster together. These results are compatible with the RNA expression of some PE markers previously reported in absence of a heartbeat (Serluca, 2008) and suggest that some dorsal wall pericardial cells express these markers even when they are not able to form the PE.

Recently, a second article pointing out the role of the heartbeat for epicardium formation has been published (Plavicki et al., 2014). In line with our own findings, in this work, the heartbeat is described to be necessary for PE cells to be advected and giving them the possibility to attach the myocardium. However, their results to not support a role for the heartbeat in PE cluster formation, as they find that *tnnt2* morphant larvae reveal a PE cluster and few epicardial cells attached to the ventricle (Plavicki et al., 2014). This phenotype has also been observed by us, when morpholino mediated gene silencing is not complete, and heart contraction is not fully stopped. Thus, a plausible explanation for the different results is, that in the experiments by Pavlicki et al, the heartbeat had not been completely stopped in the *tnnt2* morphants. This might indicate that already a very small heart contraction is enough to trigger PE formation and PE cell advection by weaker fluid forces in the pericardial cavity.

Also, similar to our approach, Plavicki and colleagues used inhibition of the heartbeat by BDM administration (Plavicki et al., 2014). When starting BDM treatment at 72 hpf, PE clusters were present, consistent with our data. From this experiment, the conclusion is made that PE clusters do not need the heartbeat for their formation. However, at 72 hpf the PE is already developed, and thus, the treatment is not interfering with initiation of PE formation. Consistent with our observations, when starting the BDM treatment at 48 hpf, larvae do not shown PE cluster formation nor epicardial cells at 120 hpf.

The fact that we did observe a change in PE cell morphology from round to flat after stopping the heartbeat suggests a function not only in PE establishment but also in its maintenance. We did not observe an increase in apoptosis of PE cells upon heartbeat inhibition. However, proliferation of pericardial cells was dramatically decreased. The link between heartbeat regulated pericardial cell proliferation and PE formation requires further studies.

When the heartbeat was altered using caffeine, which leads to a nonhomogeneous ventricular contraction, the PE size was increased significantly (**Figure R 8**). Proliferation assays would be needed to clarify whether this is due to an increase in proliferation or to a decrease in cell release. In contrast, *myh6* gene silencing led to a complete absence of PE formation. It would be interesting to perform proliferation assays also in *myh6* morphants. Taken together, these results suggest that a normal heartbeat and fluid forces profile is needed for PE cluster formation and release.

Higher forces, over 20 pN, were measured at sites where the PE clusters were formed. Mesothelial cells do not present apparent differences between them, but nonetheless PE clusters appear at a specific location. Maybe a fluid force gradient in the pericardial cavity facilitates to determine the position where the clusters will develop. The fluid forces have to be measured in embryos in which the heartbeat has been altered in different ways (using morpholinos against genes encoding proteins of the cardiac contraction machinery as well as chemical compounds) to strengthen the correlation between PE formation and fluid flow forces. In this line of thoughts, in *ace* mutants the PE cluster appeared unusually expanded towards the dorsal pericardial wall. It would be interesting to measure the fluid forces in these mutants to test whether they present a different pericardial fluid flow force map.

Another possibility to consider is that the impairment in pericardial mesothelium proliferation could be affected for the fact that pericardial fluid advections also distribute trophic factors to epicardial progenitors during development. Moreover, several growth factors, such us BMP (Laux et al., 2013), have been shown to be activated by shear stress, so stopping heartbeat could also be blocking the secretion of these molecules. Thus, genetic or epigenetic conditions that alter cardiac contraction might have a secondary adverse effect on epicardium formation, ultimately leading to a more severe phenotype. Indeed, it has been described that upon myocardial infarction, the pericardial fluid is a source of soluble factors involved in epicardial activation (Limana et al., 2010), and thus similarly it might be key in providing the necessary factors for PE maturation.

Another question to be addressed is whether PE cells are actively involved in their release from the PE clusters. It is unclear whether pericardial fluid forces are sufficient to induce PE cell detachment, and pericardial flow is likely to induce intracellular signals affecting the cytoskeleton, that trigger cells within the cluster to round up and detach, until their final release. The fact that cells within the PE cluster are in motion in synchrony with cardiac contraction for a certain period of time before their release, suggests that the effect of the fluid forces acting upon the PE cells are not enough *per se* to pull them out. The disruption of the adhesions between cells and with the basal lamina seems to be important for the release process. SEM PE cluster images showed irregularities in the cell membrane. It would be necessary to study cytoplasmic dynamics *in vivo* to find out whether changes in their cortex impulse cell movement or membrane tensions that break the adhesion among PE cells. Also, a comparison of the transcriptome of PE clusters

under normal conditions or upon impaired heartbeat could help to determine a mechanosensory pathway.

4. Role of the heartbeat in PE cell adhesion to the ventricular myocardium and epicardial layer formation.

We found that pericardial fluid advections promote the release of PE cells from the avcPE and the vpPE. Once released, cells are advected for varying periods of time until they attach the myocardial surface. As microbeads injected into the pericardial cavity were advected in exactly the same manner than PE cells, we suggest that it is the pericardial fluid rather than some PE cell intrinsic mechanisms driving this motion. Confirming the importance of the fluid forces for PE cells advection, BDM treatment at a time of formed PE clusters blocked their release and advection. The same occurs with microbeads injected into the pericardial cavity (**Movie S10** and **S12**). Advected cells in the pericardial cavity move quickly along the AVC and uppermost side of the ventricle and slower along the distal part of the ventricle. Our experiments revealed that the cells attached first to the myocardium at slow speed regions, suggesting that the fluid forces partly dictate the PE colonization of the myocardium, by facilitating the adhesion to the myocardium at low flow regions (**Figure D 3**). When impairing the heartbeat through silencing genes coding for contractile proteins the ventricle colonization behavior was altered and different adhesion patterns were observed. An abnormal pattern of epicardium formation was also observed in the axolotl *lethal* mutant, in which heart contraction is severely impaired (Fransen and Lemanski, 1990). The preferred adhesion we observed to the distal ventricle might also indicate a differential distribution of adhesion molecules of the myocardial surface. However this hypothesis is hard to reconcile with our optical tweezing experiments, which revealed that adhesion of PE cells is possible over the whole ventricular surface. However, this does also not necessarily indicate

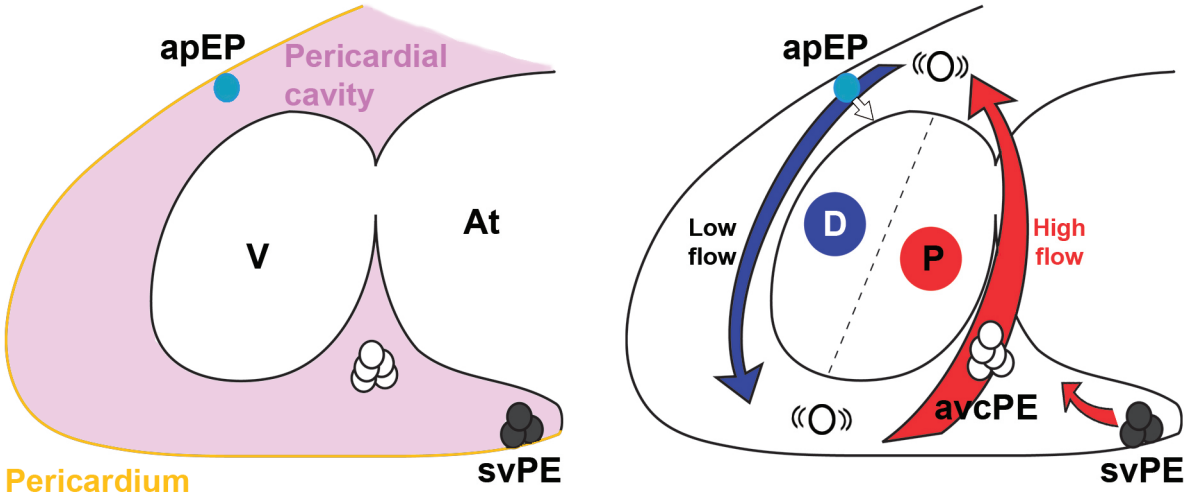

Figure D 3. Model for epicardium formation in the zebrafish. Schematic representation of the existence of three sources of proepicardial (PE) cells (avcPE, svPE and apEP) and the different ways of adhesion to the ventricular myocardium. While single apEP cells attach the ventricle directly, cells from the PE clusters are released into the high flow region in the pericardial cavity. Later they attach the distal (D) part of the ventricle preferentially, due to the low flow in that area of the cavity. At, atrium; D, distal part of the ventricle; P, proximal part of the ventricle; V, ventricle.

that the surface adhesion molecules profile is homogeneous. Several adhesion molecules and secreted molecules have been described as essential for proper epicardial layer formation. In the chick, the chemoattractant action of myocardial secreted BMP2 on PE cells has been described (Ishii et al., 2010). It would be interesting to study if abrogation of bmp2 secretion upon inhibition of cardiac contraction is the cause of impaired PE attachment of the myocardium. We propose that the whole myocardium is primed for coverage by epicardial cells but that heart morphology and associated flow patterns in the pericardial cavity expose certain regions to low fluid forces, favoring adhesion and accumulation of cells at these sites to initiate epicardium formation.

Contrary to what occurs with pericardial cell proliferation, the expansion of the epicardial layer on the myocardium seems to be less dependent on heart contraction, since proliferation of epicardial cells was observed after 5 hours of BDM treatment. In disagreement with our interpretation, the work by Plavicki et al suggests that the inhibition of heart contraction prevents epicardial development *in vitro* (Plavicki et al., 2014). *Ex vivo* 3 dpf heart cultures treated with BDM during 7 days, did not form an epicardium, while untreated hearts developed an epicardial layer. In addition, embryonic wildtype hearts were co-cultured with *tnnt2* morphant hearts. While in a control experiment, epicardial cells would crawl over the neighboring heart, in this scenario, epicardial cells do not migrate and colonize the *tnnt2* morphant heart. The lack of epicardium formation in the first experiment could be due to a long-term toxicity effect caused by BDM treatment. We have not observed a significantly increase in apoptosis in BDM 5h treatment, moreover, the decrease in proliferation was specific from the pericardium, while the neural system proliferation was not affected (not shown). However, 12h BDM treatment, in our hands, caused high embryonic lethality and pericardial edema. While we were able to efficiently induce adhesion of PE cells to BDM-treated, non-contracting cells using optical tweezers, these experiments were performed immediately after stopping the heartbeat. It is very plausible, that long-term arrest of cardiac contraction, as performed in the coculture experiment, dramatically alters cell adhesion properties of the myocardium and impedes epicardium adhesion. It will be interesting to further explore this possibility and identify putative candidate genes involved in this process using transcriptomic approaches.

Previous reports proposed that the heartbeat generates mechanical adhesion forces, which cause attachment and detachment between the PE and the myocardium or their release into the pericardial cavity (Rodgers et al., 2008). Our *in vivo* imaging analysis confirms that direct physical interaction between the myocardial surface and the pericardial mesothelium can trigger the transfer of apEP cells to the myocardium (**Figure D 3**), but release of PE cells from the other two PE cells sources did not always require direct PE-myocardium contact. We propose that the effect of the heartbeat on PE formation and PE cell release is partially mediated by pericardial fluid flow forces. Since flow results from pressure differences, it is also possible that mechanical tension exerted on the pericardial mesothelium during heart contraction participates in PE cluster formation.

5. Role of primary cilia in mechanotransduction of the pericardiac fluid forces.

Primary cilia play an important role in mechanotransduction of fluid forces. In addition, they can present receptors for signaling molecules along their membrane (Choksi et al., 2014, Freund et al., 2012). Our results showed that there were cilia protruding into the pericardial cavity from pericardial and PE cells. Before and after PE cluster formation, these cilia presented a heterogeneous location in the pericardial cells. The number was higher in the region where the avcPE will be formed. Once the PE clusters were developed, the cilia distribution was very similar to the previous one. Some PE cells showed cilia that seem to be trapped by ECM. This observation is consistent with the EM data that showed an increase of ECM produced by the PE cells. Within different regions of the pericardial cavity, cilia displayed conserved and characteristic motion pattern. Transiently stopping the heartbeat followed by reactivation revealed that cilia motions were coupled to cardiac contraction. The fact that they display several kinds of bending may imply that the signaling they are receiving and sending is specific for each region into the pericardial cavity. Higher degree of cilia deflection caused by higher flow forces might lead to more efficient or prolonged opening of associated Ca^{2+} channels, as has been reported for endothelial cells (Goetz et al., 2014). More experiments are needed to identify the role of these primary cilia in the PE formation and in the pericardial cavity. It would also be interesting to study the relationship between the proliferative cells and ciliated cells, a relasionship reporter in the endocardial cushions (Willaredt et al., 2012). We found advected broken cilia in the pericardial cavity, possibly caused by the strength of the turbulent flow in the pericardial. Our observations may be consistent with the hypothesis of threshold flow forces controlling cilia signaling or the absence of it. Further investigation is necessary to decipher whether there are ion channels or secreted signal receptors involved in intracellular signaling through cilia. Testing calcium channels and their activity in the different pericardial regions using Ca-sensing transgenic lines will help to answer this question (Wann et al., 2012).

The effects of fluid forces on mesothelial cell proliferation and cell advection in the pericardium during development might be a general mechanism operating on other mesothelia during development and disease. We have observed that epicardial cells have a very high migratory capacity. Interestingly, epicardial cells seem to be able to free-float in the pericardial wall and reattach at very distant sites on the injured myocardium in a transplantation assay (Gonzalez-Rosa et al., 2012a). This suggests, that epicardial cells might be able to “move” and “patrol” in the pericardial fluid in the adult. Thus, heartbeat driven epicardial cell release into the pericardial cavity might be a process occurring not solely during development, but might have important functions in cardiac homeostasis and injury response. Our results also support a model, in which pathophysiological conditions that alter cardiac contraction, such as those produced by genetic mutations, might have a secondary adverse effect on epicardium formation, and could serve as an additional environmental factor ultimately leading to a more severe phenotype.

CONCLUSIONS

1. The *wt1a* reporter line, *Epi:GFP*, labels most of proepicardial (PE) and epicardial cells representing a good tool to study epicardium formation *in vivo* in the zebrafish.
2. There are three sources of PE cells (avcPE, vpPE and apPE) in the zebrafish.
3. In the zebrafish, PE cell release and direct adhesion work in parallel to form the epicardial layer, revealing that both mechanisms can coexist in one species.
4. *tbx5a* is essential for PE formation but not for development of the epicardium derived from the cephalic pericardium.
5. *fgf8a* is needed for correct positioning and timing of the PE; its absence results in fewer PE cells attaching to the ventricle and delayed epicardium formation.
6. In the absence of a heartbeat, epicardium formation is disrupted, indicating that cardiac contraction triggers PE cluster formation, PE cell release and ordered adhesion to the myocardium.
7. Some of the effects of cardiac contraction on epicardium morphogenesis might be mediated through the heartbeat generated pericardial fluid flow.
8. Cells from the pericardial mesothelium and PE are ciliated.
9. Primary cilia display a specific distribution and movement patterns inside the pericardial cavity suggesting a role in mechanosensing of the pericardial fluid flow.

CONCLUSIONES

1. La línea reportera de *wt1a*, *Epi:GFP*, marca la mayoría del proepicardio (PE) y de las células epicárdicas por lo que constituye una buena herramienta para el estudio de la formación *in vivo* del epicardio en el pez cebra.

2. Existen tres fuentes de células PE (avcPE, vpPE y apPE) en el pez cebra.

3. En el pez cebra, la liberación y la adhesión directa de las células PE trabajan en paralelo para formar el epicardio, revelando que ambos mecanismos pueden coexistir en una especie.

4. *tbx5a* es esencial para la formación del PE, pero no para el desarrollo del epicardio derivado del pericardio cefálico.

5. *fgf8a* es necesario para la correcta formación temporal y espacial del PE, su ausencia da lugar a un menor número de células PE adhiriéndose al ventrículo y a un retraso en la formación del epicardio.

6. En ausencia de latido cardiaco se interrumpe la formación del epicardio, lo que sugiere que la contracción cardiaca activa la formación del PE, la liberación de las células PE y su adhesión ordenada al miocardio.

7. Algunos de los efectos de la contracción cardiaca en la morfogénesis del epicardio pueden estar mediados por de las fuerzas de fluido pericárdicas generadas por el latido.

8. Existen células ciliadas en el mesotelio pericárdico y el PE.

9. Los cilios primarios muestran una distribución y patrones de movimiento específicos en la cavidad pericárdica, lo que sugiere un papel en mecanotransducción de las fuerzas de fluido pericárdicas.

BIBLIOGRAPHY

ABU-ISSA, R. & KIRBY, M. L. 2007. Heart field: from mesoderm to heart tube. *Annu Rev Cell Dev Biol,* 23**,** 45-68.

ABU-ISSA, R., SMYTH, G., SMOAK, I., YAMAMURA, K. & MEYERS, E. N. 2002. Fgf8 is required for pharyngeal arch and cardiovascular development in the mouse. *Development,* 129**,** 4613-25.

ACHARYA, A., BAEK, S. T., HUANG, G., ESKIOCAK, B., GOETSCH, S., SUNG, C. Y., BANFI, S., SAUER, M. F., OLSEN, G. S., DUFFIELD, J. S., OLSON, E. N. & TALLQUIST, M. D. 2012. The bHLH transcription factor Tcf21 is required for lineage-specific EMT of cardiac fibroblast progenitors. *Development,* 139**,** 2139-49.

ALBALAT, R., BAQUERO, M. & MINGUILLON, C. 2010. Identification and characterisation of the developmental expression pattern of tbx5b, a novel tbx5 gene in zebrafish. *Gene expression patterns : GEP,* 10**,** 24-30.

ALSAN, B. H. & SCHULTHEISS, T. M. 2002. Regulation of avian cardiogenesis by Fgf8 signaling. *Development,* 129**,** 1935-43.

BAKKERS, J. 2011. Zebrafish as a model to study cardiac development and human cardiac disease. *Cardiovascular research,* 91**,** 279-88.

BASSON, C. T., BACHINSKY, D.R., LIN, R.C., LEVI, T., ELKINS, J.A., SOULTS, J., GRAYZEL, D., KROUMPOUZOU, E., TRAILL, T.A., LEBLANC-STRACESKI, J., RENAULT, B., KUCHERLAPATI, R., SEIDMAN, J.G. AND SEIDMAN, C.E. 1997. Mutations in Human TBX5 Cause Limb and Cardiac Malformation in Holt-Oram Syndrome. *Nature Genet.,* 15**,** 30-35.

BASSON, C. T., HUANG, T., LIN, R. C., BACHINSKY, D. R., WEREMOWICZ, S., VAGLIO, A., BRUZZONE, R., QUADRELLI, R., LERONE, M., ROMEO, G., SILENGO, M., PEREIRA, A., KRIEGER, J., MESQUITA, S. F., KAMISAGO, M., MORTON, C. C., PIERPONT, M. E., MULLER, C. W., SEIDMAN, J. G. & SEIDMAN, C. E. 1999. Different TBX5 interactions in heart and limb defined by Holt-Oram syndrome mutations. *Proceedings of the National Academy of Sciences of the United States of America,* 96**,** 2919-24.

BERBARI, N. F., O'CONNOR, A. K., HAYCRAFT, C. J. & YODER, B. K. 2009. The primary cilium as a complex signaling center. *Current biology : CB,* 19**,** R526-35.

BERDOUGO, E., COLEMAN, H., LEE, D. H., STAINIER, D. Y. & YELON, D. 2003. Mutation of weak atrium/atrial myosin heavy chain disrupts atrial function and influences ventricular morphogenesis in zebrafish. *Development,* 130**,** 6121-9.

BERG-SORENSEN, K. & FLYVBJERG, H. 2004. Power spectrum analysis for optical tweezers. *Rev. Sci. Instrum,* 75**,** 19.

BESSA, J., TENA, J. J., DE LA CALLE-MUSTIENES, E., FERNANDEZ-MINAN, A., NARANJO, S., FERNANDEZ, A., MONTOLIU, L., AKALIN, A., LENHARD, B., CASARES, F. & GOMEZ-SKARMETA, J. L. 2009. Zebrafish enhancer detection (ZED) vector: a new tool to facilitate transgenesis and the functional analysis of cis-regulatory regions in zebrafish. *Dev Dyn,* 238**,** 2409-17.

BOETTGER, T., WITTLER, L. & KESSEL, M. 1999. FGF8 functions in the specification of the right body side of the chick. *Current biology : CB,* 9**,** 277-80.

BOLLIG, F., PERNER, B., BESENBECK, B., KOTHE, S., EBERT, C., TAUDIEN, S. & ENGLERT, C. 2009. A highly conserved retinoic acid responsive element controls wt1a expression in the zebrafish pronephros. *Development,* 136**,** 2883-92.

BOROVINA, A., SUPERINA, S., VOSKAS, D. & CIRUNA, B. 2010. Vangl2 directs the posterior

tilting and asymmetric localization of motile primary cilia. *Nature cell biology,* 12**,** 407-12.

BRAITSCH, C. M., COMBS, M. D., QUAGGIN, S. E. & YUTZEY, K. E. 2012. Pod1/Tcf21 is regulated by retinoic acid signaling and inhibits differentiation of epicardium-derived cells into smooth muscle in the developing heart. *Developmental biology,* 368**,** 345-57.

BRESSAN, M., LIU, G. & MIKAWA, T. 2013. Early mesodermal cues assign avian cardiac pacemaker fate potential in a tertiary heart field. *Science,* 340**,** 744-8.

BRUNEAU, B. G. 2008. The developmental genetics of congenital heart disease. *Nature,* 451**,** 943-8.

BRUNEAU, B. G., NEMER, G., SCHMITT, J. P., CHARRON, F., ROBITAILLE, L., CARON, S., CONNER, D. A., GESSLER, M., NEMER, M., SEIDMAN, C. E. & SEIDMAN, J. G. 2001. A murine model of Holt-Oram syndrome defines roles of the T-box transcription factor Tbx5 in cardiogenesis and disease. *Cell,* 106**,** 709-21.

BUCKINGHAM, M., MEILHAC, S. & ZAFFRAN, S. 2005. Building the mammalian heart from two sources of myocardial cells. *Nature reviews. Genetics,* 6**,** 826-35.

CAI, C. L., LIANG, X., SHI, Y., CHU, P. H., PFAFF, S. L., CHEN, J. & EVANS, S. 2003. Isl1 identifies a cardiac progenitor population that proliferates prior to differentiation and contributes a majority of cells to the heart. *Developmental cell,* 5**,** 877-89.

CAI, C. L., MARTIN, J. C., SUN, Y., CUI, L., WANG, L., OUYANG, K., YANG, L., BU, L., LIANG, X., ZHANG, X., STALLCUP, W. B., DENTON, C. P., MCCULLOCH, A., CHEN, J. & EVANS, S. M. 2008. A myocardial lineage derives from Tbx18 epicardial cells. *Nature,* 454**,** 104-8.

CANO, E., CARMONA, R. & MUÑOZ-CHÁPULI, R. 2013. Evolutionary Origin of the Proepicardium. *J. Dev. Biol.,* 1**,** 3-19.

CARMONA, R., GONZALEZ-IRIARTE, M., PEREZ-POMARES, J. M. & MUNOZ-CHAPULI, R. 2001. Localization of the Wilm's tumour protein WT1 in avian embryos. *Cell Tissue Res,* 303**,** 173-86.

CARMONA, R., GUADIX, J. A., CANO, E., RUIZ-VILLALBA, A., PORTILLO-SANCHEZ, V., PEREZ-POMARES, J. M. & MUNOZ-CHAPULI, R. 2010. The embryonic epicardium: an essential element of cardiac development. *J Cell Mol Med,* 14**,** 2066-72.

CARTWRIGHT, J. H., PIRO, O. & TUVAL, I. 2009. Fluid dynamics in developmental biology: moving fluids that shape ontogeny. *HFSP journal,* 3**,** 77-93.

CASANOVA, J. C., TRAVISANO, S. & DE LA POMPA, J. L. 2013. Epithelial-to-mesenchymal transition in epicardium is independent of Snail1. *Genesis,* 51**,** 32-40.

COSSETTE, S. & MISRA, R. 2011. The identification of different endothelial cell populations within the mouse proepicardium. *Developmental dynamics : an official publication of the American Association of Anatomists,* 240**,** 2344-53.

CHOKSI, S. P., LAUTER, G., SWOBODA, P. & ROY, S. 2014. Switching on cilia: transcriptional networks regulating ciliogenesis. *Development,* 141**,** 1427-41.

CHONG, J. J., CHANDRAKANTHAN, V., XAYMARDAN, M., ASLI, N. S., LI, J., AHMED, I., HEFFERNAN, C., MENON, M. K., SCARLETT, C. J., RASHIDIANFAR, A., BIBEN, C., ZOELLNER, H., COLVIN, E. K., PIMANDA, J. E., BIANKIN, A. V., ZHOU, B., PU, W. T., PRALL, O. W. & HARVEY, R. P. 2011. Adult Cardiac-Resident MSC-like Stem Cells with a Proepicardial Origin. *Cell Stem Cell,* 9**,** 527-40.

CHRISTOFFELS, V. M., MOMMERSTEEG, M. T., TROWE, M. O., PRALL, O. W., DE GIER-DE

VRIES, C., SOUFAN, A. T., BUSSEN, M., SCHUSTER-GOSSLER, K., HARVEY, R. P., MOORMAN, A. F. & KISPERT, A. 2006. Formation of the venous pole of the heart from an Nkx2-5-negative precursor population requires Tbx18. *Circ Res,* 98**,** 1555-63.

DE PATER, E., CLIJSTERS, L., MARQUES, S. R., LIN, Y. F., GARAVITO-AGUILAR, Z. V., YELON, D. & BAKKERS, J. 2009. Distinct phases of cardiomyocyte differentiation regulate growth of the zebrafish heart. *Development,* 136**,** 1633-41.

DETTMAN, R. W., DENETCLAW, W., JR., ORDAHL, C. P. & BRISTOW, J. 1998. Common epicardial origin of coronary vascular smooth muscle, perivascular fibroblasts, and intermyocardial fibroblasts in the avian heart. *Dev Biol,* 193**,** 169-81.

DIAS, R. R., ALBUQUERQUE, J. M., PEREIRA, A. C., STOLF, N. A., KRIEGER, J. E., MADY, C. & OLIVEIRA, S. A. 2007. Holt-Oram syndrome presenting as agenesis of the left pericardium. *International journal of cardiology,* 114**,** 98-100.

DROBCZYNSKI, S., HÉBRAUD, P., MUNCH, J. P. & HARLEPP, S. 2009. Design and realization of a high-stability optical tweezer. *Opt. Eng.,* 48**,** 113601.

EISENHOFFER, G. T. & ROSENBLATT, J. 2013. Bringing balance by force: live cell extrusion controls epithelial cell numbers. *Trends in cell biology,* 23**,** 185-92.

FRANSEN, M. E. & LEMANSKI, L. F. 1990. Epicardial development in the axolotl, Ambystoma mexicanum. *Anat Rec,* 226**,** 228-36.

FREUND, J. B., GOETZ, J. G., HILL, K. L. & VERMOT, J. 2012. Fluid flows and forces in development: functions, features and biophysical principles. *Development,* 139**,** 1229-45.

GARRITY, D. M., CHILDS, S. & FISHMAN, M. C. 2002. The heartstrings mutation in zebrafish causes heart/fin Tbx5 deficiency syndrome. *Development,* 129**,** 4635-45.

GITTENBERGER-DE GROOT, A. C., VRANCKEN PEETERS, M. P., BERGWERFF, M., MENTINK, M. M. & POELMANN, R. E. 2000. Epicardial outgrowth inhibition leads to compensatory mesothelial outflow tract collar and abnormal cardiac septation and coronary formation. *Circ Res,* 87**,** 969-71.

GOETZ, J. G., STEED, E., FERREIRA, R. R., ROTH, S., RAMSPACHER, C., BOSELLI, F., CHARVIN, G., LIEBLING, M., WYART, C., SCHWAB, Y. & VERMOT, J. 2014. Endothelial cilia mediate low flow sensing during zebrafish vascular development. *Cell reports,* 6**,** 799-808.

GONZALEZ-ROSA, J. M., PERALTA, M. & MERCADER, N. 2012. Pan-epicardial lineage tracing reveals that epicardium derived cells give rise to myofibroblasts and perivascular cells during zebrafish heart regeneration. *Dev Biol,* 370**,** 173-86.

GRITSMAN, K., TALBOT, W. S. & SCHIER, A. F. 2000. Nodal signaling patterns the organizer. *Development,* 127**,** 921-32.

GUADIX, J. A., RUIZ-VILLALBA, A., LETTICE, L., VELECELA, V., MUNOZ-CHAPULI, R., HASTIE, N. D., PEREZ-POMARES, J. M. & MARTINEZ-ESTRADA, O. M. 2011. Wt1 controls retinoic acid signalling in embryonic epicardium through transcriptional activation of Raldh2. *Development,* 138**,** 1093-7.

HAENIG, B. & KISPERT, A. 2004. Analysis of TBX18 expression in chick embryos. *Dev Genes Evol,* 214**,** 407-11.

HAMBURGER, V. & HAMILTON, H. L. 1951. A series of normal stages in the development of the chick embryo. *Journal of morphology,* 88**,** 49-92.

HAMI, D., GRIMES, A. C., TSAI, H. J. & KIRBY, M. L. 2011. Zebrafish cardiac development requires a conserved secondary heart field. *Development,* 138**,** 2389-98.

HATCHER, C. J., DIMAN, N. Y., KIM, M. S., PENNISI, D., SONG, Y., GOLDSTEIN, M. M., MIKAWA, T. & BASSON, C. T. 2004. A role for Tbx5 in proepicardial cell migration during cardiogenesis. *Physiol Genomics,* 18**,** 129-40.

HIRAKOW, R. 1992. Epicardial formation in staged human embryos. *Kaibogaku Zasshi,* 67**,** 616-22.

HIROSE, T., KARASAWA, M., SUGITANI, Y., FUJISAWA, M., AKIMOTO, K., OHNO, S. & NODA, T. 2006. PAR3 is essential for cyst-mediated epicardial development by establishing apical cortical domains. *Development,* 133**,** 1389-98.

HOVE, J. R. & CRAIG, M. P. 2012. High-speed confocal imaging of zebrafish heart development. *Methods in molecular biology,* 843**,** 309-28.

HOVE, J. R., KOSTER, R. W., FOROUHAR, A. S., ACEVEDO-BOLTON, G., FRASER, S. E. & GHARIB, M. 2003. Intracardiac fluid forces are an essential epigenetic factor for embryonic cardiogenesis. *Nature,* 421**,** 172-7.

ICARDO, J. M., GUERRERO, A., DURAN, A. C., COLVEE, E., DOMEZAIN, A. & SANS-COMA, V. 2009. The development of the epicardium in the sturgeon Acipenser naccarii. *Anat Rec (Hoboken),* 292**,** 1593-601.

ISHII, Y., GARRIOCK, R. J., NAVETTA, A. M., COUGHLIN, L. E. & MIKAWA, T. 2010. BMP signals promote proepicardial protrusion necessary for recruitment of coronary vessel and epicardial progenitors to the heart. *Developmental cell,* 19**,** 307-16.

ISHII, Y., LANGBERG, J. D., HURTADO, R., LEE, S. & MIKAWA, T. 2007. Induction of proepicardial marker gene expression by the liver bud. *Development,* 134**,** 3627-37.

JAHR, M., SCHLUETER, J., BRAND, T. & MANNER, J. 2008. Development of the proepicardium in Xenopus laevis. *Dev Dyn,* 237**,** 3088-96.

KATZ, T., SINGH, M. H., DEGENHARDT, K., RIVERA-FELICIANO, J., JOHNSON, R. L., EPSTEIN, J. A. & TABIN, C. J. 2012. Distinct Compartments of the Proepicardial Organ Give Rise to Coronary Vascular Endothelial Cells. *Dev Cell,* 22**,** 639-650.

KEEGAN, B. R., MEYER, D. & YELON, D. 2004. Organization of cardiac chamber progenitors in the zebrafish blastula. *Development,* 131**,** 3081-91.

KIKUCHI, K., GUPTA, V., WANG, J., HOLDWAY, J. E., WILLS, A. A., FANG, Y. & POSS, K. D. 2011. tcf21+ epicardial cells adopt non-myocardial fates during zebrafish heart development and regeneration. *Development*.

KIKUCHI, K. & POSS, K. D. 2012. Cardiac regenerative capacity and mechanisms. *Annual review of cell and developmental biology,* 28**,** 719-41.

KIRSCHNER, K. M., WAGNER, N., WAGNER, K. D., WELLMANN, S. & SCHOLZ, H. 2006. The Wilms tumor suppressor Wt1 promotes cell adhesion through transcriptional activation of the alpha4integrin gene. *The Journal of biological chemistry,* 281**,** 31930-9.

KOMIYAMA, M., ITO, K. & SHIMADA, Y. 1987. Origin and development of the epicardium in the mouse embryo. *Anat Embryol (Berl),* 176**,** 183-9.

KREIDBERG, J. A., SARIOLA, H., LORING, J. M., MAEDA, M., PELLETIER, J., HOUSMAN, D. & JAENISCH, R. 1993. WT-1 is required for early kidney development. *Cell,* 74**,** 679-91.

KUHN, H. J. & LIEBHERR, G. 1988. The early development of the epicardium in Tupaia belangeri.

Anatomy and embryology, 177**,** 225-34.

KWEE, L., BALDWIN, H. S., SHEN, H. M., STEWART, C. L., BUCK, C., BUCK, C. A. & LABOW, M. A. 1995. Defective development of the embryonic and extraembryonic circulatory systems in vascular cell adhesion molecule (VCAM-1) deficient mice. *Development,* 121**,** 489-503.

LAUX, D. W., YOUNG, S., DONOVAN, J. P., MANSFIELD, C. J., UPTON, P. D. & ROMAN, B. L. 2013. Circulating Bmp10 acts through endothelial Alk1 to mediate flow-dependent arterial quiescence. *Development,* 140**,** 3403-12.

LAVINE, K. J., YU, K., WHITE, A. C., ZHANG, X., SMITH, C., PARTANEN, J. & ORNITZ, D. M. 2005. Endocardial and epicardial derived FGF signals regulate myocardial proliferation and differentiation in vivo. *Dev Cell,* 8**,** 85-95.

LEE, R. K., STAINIER, D. Y., WEINSTEIN, B. M. & FISHMAN, M. C. 1994. Cardiovascular development in the zebrafish. II. Endocardial progenitors are sequestered within the heart field. *Development,* 120**,** 3361-6.

LIEBLING, M., FOROUHAR, A. S., GHARIB, M., FRASER, S. E. & DICKINSON, M. E. 2005. Four-dimensional cardiac imaging in living embryos via postacquisition synchronization of nongated slice sequences. *Journal of biomedical optics,* 10**,** 054001.

LIEBLING, M., FOROUHAR, A. S., WOLLESCHENSKY, R., ZIMMERMANN, B., ANKERHOLD, R., FRASER, S. E., GHARIB, M. & DICKINSON, M. E. 2006. Rapid three-dimensional imaging and analysis of the beating embryonic heart reveals functional changes during development. *Developmental dynamics : an official publication of the American Association of Anatomists,* 235**,** 2940-8.

LIMANA, F., BERTOLAMI, C., MANGONI, A., DI CARLO, A., AVITABILE, D., MOCINI, D., IANNELLI, P., DE MORI, R., MARCHETTI, C., POZZOLI, O., GENTILI, C., ZACHEO, A., GERMANI, A. & CAPOGROSSI, M. C. 2010. Myocardial infarction induces embryonic reprogramming of epicardial c-kit(+) cells: role of the pericardial fluid. *Journal of molecular and cellular cardiology,* 48**,** 609-18.

LIMANA, F., CAPOGROSSI, M. C. & GERMANI, A. 2011. The epicardium in cardiac repair: from the stem cell view. *Pharmacol Ther,* 129**,** 82-96.

LIU, J., BRESSAN, M., HASSEL, D., HUISKEN, J., STAUDT, D., KIKUCHI, K., POSS, K. D., MIKAWA, T. & STAINIER, D. Y. 2010. A dual role for ErbB2 signaling in cardiac trabeculation. *Development,* 137**,** 3867-75.

LIU, J. & STAINIER, D. Y. 2010. Tbx5 and Bmp signaling are essential for proepicardium specification in zebrafish. *Circ Res,* 106**,** 1818-28.

LIU, J. & STAINIER, D. Y. 2012. Zebrafish in the study of early cardiac development. *Circulation research,* 110**,** 870-4.

MANNER, J. 1992. The development of pericardial villi in the chick embryo. *Anatomy and embryology,* 186**,** 379-85.

MANNER, J. 1993. Experimental study on the formation of the epicardium in chick embryos. *Anat Embryol (Berl),* 187**,** 281-9.

MANNER, J. 1999. Does the subepicardial mesenchyme contribute myocardioblasts to the myocardium of the chick embryo heart? A quail-chick chimera study tracing the fate of the epicardial primordium. *Anat Rec,* 255**,** 212-26.

MANNER, J., PEREZ-POMARES, J. M., MACIAS, D. & MUNOZ-CHAPULI, R. 2001. The origin, formation and developmental significance of the epicardium: a review. *Cells, tissues,*

organs, 169**,** 89-103.

MANNER, J., SCHLUETER, J. & BRAND, T. 2005. Experimental analyses of the function of the proepicardium using a new microsurgical procedure to induce loss-of-proepicardial-function in chick embryos. *Dev Dyn,* 233**,** 1454-63.

MARTINEZ-ESTRADA, O. M., LETTICE, L. A., ESSAFI, A., GUADIX, J. A., SLIGHT, J., VELECELA, V., HALL, E., REICHMANN, J., DEVENNEY, P. S., HOHENSTEIN, P., HOSEN, N., HILL, R. E., MUNOZ-CHAPULI, R. & HASTIE, N. D. 2010. Wt1 is required for cardiovascular progenitor cell formation through transcriptional control of Snail and E-cadherin. *Nat Genet,* 42**,** 89-93.

MIKAWA, T. & FISCHMAN, D. A. 1992. Retroviral analysis of cardiac morphogenesis: discontinuous formation of coronary vessels. *Proc Natl Acad Sci U S A,* 89**,** 9504-8.

MIKAWA, T. & GOURDIE, R. G. 1996. Pericardial mesoderm generates a population of coronary smooth muscle cells migrating into the heart along with ingrowth of the epicardial organ. *Dev Biol,* 174**,** 221-32.

MOORE, A. W., MCINNES, L., KREIDBERG, J., HASTIE, N. D. & SCHEDL, A. 1999. YAC complementation shows a requirement for Wt1 in the development of epicardium, adrenal gland and throughout nephrogenesis. *Development,* 126**,** 1845-57.

NAHIRNEY, P. C., MIKAWA, T. & FISCHMAN, D. A. 2003. Evidence for an extracellular matrix bridge guiding proepicardial cell migration to the myocardium of chick embryos. *Dev Dyn,* 227**,** 511-23.

NESBITT, T., LEMLEY, A., DAVIS, J., YOST, M. J., GOODWIN, R. L. & POTTS, J. D. 2006. Epicardial development in the rat: a new perspective. *Microscopy and microanalysis : the official journal of Microscopy Society of America, Microbeam Analysis Society, Microscopical Society of Canada,* 12**,** 390-8.

NIEDERREITHER, K., VERMOT, J., MESSADDEQ, N., SCHUHBAUR, B., CHAMBON, P. & DOLLE, P. 2001. Embryonic retinoic acid synthesis is essential for heart morphogenesis in the mouse. *Development,* 128**,** 1019-31.

PATEL, K., ISAAC, A. & COOKE, J. 1999. Nodal signalling and the roles of the transcription factors SnR and Pitx2 in vertebrate left-right asymmetry. *Current biology : CB,* 9**,** 609-12.

PERALTA, M., STEED, E., HARLEPP, S., GONZALEZ-ROSA, J. M., MONDUC, F., ARIZA-COSANO, A., CORTES, A., RAYON, T., GOMEZ-SKARMETA, J. L., ZAPATA, A., VERMOT, J. & MERCADER, N. 2013. Heartbeat-driven pericardiac fluid forces contribute to epicardium morphogenesis. *Current biology : CB,* 23**,** 1726-35.

PEREZ-POMARES, J. M., CARMONA, R., GONZALEZ-IRIARTE, M., ATENCIA, G., WESSELS, A. & MUNOZ-CHAPULI, R. 2002. Origin of coronary endothelial cells from epicardial mesothelium in avian embryos. *The International journal of developmental biology,* 46**,** 1005-13.

PEREZ-POMARES, J. M., CARMONA, R., GONZALEZ-IRIARTE, M., MACIAS, D., GUADIX, J. A. & MUNOZ-CHAPULI, R. 2004. Contribution of mesothelium-derived cells to liver sinusoids in avian embryos. *Developmental dynamics : an official publication of the American Association of Anatomists,* 229**,** 465-74.

PEREZ-POMARES, J. M., PHELPS, A., SEDMEROVA, M. & WESSELS, A. 2003. Epicardial-like cells on the distal arterial end of the cardiac outflow tract do not derive from the proepicardium but are derivatives of the cephalic pericardium. *Dev Dyn,* 227**,** 56-68.

PERNER, B., ENGLERT, C. & BOLLIG, F. 2007. The Wilms tumor genes wt1a and wt1b control

different steps during formation of the zebrafish pronephros. *Dev Biol,* 309**,** 87-96.

PESHKOVSKY, C., TOTONG, R. & YELON, D. 2011. Dependence of cardiac trabeculation on neuregulin signaling and blood flow in zebrafish. *Developmental dynamics : an official publication of the American Association of Anatomists,* 240**,** 446-56.

PLAVICKI, J. S., HOFSTEEN, P., YUE, M. S., LANHAM, K. A., PETERSON, R. E. & HEIDEMAN, W. 2014. Multiple modes of proepicardial cell migration require heartbeat. *BMC developmental biology,* 14**,** 18.

RASH, J. E., SHAY, J. W. & BIESELE, J. J. 1969. Cilia in cardiac differentiation. *Journal of ultrastructure research,* 29**,** 470-84.

REIFERS, F., BOHLI, H., WALSH, E. C., CROSSLEY, P. H., STAINIER, D. Y. & BRAND, M. 1998. Fgf8 is mutated in zebrafish acerebellar (ace) mutants and is required for maintenance of midbrain-hindbrain boundary development and somitogenesis. *Development,* 125**,** 2381-95.

REIFERS, F., WALSH, E. C., LEGER, S., STAINIER, D. Y. & BRAND, M. 2000. Induction and differentiation of the zebrafish heart requires fibroblast growth factor 8 (fgf8/acerebellar). *Development,* 127**,** 225-35.

ROBB, L., MIFSUD, L., HARTLEY, L., BIBEN, C., COPELAND, N. G., GILBERT, D. J., JENKINS, N. A. & HARVEY, R. P. 1998. epicardin: A novel basic helix-loop-helix transcription factor gene expressed in epicardium, branchial arch myoblasts, and mesenchyme of developing lung, gut, kidney, and gonads. *Dev Dyn,* 213**,** 105-13.

RODGERS, L. S., LALANI, S., RUNYAN, R. B. & CAMENISCH, T. D. 2008. Differential growth and multicellular villi direct proepicardial translocation to the developing mouse heart. *Developmental dynamics : an official publication of the American Association of Anatomists,* 237**,** 145-52.

ROJAS, A., DE VAL, S., HEIDT, A. B., XU, S. M., BRISTOW, J. & BLACK, B. L. 2005. Gata4 expression in lateral mesoderm is downstream of BMP4 and is activated directly by Forkhead and GATA transcription factors through a distal enhancer element. *Development,* 132**,** 3405-17.

RUDAT, C. & KISPERT, A. 2012. Wt1 and epicardial fate mapping. *Circ Res,* 111**,** 165-9.

SANTHANAKRISHNAN, A. & MILLER, L. A. 2011. Fluid dynamics of heart development. *Cell biochemistry and biophysics,* 61**,** 1-22.

SCHINDELIN, J., ARGANDA-CARRERAS, I., FRISE, E., KAYNIG, V., LONGAIR, M., PIETZSCH, T., PREIBISCH, S., RUEDEN, C., SAALFELD, S., SCHMID, B., TINEVEZ, J. Y., WHITE, D. J., HARTENSTEIN, V., ELICEIRI, K., TOMANCAK, P. & CARDONA, A. 2012. Fiji: an open-source platform for biological-image analysis. *Nature methods,* 9**,** 676-82.

SCHLUETER, J. & BRAND, T. 2009. A right-sided pathway involving FGF8/Snai1 controls asymmetric development of the proepicardium in the chick embryo. *Proc Natl Acad Sci U S A,* 106**,** 7485-90.

SCHLUETER, J. & BRAND, T. 2013a. Left-Right Asymmetrical Development of the Proepicardium. *J. Dev. Biol.,* 1**,** 126-140.

SCHLUETER, J. & BRAND, T. 2013b. Subpopulation of proepicardial cells is derived from the somatic mesoderm in the chick embryo. *Circulation research,* 113**,** 1128-37.

SCHLUETER, J., MANNER, J. & BRAND, T. 2006. BMP is an important regulator of proepicardial identity in the chick embryo. *Developmental biology,* 295**,** 546-58.

SCHULTE, I., SCHLUETER, J., ABU-ISSA, R., BRAND, T. & MANNER, J. 2007. Morphological and molecular left-right asymmetries in the development of the proepicardium: a comparative analysis on mouse and chick embryos. *Developmental dynamics : an official publication of the American Association of Anatomists,* 236**,** 684-95.

SEHNERT, A. J., HUQ, A., WEINSTEIN, B. M., WALKER, C., FISHMAN, M. & STAINIER, D. Y. 2002. Cardiac troponin T is essential in sarcomere assembly and cardiac contractility. *Nat Genet,* 31**,** 106-10.

SENGBUSCH, J. K., HE, W., PINCO, K. A. & YANG, J. T. 2002. Dual functions of [alpha]4[beta]1 integrin in epicardial development: initial migration and long-term attachment. *J Cell Biol,* 157**,** 873-82.

SERLUCA, F. C. 2008. Development of the proepicardial organ in the zebrafish. *Dev Biol,* 315**,** 18-27.

STAINIER, D. Y., FOUQUET, B., CHEN, J. N., WARREN, K. S., WEINSTEIN, B. M., MEILER, S. E., MOHIDEEN, M. A., NEUHAUSS, S. C., SOLNICA-KREZEL, L., SCHIER, A. F., ZWARTKRUIS, F., STEMPLE, D. L., MALICKI, J., DRIEVER, W. & FISHMAN, M. C. 1996. Mutations affecting the formation and function of the cardiovascular system in the zebrafish embryo. *Development,* 123**,** 285-92.

STAINIER, D. Y., LEE, R. K. & FISHMAN, M. C. 1993. Cardiovascular development in the zebrafish. I. Myocardial fate map and heart tube formation. *Development,* 119**,** 31-40.

STAUDT, D. W., LIU, J., THORN, K. S., STUURMAN, N., LIEBLING, M. & STAINIER, D. Y. 2014. High-resolution imaging of cardiomyocyte behavior reveals two distinct steps in ventricular trabeculation. *Development,* 141**,** 585-93.

TANAKA, M. & TICKLE, C. 2004. Tbx18 and boundary formation in chick somite and wing development. *Developmental biology,* 268**,** 470-80.

TANDON, P., MITEVA, Y. V., KUCHENBROD, L. M., CRISTEA, I. M. & CONLON, F. L. 2013. Tcf21 regulates the specification and maturation of proepicardial cells. *Development,* 140**,** 2409-21.

TORLOPP, A., SCHLUETER, J. & BRAND, T. 2010. Role of fibroblast growth factor signaling during proepicardium formation in the chick embryo. *Dev Dyn,* 239**,** 2393-403.

VAN WIJK, B., VAN DEN BERG, G., ABU-ISSA, R., BARNETT, P., VAN DER VELDEN, S., SCHMIDT, M., RUIJTER, J. M., KIRBY, M. L., MOORMAN, A. F. & VAN DEN HOFF, M. J. 2009. Epicardium and Myocardium Separate From a Common Precursor Pool by Crosstalk Between Bone Morphogenetic Protein- and Fibroblast Growth Factor-Signaling Pathways. *Circ Res*.

VANDUSEN, N. J. & FIRULLI, A. B. 2012. Twist factor regulation of non-cardiomyocyte cell lineages in the developing heart. *Differentiation; research in biological diversity,* 84**,** 79-88.

VERMOT, J., FOROUHAR, A. S., LIEBLING, M., WU, D., PLUMMER, D., GHARIB, M. & FRASER, S. E. 2009. Reversing blood flows act through klf2a to ensure normal valvulogenesis in the developing heart. *PLoS Biol,* 7**,** e1000246.

VINCENT, S. D. & BUCKINGHAM, M. E. 2010. How to make a heart: the origin and regulation of cardiac progenitor cells. *Current topics in developmental biology,* 90**,** 1-41.

VIRAGH, S. & CHALLICE, C. E. 1981. The origin of the epicardium and the embryonic myocardial circulation in the mouse. *Anat Rec,* 201**,** 157-68.

VON GISE, A. & PU, W. T. 2012. Endocardial and epicardial epithelial to mesenchymal transitions

in heart development and disease. *Circ Res,* 110**,** 1628-45.

WANN, A. K., ZUO, N., HAYCRAFT, C. J., JENSEN, C. G., POOLE, C. A., MCGLASHAN, S. R. & KNIGHT, M. M. 2012. Primary cilia mediate mechanotransduction through control of ATP-induced Ca2+ signaling in compressed chondrocytes. *FASEB journal : official publication of the Federation of American Societies for Experimental Biology,* 26**,** 1663-71.

WATT, A. J., BATTLE, M. A., LI, J. & DUNCAN, S. A. 2004. GATA4 is essential for formation of the proepicardium and regulates cardiogenesis. *Proc Natl Acad Sci U S A,* 101**,** 12573-8.

WESSELS, A. & PEREZ-POMARES, J. M. 2004. The epicardium and epicardially derived cells (EPDCs) as cardiac stem cells. *Anat Rec A Discov Mol Cell Evol Biol,* 276**,** 43-57.

WIESE, C., GRIESKAMP, T., AIRIK, R., MOMMERSTEEG, M. T., GARDIWAL, A., DE GIER-DE VRIES, C., SCHUSTER-GOSSLER, K., MOORMAN, A. F., KISPERT, A. & CHRISTOFFELS, V. M. 2009. Formation of the sinus node head and differentiation of sinus node myocardium are independently regulated by Tbx18 and Tbx3. *Circulation research,* 104**,** 388-97.

WILLAREDT, M. A., GORGAS, K., GARDNER, H. A. & TUCKER, K. L. 2012. Multiple essential roles for primary cilia in heart development. *Cilia,* 1**,** 23.

WU, S. P., DONG, X. R., REGAN, J. N., SU, C. & MAJESKY, M. W. 2013. Tbx18 regulates development of the epicardium and coronary vessels. *Developmental biology,* 383**,** 307-20.

XIN, M., OLSON, E. N. & BASSEL-DUBY, R. 2013. Mending broken hearts: cardiac development as a basis for adult heart regeneration and repair. *Nature reviews. Molecular cell biology,* 14**,** 529-41.

YANG, J. T., RAYBURN, H. & HYNES, R. O. 1995. Cell adhesion events mediated by alpha 4 integrins are essential in placental and cardiac development. *Development,* 121**,** 549-60.

ZARAGOZA, C., GOMEZ-GUERRERO, C., MARTIN-VENTURA, J. L., BLANCO-COLIO, L., LAVIN, B., MALLAVIA, B., TARIN, C., MAS, S., ORTIZ, A. & EGIDO, J. 2011. Animal models of cardiovascular diseases. *Journal of biomedicine & biotechnology,* 2011**,** 497841.

ZHOU, B., HONOR, L. B., HE, H., MA, Q., OH, J. H., BUTTERFIELD, C., LIN, R. Z., MELERO-MARTIN, J. M., DOLMATOVA, E., DUFFY, H. S., GISE, A. V., ZHOU, P., HU, Y. W., WANG, G., ZHANG, B., WANG, L., HALL, J. L., MOSES, M. A., MCGOWAN, F. X. & PU, W. T. 2011. Adult mouse epicardium modulates myocardial injury by secreting paracrine factors. *J Clin Invest*.

ZHOU, B., MA, Q., RAJAGOPAL, S., WU, S. M., DOMIAN, I., RIVERA-FELICIANO, J., JIANG, D., VON GISE, A., IKEDA, S., CHIEN, K. R. & PU, W. T. 2008a. Epicardial progenitors contribute to the cardiomyocyte lineage in the developing heart. *Nature,* 454**,** 109-13.

ZHOU, B., VON GISE, A., MA, Q., RIVERA-FELICIANO, J. & PU, W. T. 2008b. Nkx2-5- and Isl1-expressing cardiac progenitors contribute to proepicardium. *Biochem Biophys Res Commun,* 375**,** 450-3.

SUPPLEMENTARY MATERIAL

To watch the videos, please open them with Fiji or ImageJ.

Movie S 1. 3D projection of Epi:GFP pericardium at 42 hpf. Note homogeneous expression of GFP in the mesothelial cells of the pericardial cavity.

Movie S 2. Activation of Epi:GFP expression in an epicardial cell after attachment to the myocardium. High-speed confocal imaging reveals a freshly attached PE cells (circled) after attachment to the ventricle (red). 16 minutes after initiation of acquisition, the cell expresses GFP. At, atrium; V, ventricle.

Movie S 3. Proepicardial cells bulging out into the pericardial cavity. Movie of an Epi:GFP heart at 50 hpf acquired with a confocal microscope at 30 fps. Bright field and dark field images are mixed in order to appreciate better the cluster and its location. At the beginning of the movie, a GFP-positive cell cluster is visible in the dorsal pericardial wall. A single cell gets rounded and starts to move in synchrony to heart contraction. At the end of the movie, the cell is only loosely attached to GFP-positive PE cluster. At, atrium; PE, proepicardial cluster; V, ventricle.

Movie S 4. Two proepicardial clusters emerge from the dorsal pericardial wall. Movie of an Epi:GFP heart at 48 hpf acquired with a confocal microscope at 30 fps. Movement of the AVC proepicardial cluster (PE; white circle) occurs in response to heart contraction. The PE located at the ventral pole of the heart tube is circled in black (vpPE). Three GFP-positive epicardial cells already attached to the ventricle can also be seen. At, atrium; V, ventricle.

Movie S 5. Attachment of arterial pole progenitor cells to the ventricle. Fastcam imaging revealed attachment of an epicardial progenitor cell (EP) from the arterial pole (apEP; blue circle) to the ventricular myocardium. At the start of the movie, the EP cell on the inner surface of the pericardial cavity comes into close contact with the ventricle during each heart contraction. Few seconds later, the apEP detaches from the cavity wall and attaches to the ventricular surface. The epicardial cell remains attached to the ventricle during subsequent heart contractions. At, atrium; V, ventricle.

Movie S 6. Release of proepicardial cells into the pericardial cavity. Imaging of the venous pole proepicardial cell cluster (vpPE) shows movement in synch with heart contraction. During subsequent movie acquisition, this cluster gets released into the pericardial cavity. Movies were recorded 3 minutes apart. At, atrium; V, ventricle.

Movie S 7. Advection of proepicardial cells around the ventricle followed by attachment to the myocardium. Imaging at high temporal resolution was used to record a pair of proepicardial

(PE) cells advected within the pericardial cavity during heart contraction. Images were acquired at 250 fps. As the heart beats, the 2 advected PE cells (AC; white circle) can be seen circling around the ventricle. The second part of the movie, acquired 60 min after the first, shows the same cell pair attached to the ventricular myocardium. At, atrium; AC, advected cluster; V, ventricle.

Movie S 8. Genetic inhibition of heart contraction impedes epicardium formation. 3D reconstruction of a *tnnt2MO* injected *Epi:GFP* heart at 72 hpf. Myocardium is shown in red (anti-myosin heavy chain immunohistochemistry), nuclei are counterstained with DAPI (blue). Note that no Epi:GFP-positive cells attached to the myocardium; a few Epi:GFP-positive cells (green) can be seen on the pericardial wall but a proepicardium is not formed.

Movie S 9. Caffeine-treated larvae present impaired ventricular myocardium contraction during the heartbeat. Larvae without treatment, at 65 hpf. Contraction of the ventricular myocardium is homogeneous. However, larvae treated during 5 h with 100 µg/ml caffeine shown abnormal contraction of the ventricle (yellow asterisk). At, atrium; V, ventricle.

Movie S 10. Chemical inhibition of heart contraction impedes proepicardial cell advection. 2,3- butadione monoxime (BDM) was added to larvae after PE cell release. BDM was subsequently washed out (-BDM), leading to reactivation of heart contraction after 1 min and restoration of PE cell motion. Yellow circle marks position of an advected PE cell cluster, which starts its motion within the cavity after reactivation of heart contraction. At, atrium; V, ventricle.

Movie S 11. Tracking of the motion and speed of an advected proepicardial cell. The motion of a single proepicardial cell (green dot) encircling the ventricle in response to heart contraction is revealed. Note the high speed at the beginning of the movie (green tracks), when the cell is close to the atrioventricular boundary, and the slower motion when it reaches the distal ventricle (blue tracks).

Movie S 12. Motion of inert microbeads recapitulates movements of advected proepicardial cells. Red fluorescent 1 µm beads injected into the pericardial cavity are advected in an anticlockwise direction around the ventricle. Note fast movements close to the atrioventricular canal and slow motion close to the distal part of the ventricle. Treatment with 2,3- butadione monoxime (BDM) to stop the heartbeat blocks bead advection, and only Brownian motion of beads can be detected. A, atrium; V, ventricle.

Movie S 13. Optically trapped PE cells attach to the myocardium if placed close to it. Typical adhesion triggered by PE cell contact with the myocardium. A doublet of PE cells (white circle)

trapped by optical tweezers was moved towards the surface of the ventricle; the cell pair then attached and exited from the trap (red dot). V, ventricle.

Movie S 14. Optically trapped PE cells attach to the myocardium in absence of a heartbeat. BDM treated larvae just after release of a PE cells. The PE cell was trapped and placed close to the heart, which is not contracting. When put in close contact to the heart, the trapped PE cell adheres to the myocardium. Several steps of pulling the heart away from the trapped cell are shown. The strength of the trap is not enough to lead to a complete detachment of the PE cell and at the final pulling, the cell, which still has contacts with the surface, jumps back to the myocardium and releases from the trap. Red dot indicated the tweezing focus. Myo, myocardium, PE, proepicardial cell.

Movie S 15. Primary cilia protruding into the pericardial cavity. Primary cilia visualized in the *Tg(*β-actin:arl13b:GFP) by GFP expression. Cilia can be detected on cells located at the ventral pericardial wall and protruding into the pericardial cavity (white arrows). Note that faint GFP signal is also visible in some cell membranes, which should not be confounded with the ciliary axonema. V, ventricle.

Movie S 16. Primary cilia protruding from the proepicardium become immotile. Primary cilia protruding into the pericardial cavity from PE cells were immotile and bent possibly due to their trapping into ECM (white arrows). Close to the PE, a primary cilium protruding from pericardial cell can be seen in motion (white arrowhead). At, atrium; V, ventricle.

Movie S 17. Primary cilia movement in the OFT area. 1 second videos were recorded at an interval of 1 μm for a total of 18 μm and aligned based on periodic movement to obtain the 4D cilia motion. The video shows a specular reflection of the heart.

Movie S 18. Primary cilium movement at the ventral pericardium. 1 second videos were recorded at an interval 1 μm for a total of 14 μm and aligned based on periodic movement to obtain the 4D cilia motion. Note that cilium motion is affected by ventricular and atrial contractions. The video shows a specular reflection of the heart.

Movie S 19. Primary cilium movement at the deepest area of the dorsal pericardium. 1 second videos were recorded at an interval 1 μm for a total of 16 μm and aligned based on periodic movement to obtain the 4D cilia motion. Note that the cilium bents when the ventricle gets close to it. The video shows a specular reflection of the heart.

Movie S 20. Primary cilia movement at the AVC area. Shown are four cilia at the atrioventricular canal (AVC) region. A 1 second video was recorded at an interval 1 µm for a total of 8 µm and aligned based in periodic movement to obtain the 4D cilia motion. The video shows a specular reflection of the heart. Two cilia protrude into the lumen of the pericardial cavity and reveal motion. The one closer to the ventricle reveals a more prominent motion and the cilia further away moves less. The other two cilia are immotile and are bent, as trapped by extracellular matrix.

Movie S 21. Chemical inhibition of heart contraction impedes cilia motion. 2, 3- butadione monoxime (BDM) was added at 20 µM to stop the heartbeat. This leads to immediate block of cilia motion. At, atrium; V, ventricle.

Movie S 22. Primary cilia movement is coupled to the hearbeat. 20 µM 2,3- butadione monoxime (BDM) was added to larvae and subsequently washed out, leading to a reactivation of heart contraction. This led to concomitant reactivation of cilia motion. Note, however, that the cilia motion is different to the normal motion for that area, due to the abnormal cardiac contraction. At, atrium; V, ventricle.

Movie S 23. In vivo imaging revealing the dynamics of a PE-myocardial contact. *Epi:GFP* embryos at 60 hpf (myocardium in red and PE and epicardial cells in green).Yellow asterisk mark PE cells contacting with the ventricle apparently forming a bridge, which is undone with the heartbeat. At, atrium; V, ventricle.

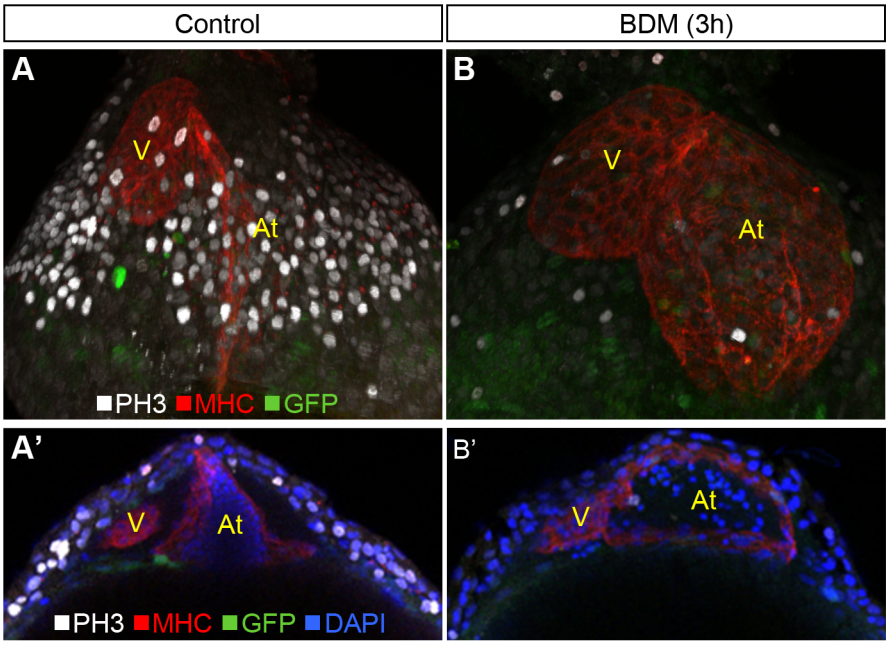

Figure S 1. BDM treatment reduces pericardial cell proliferation. (A) 3D model of phosphohistone 3 (PH3) immunohistochemistry (white dots), myosin heavy chain (MHC) and GFP in control embryos at 63 hpf. (B) 3D model of a BDM treated (3 h) embryo. (A',B') 15 µm sections from the 3D models. At, atrium; V, ventricle.

APPENDIX